Monte Carlo Studies of Interface Behavior in Ising Films

by

Lijun Pang

(Under the direction of David P. Landau)

Abstract

The interesting effects resulting from a linearly varying magnetic field on a thin Ising film is studied. The phase diagram is determined by looking for bulk two-phase coexistence at different values of g, the magnetic field gradient, and temperature T. We confirm the qualitative phase diagram predicted by theoretical work by Rogiers and Indekeu in 1993. As g increases, the temperature bounding bulk two-phase coexistence is re-entrant. We also studied non-local correlation functions in Ising films with opposite surface fields by calculating the spin-spin correlations for multiple choices of lattice size L and thickness D, between surface and interface, and within the interface. Fourier transformation of these correlations as well as the ratio between the real-space correlations and their Fourier transformation are calculated. We found that the ratio does decay exponentially as the non-local theory predicted, in the region of small wave vector q. The linear D dependence of the non-local correlation length ξ_{NL} is not confirmed, instead, we observed a power law relationship with the power of 1.20. The values of ξ_{NL} are also estimated.

Index words: Ising; wetting; phase transition; Monte Carlo; histogram reweighting; non-local correlation length; fourier transformation; finite size effects

Monte Carlo Studies of Interface Behavior in Ising Films

by

Lijun Pang

B.S., Nankai University, Tianjin, China, 1998

M.S., Nankai University, Tianjin, China, 2001

M.S., University of Georgia, Athens, GA, 2009

A Dissertation Submitted to the Graduate Faculty

of The University of Georgia in Partial Fulfillment

of the

Requirements for the Degree

Doctor of Philosophy

Athens, Georgia

2010

Monte Carlo Studies of Interface Behavior in Ising Films

by

Lijun Pang

Approved:

Major Professor: David P. Landau

Committee: Uwe Happek
Steven P. Lewis
Shan-ho Tsai

Electronic Version Approved:

Maureen Grasso
Dean of the Graduate School
The University of Georgia
Decembert 2010

Dedication

This paper is dedicated to my husband, my daughter and my parents.

Acknowledgments

I would first thank my major advisor, Prof. David P. Landau, for providing insightful advice with constant encouragement, strong support, and great patience throughout my entire research and academic years. I have learned to analyze problems thoroughly, pay attention to details, and communicate efficiently.

I would also like to thank all the other members in my advisory committee, Profs. Steven P. Lewis, Uwe Happek and Shan-Ho Tsai, for their insights and perspective as physicists and for spending time on serving as my committee members. Prof. Stevem P. Lewis gave me a lot of advice and help in my academic endeavor, especially in my job search. Prof. Uwe Happek also served in my advisory committee before I was accepted as phD candidate. I owe Prof. Shan-Ho Tsai a great deal for her great patience in helping me understand the simulation code and simulation techniques.

I want to express my sincere appreciation to Prof. Kurt Binder, who helped to propose the topics of my phD research projects and gave me tremendous advice and guidance these years.

I would also like to express special thanks to Linda Lee, administrative specialist in CSP, for her extremely cordial and kind help during my years in CSP.

I appreciate Prof. Joao Plascak and my fellow graduate student Xiuping Tao, Chongshan Zhang, and Junqi Yin at CSP for a lot of helpful discussions.

I should also thank my church family who gave me and my family tremendous help and encouragement through years.

I thank my parents and my parents-in-law for being supportive all the time. Finally, in a very inadequate manner, I want to thank my husband and my dear daughter for standing with me as a family.

Table of Contents

List of Figures

Chapter 1

Introduction

Wetting phenomena have formed a topic of interest with a long history, but interesting questions remain unanswered. The observation that the contact angle between a fluid and underlying surface (see Fig. 2.3 in Section 2.2) may be either zero or nonzero dates back at least to Young [1]. In recent years, wetting phenomena have attracted a lot of theoretical [2-15] and experimental [16-20] attention. A wetting transition basically refers to the formation of an infinitely thick film being deposited on a surface. The surface may be between two different liquids, or something else, and the transition itself is defined by the thickness of the film going to infinity . It may occur in the surface layers of bulk systems and is induced by symmetry-breaking surface fields. For example, in binary liquid mixtures below the consolute point, one phase will be adsorbed on the wall of the container, and may wet its surface. It can be viewed as a delocalization of the interface between the adsorbed phase and the bulk phase of the mixture. The transition from the nonwet to the wet state may be either first order [3, 4, 5] or second [6, 7, 8, 10, 11, 12].

Nakanishi and Fisher [6] made an important advance in our theoretical understanding of wetting phenomena by drawing the analogy between wetting phenomena and surface critical behavior in the Ising model. In the latter problem, one is interested in the ordering of the surface in the absence of bulk and surface fields. It's known that the surface orders before the bulk, if the exchange J_s in the surface plane exceeds a critical value J_{sc}. Nakanishi and Fisher [6] related surface criticality and "prewetting" which is a wetting transition occurring in the presence of a nonzero bulk symmetry breaking field, $H \neq 0$ (Fig. 2.6 in section 2.3). Binder, Landau *et al.* [21, 22, 23, 24] used an Ising-lattice-gas model and well-developed

Monte Carlo simulation techniques in an Ising model to examine the wetting behavior. They considered a semi-infinite Ising model with a simple interaction between "spins" and between "spins" and the walls and realized this geometry on a finite computer by using a very thick Ising slab for which the top and bottom surfaces are so widely separated that each acts as though it is the boundary to a semi-infinite system. On the other hand, thin fluid films that are adsorbed on substrates or confined in slit-like capillaries also attracted enormous interest [9, 25, 26, 27, 28, 30, 32, 33, 34, 35, 51, 52] since they pose challenging fundamental questions due to an interplay between finite size behavior and surface phenomena. These systems can readily be simulated using the same Ising slab described earlier for the study of semi-infinite systems by merely reducing the thickness of the system being simulated. Thus, Monte Carlo simulation in Ising-lattice-gas provided a natural testing ground for theoretical predictions for wetting phenomena and interface behavior.

This dissertation describes extensive Monte Carlo studies of interface behavior in Ising films and has concentrated on the following two controversial topics: The first controversy can be dated back to 1980's. Although a wetting transition can be either first order or second order, the latter case, "second order wetting transition" or "critical wetting", is particularly interesting. The initial theoretical interest in study of critical phenomena concerning the nature of fluctuation effects for critical wetting transitions in three-dimensional systems with short-ranged forces stems from the fact that the physical dimension $d = 3$ is also the upper critical dimension for the transition. Renormalization group (RG) analyses of a simple interfacial (capillary-wave) Hamiltonian by Brezin, Halperin and Leibler [10] and later Fisher and Huse [13] predicted that all critical properties are strongly non-universal (see Section 2.3), which differs dramatically from the mean-field result [10, 11, 13]. However, Binder, Landau and coworkers [21, 22, 23, 24] did extensive Monte Carlo simulations to study wetting phenomena. They compared their results for critical wetting to theoretical predictions and surprisingly found that their results were consistent with simple mean-field behavior, i.e. the different singular behavior predicted by various renormalization-group treatments was

not observed. Different models and RG analyses based on local interfacial Hamiltonians [38-47] were proposed to explain the differences between the theoretical predictions and Monte Carlo simulations by introducing the stiffness-instability mechanism which allows for a spatially dependent interfacial stiffness. This, however, is claimed to be flawed by Parry *et al.* [49]. The first reason is that the stiffness-instability mechanism does not provide a quantitative explanation of the near mean-field-like criticality observed for the Ising model. The other reason is that the mechanism, which is present in microscopic models, would serve to exchange the lines of first-order and critical wetting appearing in the equilibrium global surface phase diagram by Nakanishi and Fisher [6] and contradict much of our understanding of wetting and surface criticality. Parry *et al.* [48, 49, 60, 61, 62, 63, 64, 65] revisited these problems using a non-local (NL) interfacial Hamiltonian [66, 67]. The new ingredient in the NL model is the presence of long-ranged two-body interfacial interactions controlling the repulsion from the wall which was not modeled correctly in previous interfacial descriptions. The analysis of the NL model shows that correlation functions are characterized by not one, but two diverging correlation lengths, the parallel correlation length $\xi_{\|}$ and the non-local correlation length ξ_{NL}, which turns out to be proportional to $\sqrt{ln\xi_{\|}}$. This second length serves to lower the cut-off in the spectrum of interfacial fluctuation determining the repulsion from the wall in critical wetting. Analyses based on this non-local Hamilonian claim to correct previous renormalization group predictions for fluctuation effects.

Inspired by this new non-local Hamiltonian, we did extensive Monte Carlo simulation in an Ising film confined between two opposite walls and calculated non-local correlation functions defined by Parry *et al.*. This work provides the first and most direct confirmation of the non-local theory.

The other topic we studied was the effect of gravity on phase equilibria. Parry and Evans [51, 52] investigated the phase diagram of a d-dimensional Ising model in an $D \times \infty^{d-1}$ geometry, i.e., confined between two walls separated by a finite distance D, using detailed mean-field theory and scaling arguments. They considered opposing walls, where one wall

favors the liquid phase and the other favors the vapor phase(corresponding to introducing surface magnetic fields H_1 and H_2 with opposite sign ($H_1 H_2 < 0$)). It was found [51] that two phase coexistence is restricted to temperatures below the wetting temperature T_W; Brochard and de Gennes reached a similar conclusion by doing experiments on the spreading of liquid droplets deposited on a liquid substrate [53]. These results were later confirmed by extensive Monte Carlo simulations, both in two and three dimensions [28, 36]. What is surprising about the results of Parry and Evans is that one does not seem to recover information about the bulk critical point when the limit $L \to \infty$ is taken: for all values of L two phase coexistence is restricted to $T < T_W$.

To clarify the remarkable properties of this system, Rogiers and Indekeu [54] introduced an extra bulk field which varies linearly with the distance between the walls, and which plays the role of gravity in the fluid. Using a mean-field analysis, they found that the competing effect of opposing surface fields and gravity restores phase coexistence up to the bulk critical temperature. Carlon and Drzewiński [55, 56] studied Rogiers and Indekeu's model using a density matrix renormalization group method and confirmed the mean field calculations.

We used Monte Carlo simulation to study the effect of a linearly changing field on an Ising film confined between two opposing walls to determine the interface-binding-unbinding phase transitions when varying both the temperature and the field gradient.

The rest of this dissertation is organized as follows. The theoretical background is presented in Chapter 2. The model and methods are decribed in Chapter 3. In Chapter 4, the simulation results for the non-local correlation is reported. The simulational results for the gravity effects is discussed in Chapter 5. Finally, the dissertation concludes in Chapter 6.

Chapter 2

Background

2.1 Phase transitions

In physics, a thermodynamic phase of a simple material is an open, connected region in the space of thermodynamic states. A phase transition is the transformation of a thermodynamic system from one phase to another. During a phase transition, certain properties of the system will change as a result of a alteration of some external condition, such as temperature, pressure, and others. For example, a liquid may become gas upon heating to the boiling point, resulting in an abrupt change in volume.

For most phase transitions, we have an "order parameter" which will have a non-zero value in the ordered phase but identically zero in the disordered phase. In different kinds of systems, the order parameter has different definitions. For example, the order parameter is defined as the spontaneous magnetization in a ferromagnet; in liquid-gas system, it is the density difference between the liquid and gas phases at the transition.

If the first derivatives of the free energy are discontinuous at the transition temperature, the transition is called first order, whereas second order phase transitions are continuous in the the first derivatives but exhibit discontinuities in the second derivatives of the free energy. The characteristic behavior for these both kinds of phase transitions is shown below in Fig. 2.1 [57].

Let's take Ising model as an example to discuss the phase transition . The Hamiltonian of a typical ferromagnetic Ising model is :

$$\mathcal{H} = -J_{\mathrm{nn}} \sum_{nn} \sigma_i \sigma_j - H \sum_i \sigma_i \tag{2.1}$$

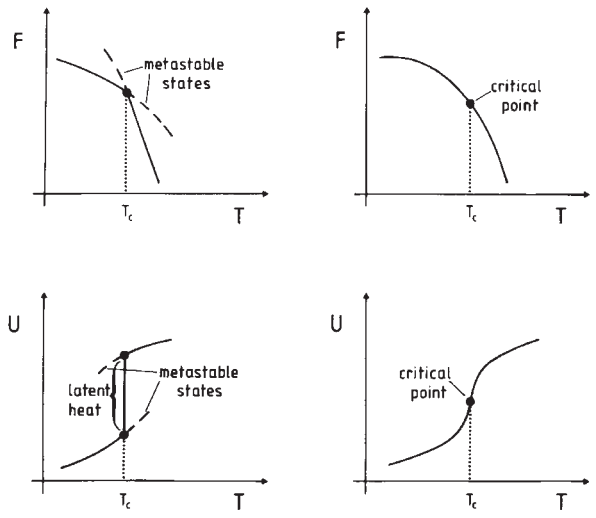

Figure 2.1: (left) Schematic temperature dependence of the free energy F and the internal energy U for a system undergoing a first order transition; (right) schematic temperature dependence of the free energy and the internal energy for a system undergoing a second order transition. From Ref.[57]

where $\sigma = \pm 1$ is the spin at lattice site i which interacts with nearest neighbors on the lattice with interaction constant $J_{\rm nn} > 0$. The summation in the first term is over all distinct pairs of nearest-neighbor spins, and H is the bulk magnetic field. The order parameter here is the average magnetization defined as:

$$\langle m \rangle = \frac{1}{N} \sum_i \sigma_i \ . \tag{2.2}$$

In two or more dimensions, the Ising system may undergo phase transitions by changing temperature T or magnetic field H. Fig. 2.2 shows the phase diagram in $H - T$ space. When $T < T_c$, most spins point upward at $h > 0$ and point downward at $h < 0$. At low temperatures, when h is swept through zero, a first order transition occurs. The first order line (or phase boundary) ends at T_c, where the transition becomes second order. For example, along the path $A \to B \to C$, a first order phase transition occurs at B. However along $A \to D \to C$, no transition occurs.

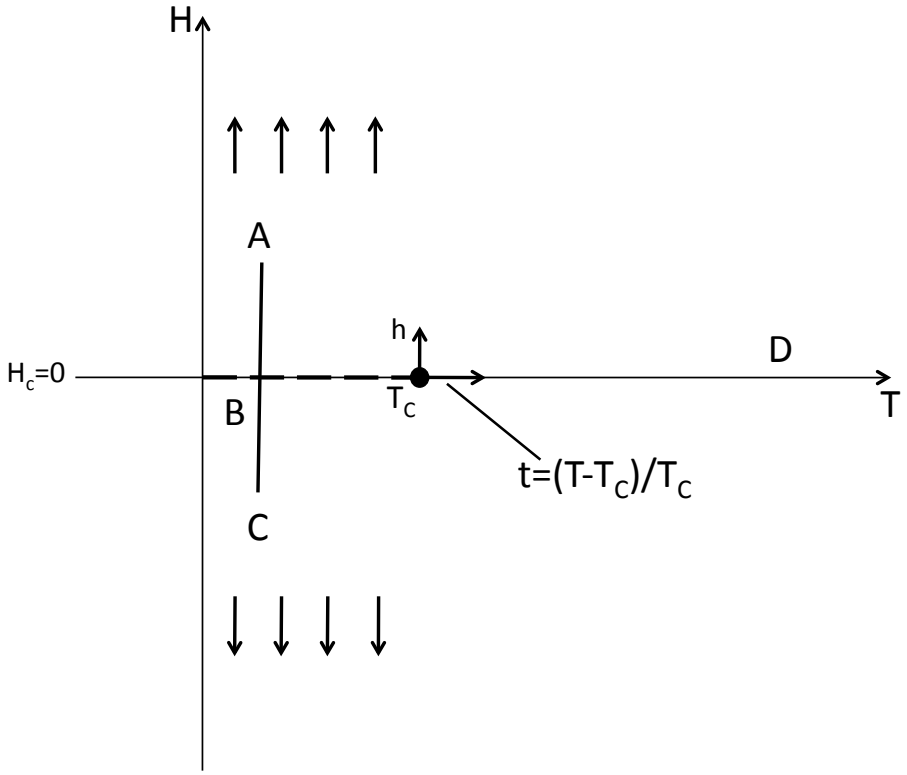

Figure 2.2: Phase diagram of a typical Ising model. The dashed line indicates a first order transition. The dot at the end of the dashed line indicates the critical point (in second order transiton). The parallel arrows indicate the spin directions. A, B, C represent three different states in the phase diagram.

At criticality, the thermodynamic properties, like the order parameter m, the specific heat C, the susceptibility χ and the correlation length ξ exhibit power-law singularities as follows:

$$m = m_o \varepsilon^{\beta} \tag{2.3}$$

$$\chi = \chi_o \varepsilon^{-\gamma} \tag{2.4}$$

$$C = C_o \varepsilon^{-\alpha} \tag{2.5}$$

$$\xi = \xi_o \varepsilon^{-\nu} \tag{2.6}$$

where $\varepsilon = |1 - T/T_c|$ is the reduced temperature and the powers are critical exponents that are unique for systems with the same symmetries. The equations are only valid when $\varepsilon \to 0$. The fundamental source of these singularities is the divergence in the correlation length ξ at criticality.

Since critical phenomena arise from long-ranged correlations, one expect that some of the details of the interatomic potential might be quite irrelevant to the behavior in the critical region. So it is usually asserted that the values of the critical indices are independent of interaction details, as the universality hypothesis states. The universality hypothesis says that all critical problems may be divided into classes differentiated in part by: (1) The dimensionality of the system; (2) The symmetry group of the system; and (3) Spin dimensionality. Within each class, the systems have the same set of critical exponents.

2.2 WETTING TRANSITIONS - PHENOMENOLOGICAL DESCRIPTION

As is shown in Fig. 2.3, when a small amount of liquid is on the surface of a solid substrate and also surrounded by saturated gas, one may either observe that this liquid stays in the form of droplets which touch the solid surface with a contact angle Θ, or it is spread out and forms a homogenous film covering the solid surface. In the former case one says that the

solid surface is "non-wet" or "incompletely wet" (i.e., if $0 < \Theta < \pi/2$, not including $\Theta = 0$), while in the latter case the substrate surface is wetted by the liquid.

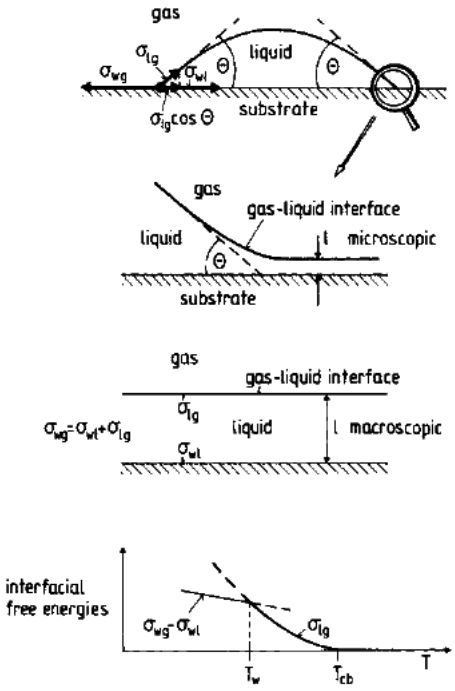

Figure 2.3: Schematic cross section of a (macroscopic) droplet of liquid, coexisting with saturated gas, on a non-wet substrate surface showing: (upper part) the contact angle Θ and the interpretation of Youngs equation in terms of mechanical equilibrium of the surface tensions on the contact line; (middle part) A magnified view of the three-phase contact line where the liquid-gas interface meets the substrate surface. (bottom part) Illustration of a (first-order) wetting transition in terms of the temperature dependence of the various interface free energies.(From ref. [24])

According to the famous Young's equation [1] established over 200 years ago, the contact angle is determined by a competition between three interface free energies: the surface tension between wall and gas σ_{wg}, the surface tension between wall and liquid σ_{wl}, and the interface tension between liquid and gas σ_{lg}.

$$cos\Theta = (\sigma_{wg} - \sigma_{wl})/\sigma_{lg} \text{ if } \sigma_{wg} \leq \sigma_{wl} + \sigma_{lg} \tag{2.7}$$

If a system is incompletely wet in its original state, it lowers its free energy by forming a liquid film of mesoscopic thickness which uniformly covers the solid substrate surface. So, the wet surface corresponds to $\Theta = 0$.

Because the interface free energies depend on temperature, and possibly other parameters, one would expect to be able to induce a transition in a system from incompletely wet to completely wet by variation of temperature or other parameters. However, it was not until about 30 years ago that a Landau-type theory about wetting transition was first proposed [3]. The resulting generic phase diagram, density profile and the variation of the surface excess density ρ_s in different situations are shown in Fig. 2.4.

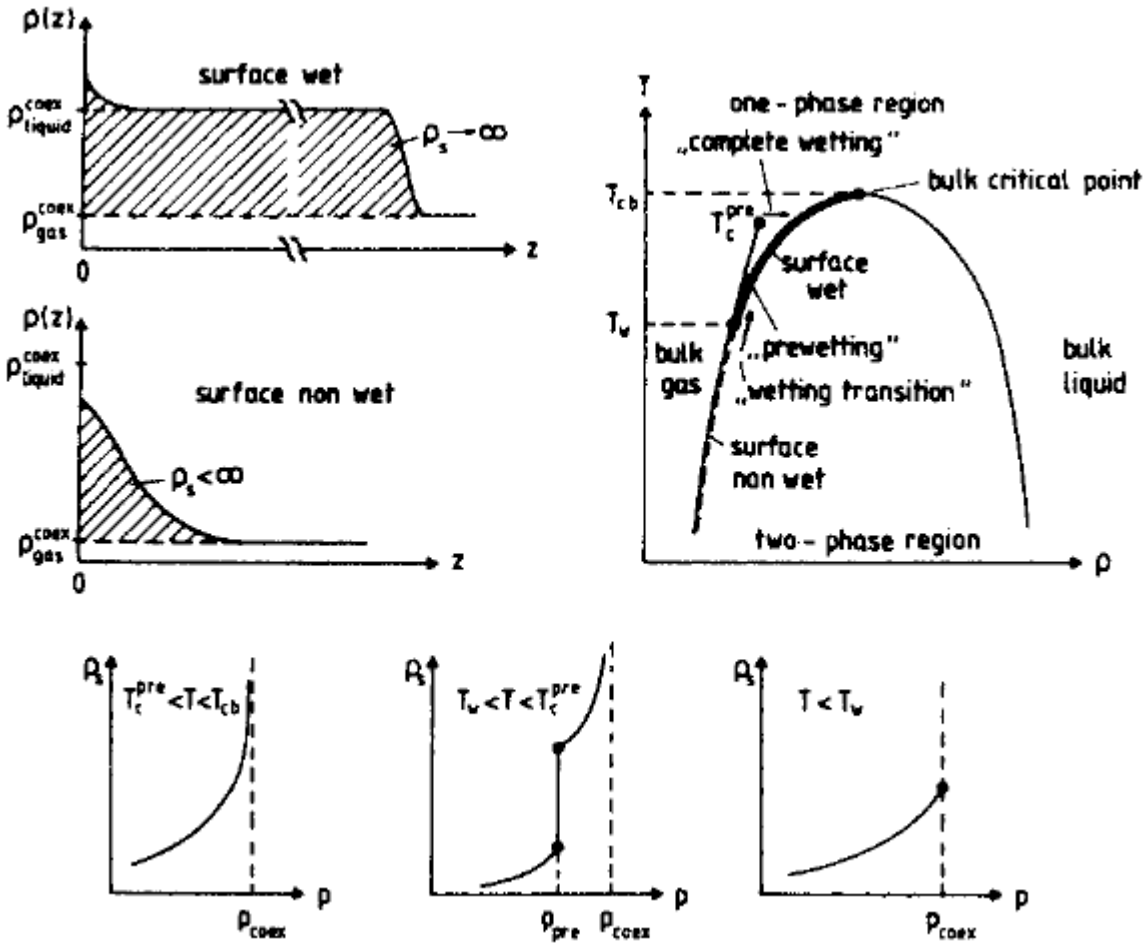

Figure 2.4: (right part) Schematic phase diagram of a semi-infinite fluid in contact with a wall; (left part) corresponding profiles of the coarse-grained local density $\rho(z)$ as function of the distance z from the wall at $z = 0$.(From ref. [24])

In the phase diagram, the coexistence curve separates saturated gas with liquid in the bulk. At the bulk critical point (T_{cb}), the enclosed two-phase region ends. A wetting transition occurs at a temperature T_w along the gas branch of the coexistence curve. Since the wetting

transition is a singularity of the surface excess free energy (see Eqn.2.17) associated with the wall, if the corresponding density profile changes from a non-wet state of the surface to a wet state continuously, the transition is critical wetting; while the transition is first-order if the density profile changes via a discontinuous jump at T_w. In the latter case, a prewetting transition (a wetting transition occuring in the presence of a non-zero bulk symmetry breaking field, $H \neq 0$) occurs in the one-phase region, ending at a prewetting critical temperature T_c^{pre}.

It is interesting that the surface critical behavior of Ising ferromagnets is also related to the singular behavior of a surface excess free energy contribution of a semi-infinite system [2]. The associated phase diagram is shown in Fig. 2.4 [2, 9]

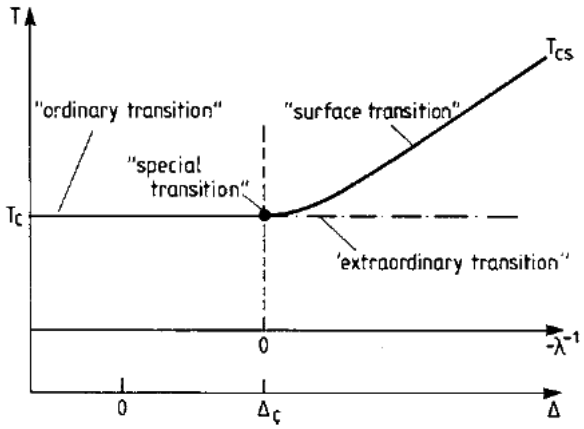

Figure 2.5: Surface phase diagram of a semi-infinite Ising ferromagnet with nearest-neighbor interaction J in the bulk and coupling J_s in the surface plane, and zero surface field $H_1 = 0$ as a function of temperature T. ($\Delta = J_s/J - 1$) (From ref. [24])

If $\Delta = J_s/J - 1$ is greater than the critical value Δ_c, the surface orders before the bulk at a temperature $T_{cs} > T_{cb}$. This surface transition merges with the bulk transition at a point, $T = T_{cb}$, $J_s/J = J_{sc}/J$, and this point is called the "special transition" or "surface-bulk multicritical point".

It is well known that the Ising model in a magnetic field H is equivalent to a lattice gas model in a chemical potential. One only needs to relate a density variable c_i to an Ising spin

σ_i by the following equation:

$$c_i = (1 + \sigma_i)/2 \tag{2.8}$$

where

$$c_i = \begin{cases} 1 & \text{if lattice site i occupied} \\ 0 & \text{if lattice site i empty} \end{cases} \tag{2.9}$$

and

$$\sigma_i = \begin{cases} 1 & \text{if spin i pointing up} \\ -1 & \text{if spin i pointing down} \quad . \end{cases} \tag{2.10}$$

So it is natural to consider wetting transitions in an Ising model. As mentioned earlier, Nakanishi and Fisher [6] made an important advance in our theoretical understanding of wetting phenomena by clarifying the relation between wetting and surface critical phenomena more precisely. Fig. 2.5 illustrated the phase diagrams for a semi-infinite Ising magnet.

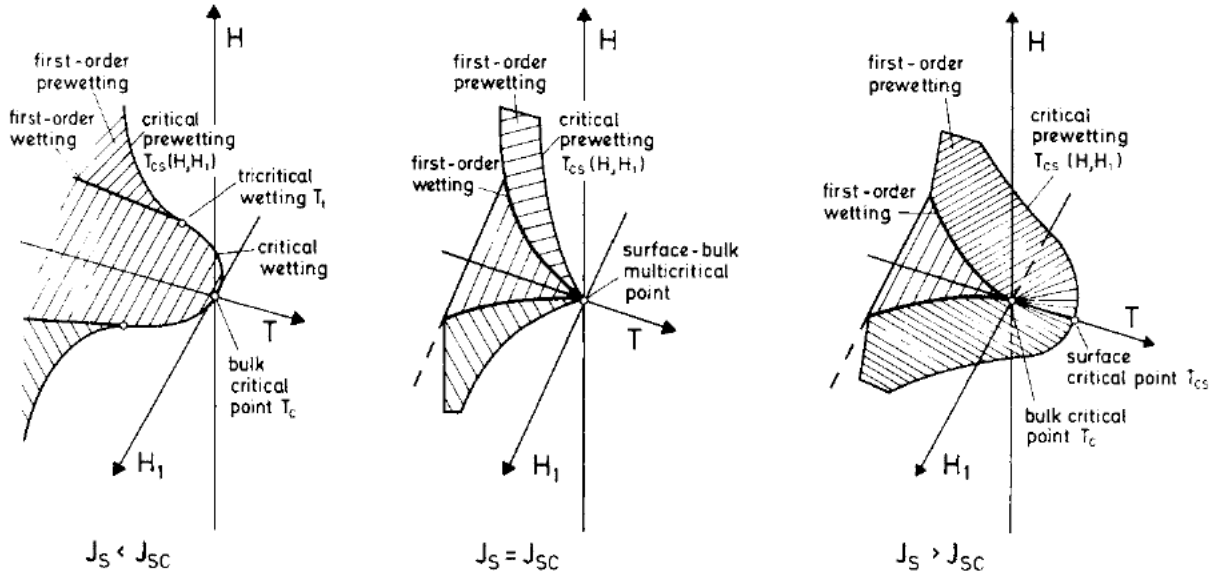

Figure 2.6: Schematic phase diagrams for a semi-infinite Ising magnet in the vicinity of the bulk critical point T_{cb} as a function of temperature T, bulk field H, and surface field H_1 . In the shaded part of the plane H=0 the system is non-wet for $T < T_c$, while outside of it, for $T < T_c$, it is wet. The wetting transition is shown by a thin line where it is second-order and by a thick line where it is first-order. First-order prewetting surfaces terminate in the plane $H = 0$ at the first-order wetting line. Critical and multicritical points are indicated in the figure. From ref. [6]

Here, the surface criticality is related to "prewetting" by Nakanishi and Fisher [6]. Prewetting is a wetting transition which occurs when there exists a nonzero bulk symmetry breaking field, $H \neq 0$. At the prewetting transition, the interface will jump from a position close to the surface to a more distant position, although it does not get completely delocalized. In addition, some corresponding singularities in other quantities also occur, i.e. surface excess energy (See Eqn. 2.17) or excess magnetization (See Eqn. 2.16). In the phase diagram shown in Fig. 2.5, the prewetting surface is bound by two lines: One line is at $H = 0$ and is a first-order wetting transition. The other line is composed of critical points which describe "critical prewetting". Along the line of critical prewetting, the singularities in the surface excess quantities will vanish and only two-dimensional critical fluctuations in the surface plane exist, as at the surface critical point mentioned above. For different enhancement of the surface layer coupling, the position of a tricritical wetting transition is located differently in the phase diagram, or may even disappear completely.

2.3 non-local correlation length - Resolution of a long standing puzzle?

It has been a long-standing puzzle within the renormalization group (RG) theory about the nature of fluctuation effects for critical wetting transitions in three-dimensional systems with short-ranged forces [58]. According to the renormalization group theory prediction made by Brezin, Halperin and Leibler [10] and later Fisher and Huse [13] based on isotropic continuum models, all the critical properties are strongly non-universal and depend on the dimensionless wetting parameter [11]

$$\omega = \frac{k_B T \kappa^2}{4\pi\Sigma} \tag{2.11}$$

where, Σ is the stiffness of the $\alpha\beta$ interface (or interface tension of the free interface) which continuously unbinds from an inert wall when approaching the wetting temperature T_W, and $\kappa = 1/\xi_\beta$ is the inverse correlation length of the bulk phase β. Non-universality predictions [10, 13] are made for the divergence of three characteristic length-scales: the equilibrium film

thickness, $\langle l \rangle$, the interfacial roughness, $\xi_\perp$ ($\propto \sqrt{D}$), and the parallel correlation length $\xi_\parallel$ ($\propto \sqrt{\frac{l}{k}}$, where $k = 1/\xi_{bulk}$, is the inverse bulk correlation length). Particularly, the exponent $\nu_\parallel$ describing the singularities occuring at critical wetting $\xi_\parallel \sim (T_W - T)^{-\nu_\parallel}$ deviates distinctly from its mean-field value, $\nu_\parallel^{MF} = 1$ [15, 6], and is highly dependent on the parameter ω. When $\omega > 2$, the correlation length $\xi_\parallel$ diverges exponentially quickly.

$$\nu_\parallel(\omega) = \begin{cases} (1-\omega)^{-1} & \text{for } 0 < \omega < 1/2 \\ \left(\sqrt{2} - \sqrt{\omega}\right)^{-2} & \text{for } 1/2 < \omega < 2 \\ \infty & \text{for } \omega > 2 \quad . \end{cases} \tag{2.12}$$

Critical wetting in $d = 3$ is very important for us to understand interfacial critical phenomena. The natural testing ground for these predictions is the wetting transition in the semi-infinite, simple cubic Ising model, above its roughening temperature (the temperature at which the layer-by-layer behavior occurs). It is known that the wetting parameter tends to a universal value $\omega \approx 0.8$ on approaching the bulk critical temperature T_c suggesting that $\nu_\parallel^{RG} \approx 3.7$, strikingly different from its mean-field value $\nu_\parallel = 1$. However, these predictions are not supported by extensive Monte Carlo simulation studies of wetting in the Ising model due to Binder, Landau and coworkers [21, 22, 23, 24]. They found out that the critical singularities at critical wetting are broadly consistent with simple mean-field behavior, and they did not observe the singularities predicted by various renormalization-group treatments.

In a series of articles in the early 1990s, this controversy was reconsidered by Fisher and Jin [38, 39, 40, 41, 42]. They suggested that the customary effective interface Hamiltonian (Landau-Ginzburg-Wilson Hamiltonian, or LGW model) must be modified in the presence of a wall or other externally imposed inhomogeneity, not only by including a direct wall-interface potential, but also by allowing for a spatially dependent interfacial stiffness (FJ model). They constructed this interfacial model perturbatively as a gradient expansion by considering small derivations from planar (constrained) profiles. They suggested that actually one should have a very weak first-order wetting transition in the Ising model, while Monte

Carlo simulations showed it is second order. Although it is possible that a very weak first-order transition in a simulation (as well as in experiments) is mistakenly identified as a second-order transition, there are no specific predictions of any quantities resulting from the work of Fisher and Jin that could provide a more critical test of what actually happens.

Parry, Boulter and coworkers [43, 44, 45, 46, 47] developed a slightly generalized model which allows for coupling between fluctuations in the order parameter near the interface and near the wall. They did a renormalization group analysis and pointed out that there is a second length scale in Monte Carlo simulation results as shown in Fig.2.7 . Although the results of their analysis are in excellent quantitative agreement with the Ising model simulation studies [21, 22, 23, 24], these methods show a stiffness-instability and therefore are flawed.

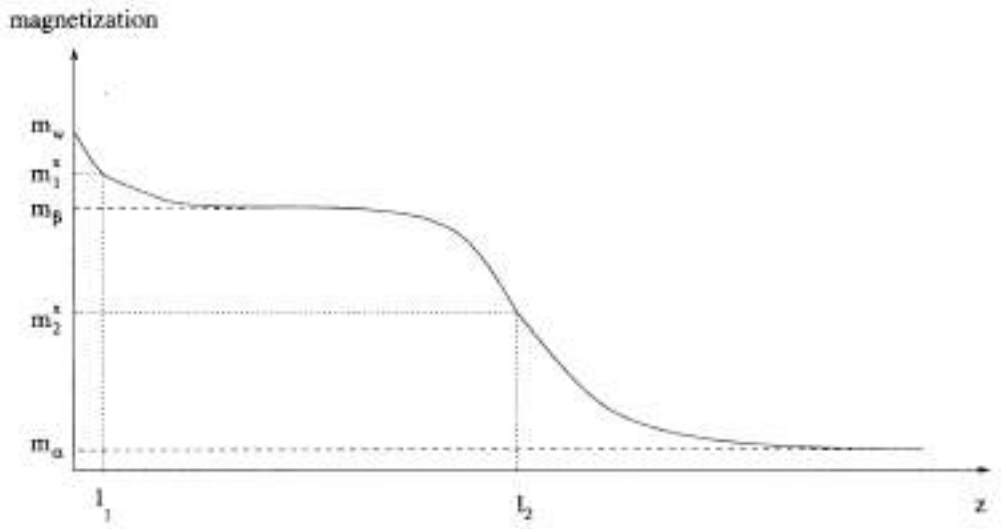

Figure 2.7: Schematic section of a typical magnetization profile near complete wetting (in a semi-infinite space $d > 0$ with the wall in the plane $z = 0$). The locations and fluctuations of inhomogeneities in the magnetization density near the wall-β and $\alpha\beta$ interfaces may be modeled by generalized collective coordinates l_1 and l_2 which denote surfaces of fixed magnetization m_2^X, m_1^X chosen such that $m_\beta > m_2^X > m_\alpha$ and $m_1 > m_1^X > m_\beta$. (From ref. [45])

In a recent series of papers, Parry and coworkers [48, 49, 60, 61, 62, 63, 64, 65] revisited these problems using a non-local (NL) interfacial Hamiltonian [66, 67]. The new ingredient in the NL model is the presence of long-ranged two-body interfacial interactions controlling the repulsion from the wall that were not modeled correctly in previous interfacial descriptions.

The analysis of the NL model shows that correlation functions are characterized by, not one, but two diverging parallel correlation lengths, parallel correlation length $\xi_{\|}$ and non-local correlation length $\xi_{NL} \propto \sqrt{ln\xi_{\|}}$.

We did Monte Carlo simulations to study the interface behavior of Ising model, calculated correlation functions and tested the presence of this second correlation length.

2.4 WETTING IN THE NEAREST-NEIGHBOR SIMPLE-CUBIC ISING LATTICE - PREVIOUS MONTE CARLO SIMULATIONS

It's well known that wetting phenomena for long-range forces should be very different from the short-range case; particularly, the interesting fluctuation effects predicted for critical wetting don't occur in the long-range forces case. According to the experiments on systems where long-range forces are negligible by Ross, Bonn and Meunier [92], the critical wetting is mean-field like. In order to get more understanding of the theory of wetting for the short-range case is an important theoretical challenge, Monte Carlo computer experiments provide a reasonable way to test the theories. Binder, Landau and coworkers did an extensive work studying wetting phenomena in the nearest-neighbor simple-cubic Ising lattice by Monte Carlo simulations in the 1990s and early 2000s [21, 22, 23, 24]. They considered a simple-cubic Ising $L \times L \times D$ system, with two free surface $L \times L$ layers, and periodic boundary conditions in the two remaining directions. The exchange constant in the two free surface layers is J_s, while J in other layers. The Hamiltonian can be expressed as follows

$$\mathcal{H} = -J \sum_{bulk} \sigma_i \sigma_j - J_s \sum_{surfaces} \sigma_i \sigma_k - H \sum_{bulk} \sigma_i - H_1 \sum_{surfaces} \sigma_k \tag{2.13}$$

where $\sigma_i = \pm 1$ represents the up-pointing or down-pointing spins, and a bulk field H and surface field H_1 are included. As is known, the three-dimensional Ising model orders ferromagnetically at $J/k_B T_c \approx 0.2217$ [68]. Monte Carlo runs were performed for different values of $J/k_B T$. The ratio J_s/J was varied over a wide range to locate the tricritical wetting transition. The thickness of the system $D = 40$ is rather large in comparison with the bulk

correlation length ξ_b, which is less than two lattice spacings for all temperatures deep in the non-wet phase. So, the two free surfaces are far enough from each other and the system can be taken as if it were semi-infinite. Among the quantities recorded, they concentrate on the profiles of magnetization m_n and energy U_n (n is from 1 to D, representing the layer index). Besides, they also record the bulk magnetization m_b and energy U_b which are defined as

$$m_b \equiv \frac{1}{20} \sum_{n=11}^{30} m_n \tag{2.14}$$

$$U_b \equiv \frac{1}{20} \sum_{n=11}^{30} U_n \tag{2.15}$$

They also obtained the surface excess magnetization m_s, and surface excess energy U_s as follows:

$$2m_s = \sum_{n=1}^{D} (m_b - m_n) \tag{2.16}$$

$$2U_s = \sum_{n=1}^{D} (U_b - U_n) \tag{2.17}$$

where the factor 2 is simply due to the fact that there are two free surfaces. They also use fluctuation relations to calculate the susceptibilities χ_{11} and χ_1. They are defined as follows:

$$\chi_{11} = \frac{\partial m_1}{\partial H_1} \tag{2.18}$$

$$\chi_1 = \frac{\partial m_1}{\partial H} \quad , \tag{2.19}$$

and they are calculated using the fluctuation relations as follows:

$$k_B T \chi_{11} = L^2 \left[\langle \left[\frac{1}{2L^2} \sum_{surfaces} \sigma_k \right]^2 \rangle - m_1^2 \right] \tag{2.20}$$

$$k_B T \chi_1 = L^2 D \left[\langle \frac{1}{2L^2} \sum_{surfaces} \sigma_k \frac{1}{L^2 D} \sum_i \sigma_i \rangle - m_1^2 \right] \quad . \tag{2.21}$$

Fig.2.8 is a typical description of the wetting phenomena for $J_s/J = 0.5$ and $J/k_B T = 0.25$, which is deep in the critical wetting regime. It shows the profiles of magnetization and energy across the film, for a field in the nonwet region ($H_1/J = -1.2$) close to the wetting transition

which occurs roughly at $H_{1c}/J = -1.3$, and two fields ($H_1/J = -1.4$ and $H_1/J = -1.5$) in the wet regime. In the nonwet case ($H_1/J = -1.2$) the magnetization increases until it reaches the bulk magnetization value in the center of the film, and the surface energy U_n is largest close the surface and then decreases monotonically to the bulk values in the center of the film. However, in the wet cases ($H_1/J = -1.4$ and $H_1/J = -1.65$), the magnetization profile in the first few layers is rather flat. The energy profile is also rather flat in the first few layers, and then increases to a maximum value at a layer number which represents the average interface position. This average interface position coincides very well with the inflection point of the magnetization profile. This behavior indicate that the interfaces have depinned from the surface. Take the left-hand side of the profiles for $H_1/J = -1.65$ as an example. The local energy U_n for $n = 2, 3, 4$ nearly coincides with the energy in the bulk, and the magnetization m_n for 2,3,4 nearly coincides with the negative value of the spontaneous magnetization. This is the demonstration of the microscopic significance of "wetting phenomena" in this nearest-neighbor simple-cubic Ising lattice model. Not only critical wetting, but also tricritical and first-order wetting transitions in this model were studied. The qualitative structure of the global surface phase diagram by Fisher and Nakanishi [6] was confirmed by the simulations. And as mentioned in previous section, a quantitative test was attemped with resppect to the NG predictions for singularities at critical wetting, however, these predictions could not be verified, but rather a simple mean-field critical behavior was confirmed.

2.5 Thin Ising films with competing walls

In recent years thin films have attacted enormous attention and extensive research because of their growing technological importance for technical applications as well as for their theoretical scientific interest. It is well known that in confined systems, phase equilibria and critical phenomena may be significantly different from their counterparts in systems that are infinitely extended in all of their dimensions. A fluid between parallel surfaces, or walls, is

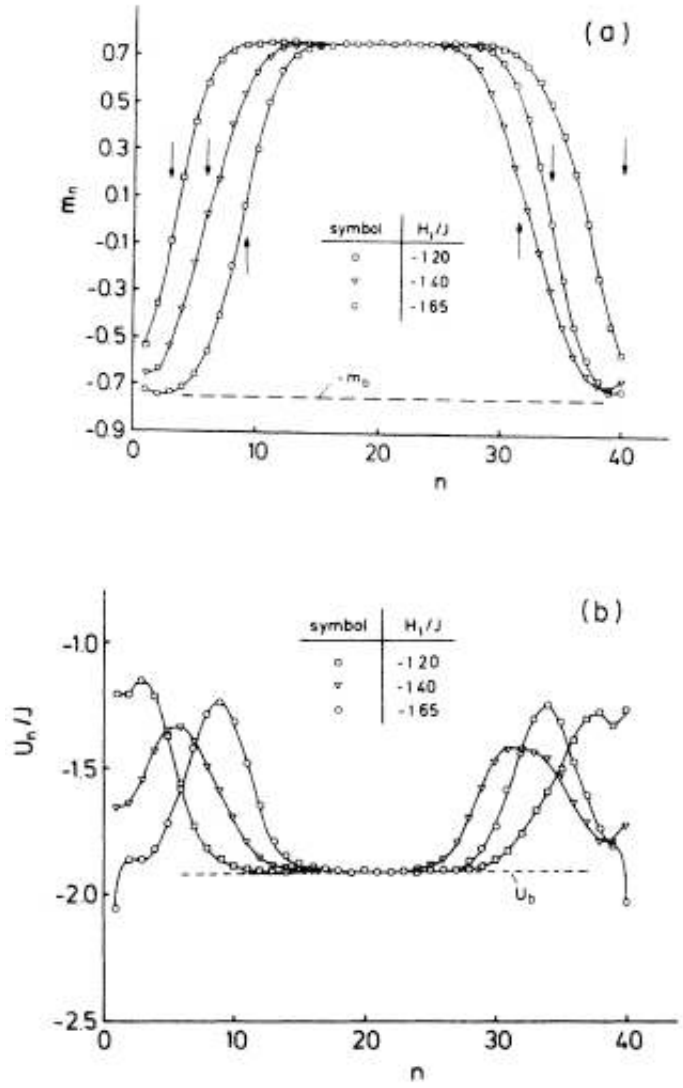

Figure 2.8: (a) Profile of the layer magnetization m_n, and (b) layer energy U_n across the film, for a $30 \times 30 \times 40$ lattice with $J_s/J = \frac{1}{2}$, $J/k_BT = 0.25$, and three choices of the surface field. The index n labels the layers. The arrows in part (a) show the positions where U_n has maxima, the straight line indicates the value of $-m_b$, the negative value of the bulk magnetization. From ref. [13]

a familiar example. In this system, capillary condensation occurs at a slightly lower pressure than the normal saturated vapor pressure. The bulk liquid-vapour critical point also undergoes a shift [50, 27, 59]. Parry and Evans [51] (and, independently, Albano et al. [28]) drew attention to Ising models with competing walls (refer to Eqn.2.15): In magnetic terminology (the Ising model), one surface exhibits a positive surface field, and the other surface exhibits a negative one; in the lattice gas model, one wall favors a liquid phase while the other wall favors a gas phase. It is physically very natural that the two surfaces of a thin film are different. Binder, Landau and Ferrenberg [36] focused on the statistical mechanics of phase transitions in a thin film geometry, studying the interplay between confinement and competing wall forces using Monte Carlo simulation. They studied the Ising Hamiltonian on the simple cubic lattice in a $L \times L \times D$ geometry, applying periodic boundary conditions in the x and y directions. At the two free $L \times L$ surfaces at layer numbers $n = 1$ and $n = D$, fields H_1 and H_D are applied:

$$\mathcal{H} = -J \sum_{nn} \sigma_i \sigma_j - H \sum_{i} \sigma_i - H_1 \sum_{i \in surface1} \sigma_i - H_D \sum_{i \in surfaceD} \sigma_i \tag{2.22}$$

In this work, $\sigma_i = \pm 1$, the bulk field is confined to $H = 0$, and the surface fields $H_1/J = -H_D/J = -0.55$, for which the wetting temperature has already been located, $k_B T_W/J \approx 4.00$ [69]. T_W lies sufficiently below T_{cb} ($k_B T_{cb}/J \approx 4.51142 \pm 0.00005$) [70]. The competing surface fields lead to a rather unusual behavior described in Fig. 2.9, which shows the profiles of the layer magnetization m_n, the layer internal energy U_n, and the layer susceptibility $\chi_{nn} = \partial m_n / \partial H_n$ for a variety of temperatures. One sees that above the transition when the mean interface position is in the center of the film, the overall magnetization is zero. At a temperature $T_c(D) < T_{cb}$ the interface gets bound to one of the walls and an interface localization transition takes place. When the temperature is below $T_c(D)$, The simulation results also show that the transition is shifted below the wetting transition temperature in a semi-infinite system and belongs to the universality class of the two dimensional Ising model.

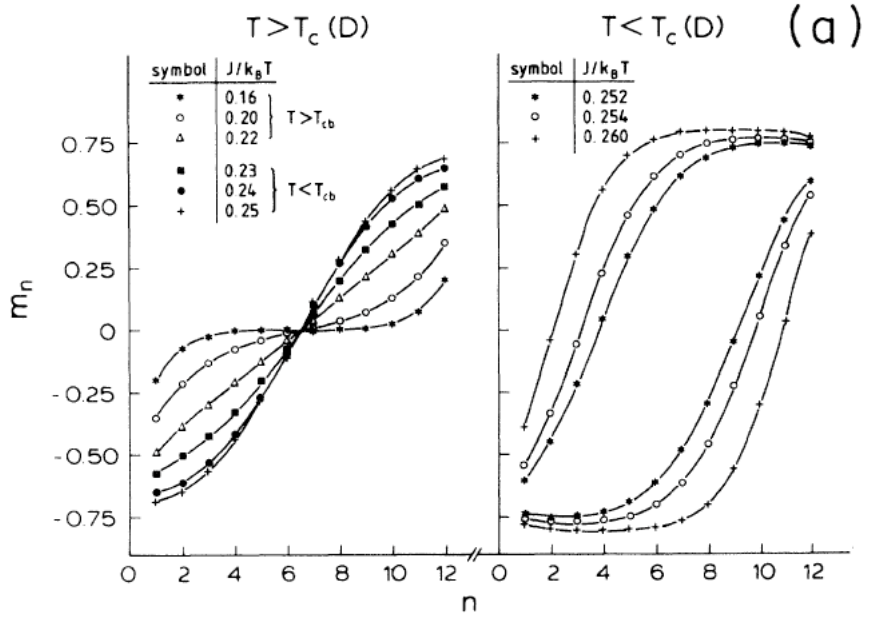

Figure 2.9: Profiles of the layer magnetization $m_n(a)$, the normalized layer energies $U_n/J(b)$, and the layer susceptibilities $\chi_{nn}J(c)$ vs layer number n, for a thin film of thickness $D = 12$. The left-hand part of each panel shows data for temperatures T above the thin film critical temperature $T_c(D)$, while the right-hand part shows data for three temperatures below $T_c(D)$. (From ref. [36])

2.6 Effect of gravity on phase equilibria

A gravitational field is present in most experimental environments. In a gravitational field, phase equilibria in fluids undergo seemingly small but important modifications. Let's first look at the effect of gravity in systems which are infinite in all their dimensions. Consider a grand canonical ensemble, and let z represent the vertical coordinate which is parallel to the gravitational field. At liquid-vapor phase coexistence, a fluid shows a horizontal interface (assume to be at $z = 0$). Around the interface, the chemical potential $\mu_{hom}(\rho(z))$ of a homogeneous reference system with a uniform density equal to the actual local density $\rho(z)$, takes the value μ_{co} which is corresponding to two-phase coexistence in bulk. However, the liquid at a depth $-z$ below and the vapor at a height z above this interface are characterized

to a first approximation by $\mu_{hom}(\rho(z)) - \mu_{co} = -gz$, where g is the gravitational acceleration. The fluid is in an inhomogeneous state and a small variation of the chemical potential will induce a finite vertical interface displacement, for finite g. In an infinite system, a very sharp first-order liquid-vapor phase transition occurs only when gravity is zero. And the bulk critical phenomenon is also attenuated by gravity. According to Van Leeuwen and Sengers [71], the bulk correlation length ξ becomes anisotropic and remains finite, not only in the gravitational field direction, but also in the $d-1$ perpendicular directions.

Now let's look at the effect of gravity in confined systems. Rogiers and Indekeu [54] studied a fluid or Ising lattice gas confined between two horizontal walls with separation L in a gravitational field of strength g using a mean field approach. They found that the $(d-1)$-dimensional phase equilibria and critical phenomena are not necessarily attenuated by gravity, but may extend into the space of non-zero g. For identical walls (surface fields $H_1 = H_L$) the familiar capillary condensation and capillary criticality extend to non-zero g. The case with opposing walls case ($H_1 = -H_L$) has drawn more interest in recent years [28, 30, 53, 51, 72, 73]. Brochard and de Gennes [53] argued that the bulk critical temperature shifts, or rather leaps, from $T_c(\infty)$ to $T_c(L) \approx T_W$, the wetting temperature of the semi-infinite system (with only a single wall surface field H_1) in this type of confinement. Parry and Evans [51, 52, 72] also uncovered this using detailed mean-field theory and scaling arguments. Swift *et al.* [30] and Indekeu *et al.* [73] interpreted this as the shift of the wetting temperature, and proposed that the question of the bulk critical point shift remains open. Rogiers and Indekeu [54] believed that a crucial step towards the solution of the controversy is made by extending the space of thermodynamic fields to include what is already naturally present in numerous physical systems: gravity. They found that the interface imposed by the opposing walls above T_W can be counteracted by a weak linearly varying field with a gradient $g > 0 (< 0)$ for $H_1 = -H_L > 0$ (< 0) and the bulk two-phase coexistence can be restored. The field gradient can compete with opposite surface fields when the signs are chosen properly. For example, for a fluid in the earth's gravity field, we need to choose a

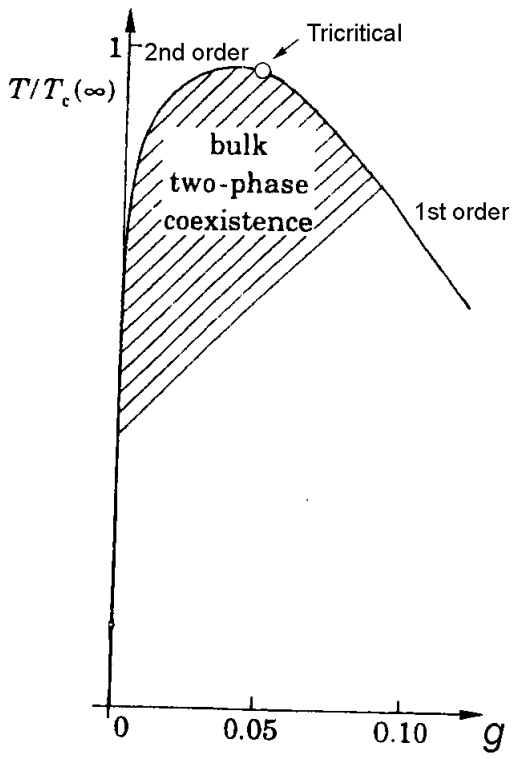

Figure 2.10: Phase equilibria between opposing walls ($H_1 = -H_L$), calculated in the Landau theory for a slab of thickness $L/c^{1/2} = 10$(where $c/2$ is the coefficient of the gradient squared contribution to the free energy [30]). From Ref. [46]

bottom surface which prefers the vapor, and a top surface which prefers the liquid. Their claim is supported by mean-field and continuum Landau Theory calculations [30, 51, 72, 73]. The above Fig. 2.10 is the typical phase diagram they obtained.

Carlon and Drzewiński [55] also investigated the effect of gravity and confinement on phase equilibria by a density matrix renormalization approach. They cosidered the following Hamiltonian:

$$\mathcal{H} = -J\sum_{nn}\sigma_i\sigma_j - H\sum_i \sigma_i - H_1 \sum_{i\in surface1} \sigma_i - H_D \sum_{i\in surfaceD} \sigma_i + g\sum_{i=1}^{D}(2i-1-D)\sum_j \sigma_i \quad (2.23)$$

where the parameter g is the equivalent of the gravitational gradient. Carlon and Drzewiński studied the phase diagram of the model described by the above Hamiltonian for an $D \times \infty$

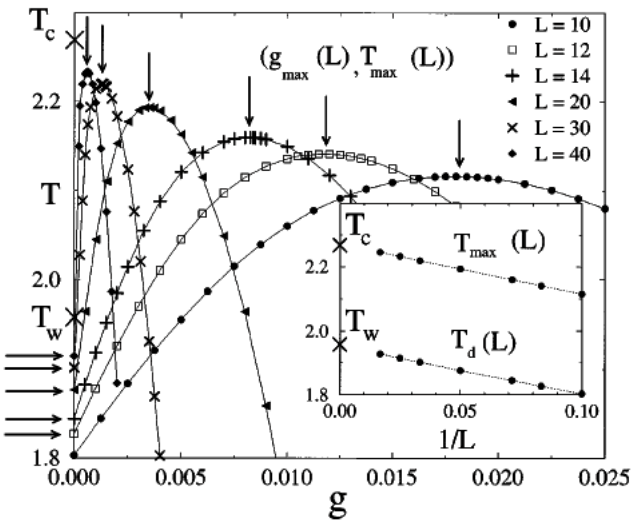

Figure 2.11: Phase diagram of the model for different strip widths in the (g, T) plane for $H_1 = 0.5$ and $J = 1$; the area below the curves is the two phase coexistence region. Inset: Scaling of $T_{max}(L)$ and $T_d(L)$ vs $1/L$.From Ref. [52]

strip, beyond the mean field approximation. They tested the validity of the conclusions of Rogiers and Indekeu [54] at the lower critical dimension ($d = 2$) and clarified the mechanism of the critical point shift for a system confined between opposing walls. According to their study, gravity restores two phase coexistence up to the bulk critical point, in agreement with mean field calculations. Fig. 2.10 and Fig. 2.11 show the phase diagram of the model for different strip widths in the (g, T) plane and magnetization profiles.

We used Monte Carlo simulation to study the effect of a linearly changing magnetic field on an Ising film confined between two opposing walls, and got a phase diagram which is qualitatively in agreement with the theoretical predictions.

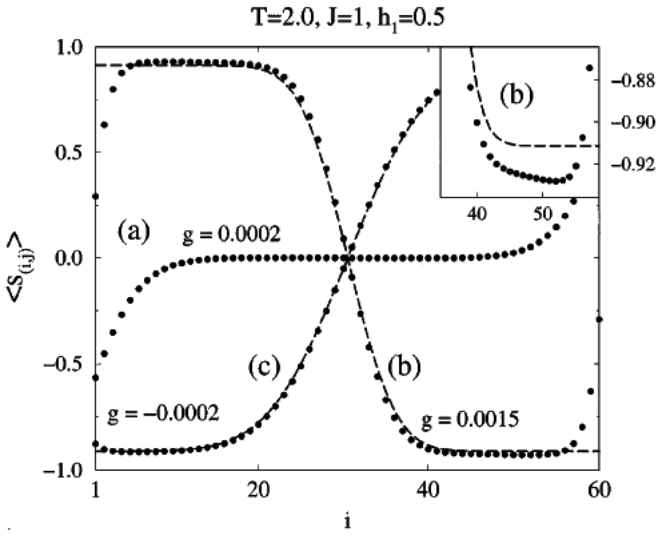

Figure 2.12: (Circles)Magnetization profiles in the two phase coexistence region (a) and in the single phase region [(b) and (c)] calculated by DMRG (Density matrix renormalization). (Dashed lines) Profiles calculated with a SOS approximation [56]. Inset: Details of the profile (b) far from the interfacial region. From Ref. [52]

Chapter 3

Model and Methods

3.1 Ising thin films model

We studied the simple cubic Ising model with the same Hamiltonian that Rogiers *et al.* [54] and Carlon *et al.* [55] used (see Eqn.2.25). The Hamiltonian is put down here again in Eqn. 3.1. As illustrated in Fig. 3.1, the model is an Ising film on the simple cubic lattice in a $L \times L \times D$ geometry. Periodic boundary conditions are applied in the x, and y, direction to better approximate the limit $L \to \infty$, while free boundary condition is imposed in the z direction. The thickness of the film is D, which means the number of spin layers is D.

$$\mathcal{H} = -J_{nn} \sum_{nn} \sigma_i \sigma_j - H \sum_i \sigma_i - H_1 \sum_{i \in surface1} \sigma_i - H_D \sum_{i \in surfaceD} \sigma_i + g \sum_{i=1}^{D} (2i - 1 - D) \sum_j \sigma_i, \quad \sigma_i = \pm 1 \tag{3.1}$$

where σ_i represents the up-pointing or down-pointing spins, which interact with nearest neighbors on the lattice with interaction constant $J_{nn} > 0$. The summation in the first term is over all distinct pairs of nearest-neighbor spins. In this work, we confine ourselves to zero uniform bulk field in the second term. At the two free $L \times L$ surfaces at layer numbers $n = 1$ and $n = D$, competing surface fields H_1 and H_D are applied: $H_1 = -H_D$. We restricted the value of H_1 to $-0.55J$, for which Binder, Landau and Ferrenberg [36] have done extensive Monte Carlo simulation in Ising films without gravity. The last term is the linearly changing layer field corresponding to the introduction of gravity into the lattice-gas model.

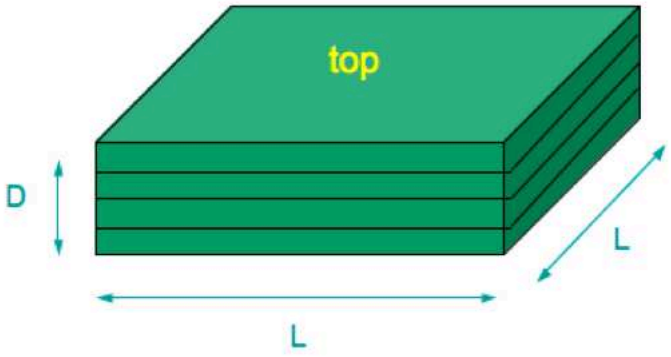

Figure 3.1: An illustration of the thin Ising film model, an $L \times L \times D$ symmetry. Periodic boundary conditions are applied along the both directions with size L. Free boundary conditions are applied in the other direction. D is the number of layers.

3.2 Monte Carlo Simulation

The Monte Carlo method was named after Monte Carlo, Monaco, where the primary attractions are casinos containing games of chance. In the 1940s, Fermi, Ulam, von Neumann, Metropolis and others [74] started developing a modern Monte Carlo simulation method, a stochastic sampling technique where random numbers are generated to mimic the fluctuations that occur in physics. Due to its advantage of simplicity and power, the Monte Carlo methods can be applied to a broad spectrum of interesting problems. Usually, Monte Carlo methods can be divided into two classes: simple Monte Carlo methods and importance sampling Monte Carlo methods. The difference between them is that the former is dealing with variables that are uniformly distributed over the integration region, while the latter is

choosing a good distribution from which to simulate one's random variables. Simple Monte Carlo methods can be used to evaluate definite integrals that are intractable by analytic techniques, and in statistical physics, can be applied to various problems like fluid flow or percolation. However, to study phase transitions at finite temperature, one needs to use importance sampling Monte Carlo methods, among which the most popular and straightforward way is the Metropolis sampling method.

In the simulation, the Metropolis importance sampling method is used to generate configurations from a previous state with a transition probabiliy which depends on the energy difference between the initial and final states. The time dependent behavior is described as follows

$$\partial P_n(t)/\partial t = -\sum_{n\neq m}[P_n(t)W_{n\to m} - P_m(t)W_{m\to n}] \tag{3.2}$$

where $P_n(t)$ is the probability of the system being in state n, and $W_{n\to m}$ is the transition rate for $n \to m$. In equilibrium $\partial P_n(t)/\partial t = 0$, so the transition probability has to satisfy detailed balance

$$P_n(t)W_{n\to m} = P_m(t)W_{m\to n} \tag{3.3}$$

In a classical system that follows the Boltzmann distribution, $P_n(t)$ is given by

$$P_n(t) = exp(-E_n/k_BT)/Z \tag{3.4}$$

where Z is the partition function. So we have

$$\frac{W_{n\to m}}{W_{m\to n}} = \frac{P_m(t)}{P_n(t)} = exp(-\Delta E/k_BT) \tag{3.5}$$

where $\Delta E = E_m - E_n$. Any transition rate which satisfies detailed balance is acceptable. The first choice of rate that was used in statistical physics is the Metropolis form [75]

$$\begin{aligned} W_{n\to m} &= exp(-\Delta E/k_BT), \qquad if \Delta E > 0 \\ &= 1, \qquad\qquad\quad if \Delta E < 0 \end{aligned} \tag{3.6}$$

where the time unit is set to unity and suppressed in the equations. The recipe for the Metropolis algorithm follows.

1. Choose an initial state
2. Choose a site i in order
3. Calculate the energy change ΔE which results if the spin at site i is overturned
4. Generate a uniform random number r in the interval [0,1]
5. If $r < exp(-\Delta E/k_B T)$, flip the spin
6. Go to 2

The 'standard' measure of Monte Carlo time is the Monte Carlo step/site (MCS/site) which corresponds to the consideration of every spin in the system once. After a sufficiently long run, this algorithm generates a series of states that follow the Boltzmann distribution, i.e., the occurrences of a state are proportional to Eqn. 3.4. And then, the desired average $\langle A \rangle = \sum_n P_n A_n$ of a variable A simply becomes the average over the entire sample of states which is kept.

Besides the Metropolis algorithm, we also consider the heatbath method [93] which was first suggested for application to lattice gauge theories. It corresponds to touching each spin in turn (selected either in order or randomly) to a 'heat bath' [77]. The difference between the heatbath method and Metropolis algorithm is that for the latter, one allows the change in energy to determine the 'new' spin configuration, while for the former, one can simply randomly select a new spin direction and then compare a random number rn with the Boltzmann probability of the trial configuration, i.e. accept the new configuration if $rn < exp(-E'/k_B T)$ where E' is the energy of the trial state. It is most useful in circumstances where the Metropolis-like approach has a very low acceptance rate. When the heatbath method is applied in an Ising model, the spin may be set equal to +1 with probability p_i and equal to -1 with probability $1 - p_i$ where

$$p_i = \frac{e^{2\beta \sum_{nn} \sigma_j}}{1 + e^{2\beta \sum_{nn} \sigma_j}} \tag{3.7}$$

This may be easily implemented by generating a random number rn and setting

$$\sigma_i' = sign(p_i - rn) \tag{3.8}$$

We applied the heatbath method, and simulated lattice sizes of $L = 128$ and occasionally 16, 32, 64, 256. We also did preferential layer selection which means we sampled 10 times more frequently in surface layers than the bulk layers since in the surface layers, the correlation times are longer than the bulk layers due to the surface fields. For $L = 128$, the correlation times of the averaged magnetization are less than 10 Monte Carlo steps. The random number generator R250 was used. Multiple independent runs were performed to estimate the statistical errors.

3.3 Finite size effects and determination of critical temperatures

In interpreting simulational data, one often encounters a fundamental difficulty: the equilibrium, thermodynamic behavior of a finite system is smooth as it passes through a phase transiton for both first order and second order transitions. So it is important for one to be able to distinguish the order of the transition. And for a second order phase transition, locating the critical temperature T_c is also a topic in which we are most interested.

3.3.1 Finite size effects

Computer simulations can only handle finite size systems, however, often properties of infinite systems are of interest to us. Fortunately, we can extract such properties from the results obtained on finite systems. According to Fisher's finite-size scaling theory [90], the critical behavior of a system at a second order phase change in the thermodynamic limit can be extracted from the size dependence of the singular part of the free energy which has such a scaling form

$$F(L,T) = L^{-(2-\alpha)/\nu}\mathcal{F}(\epsilon L^{1/\nu}) \tag{3.9}$$

where $\epsilon = (T - T_c)/T_c$ and $\mathcal{F}$ is a scaling function. The thermodynamic quantities (Magnetization M, Specific heat C, and Susceptibility χ) can be derived by appropriately differentiating the free energy scaling

$$M = L^{-\beta/\nu}\mathcal{M}^o(\epsilon L^{1/\nu}) \tag{3.10}$$

$$\chi = L^{\gamma/\nu}\chi^o(\epsilon L^{1/\nu}) \tag{3.11}$$

$$C = L^{\alpha/\nu}\mathcal{C}^o(\epsilon L^{1/\nu}) \tag{3.12}$$

where $\mathcal{M}^o$, χ^o and $\mathcal{C}^o$ are scaling functions. At T_c, $\epsilon = 0$, we have

$$M \sim L^{-\beta/\nu} \tag{3.13}$$

$$\chi \sim L^{\gamma/\nu} \tag{3.14}$$

$$C \sim L^{\alpha/\nu} \tag{3.15}$$

and critical exponent ratios can be determined from power law fits to these quantities as a function of size L.

3.3.2 Binder Cumulant Crossing

The above quantities are basically just first or second order moments of the probability distribution of order parameter or energy. If we examine higher order moments of the finite size lattice probability distribution, we may obtain important, additional information. We can do this effectively by considering the Binder cumulant, i.e. the fourth order cumulant of the order parameter introduced by Binder [78]. For an Ising model in zero field, the fourth order cumulant simplifies to the following format due to the fact that all odd moments disappear by symmetry:

$$U_4 = 1 - \frac{\langle m^4 \rangle}{3\langle m^2 \rangle^2} \quad . \tag{3.16}$$

As the system size $L \to \infty$, U_4 has the following behavior:

$$U_4 = \begin{cases} 2/3 & T < T_c \\ 0 & T > T_c. \end{cases} \tag{3.17}$$

When the lattice size is large enough, curves for U_4 as a function of temperature cross at a fixed point value U_4^* and the location of the crossing point is the location of the critical point. For different universality classes, the value of U_4^* should be different. For example, for the two-dimensonal Ising model, the U_4^* value is found out to be 0.615 [79], while it is found to

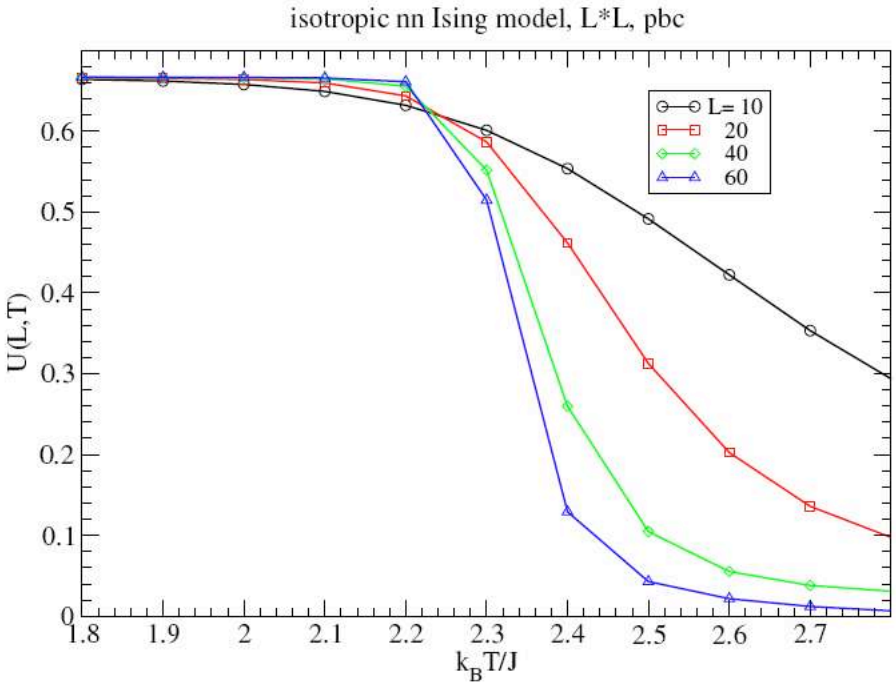

Figure 3.2: Temperature dependence of the fourth order cumulant of magnetization for $L \times L$ Ising square lattices with periodic boundary conditions. From Ref. [80]

be 0.624 in the three-dimensional model [76]. So, making such plots for different size lattices provides an efficient way for us to make a preliminary identification of the universality class from the value of U_4^* and obtain an estimate for T_c from the location of the crossing point. However, if the sizes used are too small, the curves will not have a common intersection. Instead, there should then be a systematic crossing behavior with increasing lattice size.

Fig. 3.2 shows an example of crossing behavior with a common intersection on a coarse scale.

3.4 First Free Energy Integration

As is well known, the partition function, is an important quantity that encodes the statistical properties of a system in thermodynamic equilibrium. The general form for the partition

function for a classical system is

$$Z = \sum_{all\ states} e^{-\mathcal{H}/k_B T} \tag{3.18}$$

where $\mathcal{H}$ is the Hamiltonian for the system, T is the temperature, k_B is the Boltzmann constant, and the sum is over all possible states of the system. The free energy of a system can be determined from the partition function [81] from

$$F = -k_B T ln Z \tag{3.19}$$

and all other thermodynamic quantities can be calculated by appropriate differentiation of Eqn. 3.18. This relation connects statistical mechanics and thermodynamics. The internal energy of a system can be obtained from the free energy via

$$U = -T^2 \partial(F/T)/\partial T \tag{3.20}$$

Another important quantity, the entropy, which measures the amount of disorder in the system, is defined in statistical mechanics by

$$S = -k_B ln P \tag{3.21}$$

where P is the probability of occurrence of a state. The entropy can be determined from the free energy from

$$S = -(\partial F/\partial T)_{V,N} \quad . \tag{3.22}$$

There is also the following relationship between the free energy and the internal energy

$$F = U - TS \tag{3.23}$$

The free energy is important due to the fact that it is a minimum in equilibrium when T and V are held constant. What is more interesting about this quantity is that the difference in free energy between any two states does not depend on the path between the states. As illustrated in Fig. 3.5, when we consider two points in the pressure-temperature $p-T$ plane,

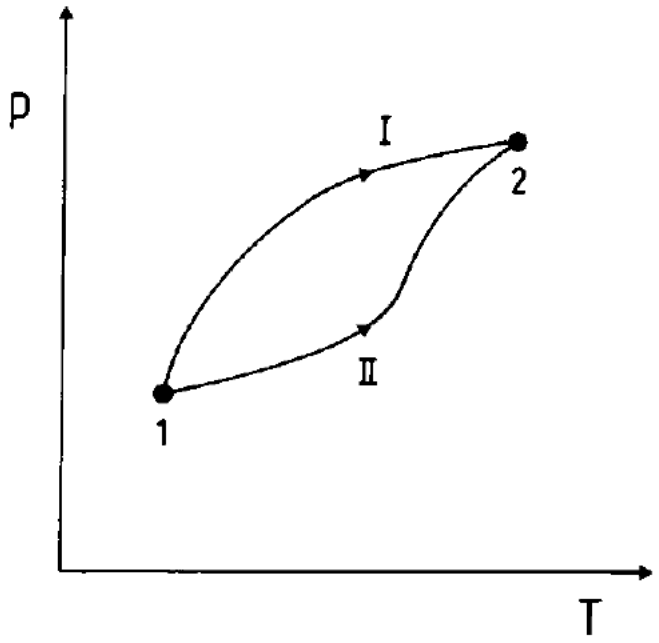

Figure 3.3: Schematic view of different paths between two different points in thermodynamic $p-T$ space. From Ref. [57]

two different paths which connect points 1 and 2 are shown. The difference in free energy between these two points is identical for both paths, i.e.

$$F_2 - F_1 = \int_{path\ I} dF = \int_{path\ II} dF \tag{3.24}$$

Similarly, in a magnetic system like Ising model, when we consider two points in the field-temperature $H - T$ plane, the difference in free energy between these two points is also identical for any two paths connecting these two points.

In some circumstances, knowledge of the free energy itself, and not just its derivatives, is important. For example, for a strongly first order phase transition, we can use the method of free energy integration to determine the location of the transition. In an Ising model, when the temperature is varying, we could estimate the free energy along two different directions

by doing the following integrations: (1) from low T to high T,

$$F(T) = U(T) - T\int_0^T \frac{C(T')}{T'}dT' \tag{3.25}$$

(2) from high T to low T

$$\frac{F(T)}{k_BT} = \frac{S(\infty, H)}{k_B} + \int_0^{1/k_BT} Ud(1/k_BT) \tag{3.26}$$

The intersection of three pairs of two free energy branches can be used to determine the location of the phase transition (see Fig. 3.4 (a)). In cases where the transition is caused by varying an applied field or chemical potential, we need to do the thermodynamic integration in two steps as illustrated in Fig. 3.3(b): integrating to the desired temperature first, and then sweeping the field across the transition while fixing the temperature:

$$F(H) = F(H_1, T) + \int_{H_1}^{H} MdH' \tag{3.27}$$

$$F(H) = F(H_2, T) + \int_{H_2}^{H} MdH' \tag{3.28}$$

and again in these cases the point of intersection can be used to locate the transition.

3.5 Probability Distribution of the Order Parameter

The order parameter distribution function has been proved to be a powerful tool for studying not only magnetic systems [78, 82, 84, 85, 86], but also the liquid-gas critical point [87], the critical point in the unified theory of weak and electromagnetic interactions [88], and the critical point in quantum chromodynamics [89]. For the specific case of magnetic systems the order parameter can be chosen as the magnetization per spin, namely $M = \frac{1}{N}\sum_{i=1}^{N}\sigma_i$, where N is the total number of spins and σ_i is the spin at site i. In finite-size systems, the magnetization M is a fluctuating quantity, which is characterized by the probability distribution $P(M)$ [78, 82]. In Ising-like models undergoing a second-order phase transition, it is well known that at temperatures lower than the critical temperature T_c, the distribution $P(M)$ has a double peak, centered at the spontaneous magnetizations $+M_0$ and $-M_0$. At

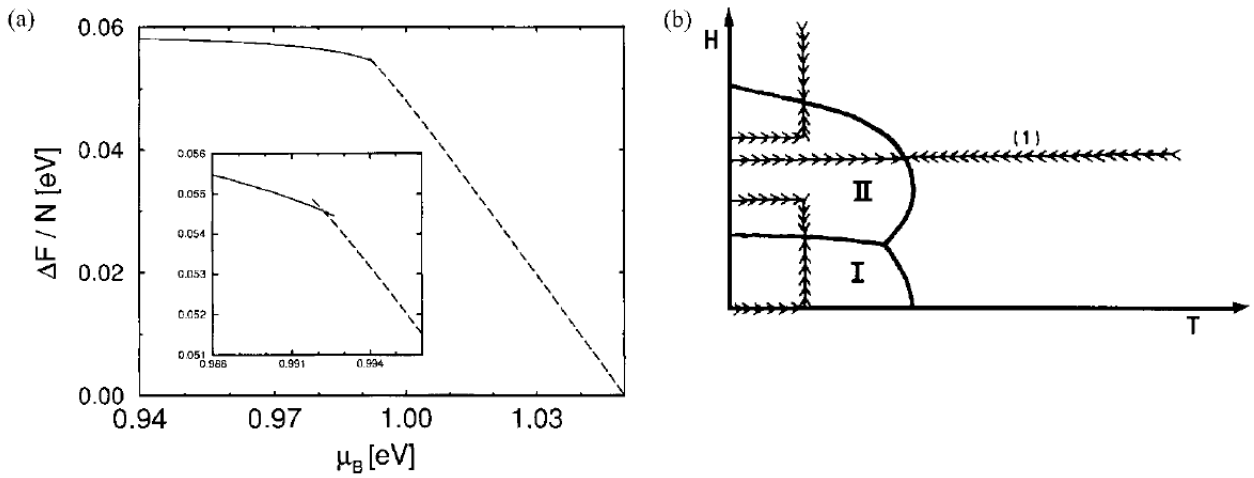

Figure 3.4: (a) Comparison of free energies obtained with the chemical potential swept in opposite directions for the model of Si/Ge. (b) Schematic view of paths for free energy integration. There are three first order phase boundaries separating a high temperature disordered phase, and two low temperature ordered phases. From Ref. [57]

temperatures above T_c, $P(M)$ has a single peak at zero magnetization, and exactly at T_c a double-peak shape is observed [78].

Analogously to the usual finite-size scaling assumptions [90], one expects that , for a large finite system of linear dimension L at the critical point, $P(M)$ takes the form

$$P(M) = bP^*(\tilde{M}) \tag{3.29}$$

where $b = b_0 L^{\beta/\nu}$, β and ν are critical exponents, $\tilde{M} = bM$, b_0 is a constant, and $P^*(M)$ is a universal scaling function, normalized to unit norm and unit variance. Scaling functions, such as P^*, are characteristic of the corresponding universality class, i.e. systems belonging to the same universality class share the same scaling functions. Thus, from the precise knowledge of $P^*(M)$ one can characterize critical points and also identify universality classes.

In Monte Carlo simulations, the probability distribution $P(M)$ corresponds to the fraction of the total number of realizations in which system magnetization is M, i.e.,

$$P(M) = \frac{\mathcal{N}_M}{\mathcal{N}_{MCS}} \tag{3.30}$$

where $\mathcal{N}_M$ is the number of times that magnetization M appears and $\mathcal{N}_{MCS}$ is the total number of Monte Carlo steps. To compute the normalized distribution $P^*(M)$, the pre-factor b has to be evaluated first. This can be done by noting that $b = 1/\sigma$, where σ is the square root of the magnetization variance ($\sigma^2 = \langle M^2 \rangle - \langle M \rangle^2$). So the universal function $P^*(M)$ is obtained by simply rescaling the magnetiztion and by using Eqn. 3.29.

3.6 Histogram Reweighting Methods

The Monte Carlo method had suffered from, the huge amount of computer resources required for thorough and accurate results for multiple data points until the introduction of the histogram reweighting method by Ferrenberg and Swendsen [91]. This method increases the amount of information obtained from a single simulation, rather than just taking the averages and standard deviations of thermodyamic quantities. This method is based on the realization that the properties of the systems will be determined by a distribution function in an appropriate ensemble.

The Hamiltonian for an Ising model is given in Eqn. 2.1. We can also write it in the following way

$$-\beta\mathcal{H} = -J_{\text{nn}} \sum_{nn} \sigma_i \sigma_j - H \sum_i \sigma_i = KS + hM \tag{3.31}$$

where K is the dimensionless coupling constant (J/k_BT) and h is an applied magnetic field (H/kT), i.e. this h includes J/k_BT. The probability distribution of S and M at a point in the parameter space (K, H) is given by

$$P_{(K,h)}(S, M) = \frac{1}{Z(K, h)} \mathcal{N}(S, M) exp(KS + hM) \tag{3.32}$$

where $\mathcal{N}(S, M)$ is the number of configurations at the point (S, M) in the phase space, and $Z(K, h)$ is the canonical partition function given by

$$Z(K,h) = \sum_{S,M} \mathcal{N}(S,M) exp(KS + hM) \quad . \tag{3.33}$$

The histogram of values of (S, M) generated by the Monte Carlo simulation is proportional to $P_{(K,h)}(S, M)$. From the histogram, it is straightforward for one to obtain the normalized probability distribution. Then, the histogram can be used to generate data for different parameters. For new parameters (K', h'), the normalized probability distribution can be expressed in terms of the distribution with (K, h)

$$P_{(K',h')}(S,M) = \frac{P_{(K,h)}(S,M) exp[(K'-K)S + (h'-h)M]}{\sum_{(S,M)} P_{(K,h)}(S,M) exp[(K'-K)S + (h'-h)M]} \quad . \tag{3.34}$$

We could then use $P_{(K',h')}(S, M)$ to calculate the quantities of interest without having to do time-consuming Monte Carlo simulations at (K', h').

3.7 Spatial Correlation and Fourier Transformation

As mentioned in section 2.4, Parry *et al.* [66, 67] revisited the controversy in critical wetting transitions in three-dimensional systems with short-ranged forces and introduced a non-local (NL) interfacial Hamiltonian. According to their analysis, they showed that spatial correlation functions are characterized by, not one but, two diverging transverse length scales, parallel correlation length $\xi_{\parallel}$ and non-local correlation length $\xi_{NL} \propto \sqrt{ln\xi_{\parallel}}$. Thus, to measure and examine the correlation functions directly from Monte Carlo simulation would provide a most direct test of the non-local theory by Parry *et al.* since one can see the influence of ξ_{NL} in the correlation functions between the surface and interface, and correlation within the interface.

Based on our model, which was described in detail in section 3.1, the general form of the spin-spin correlation function we measured has the following format

$$Corr(z_1, z_2; \vec{r}) = \langle S(\vec{r_1}) S(\vec{r_2}) \rangle - \langle S(\vec{r_1}) \rangle \langle S(\vec{r_2}) \rangle \tag{3.35}$$

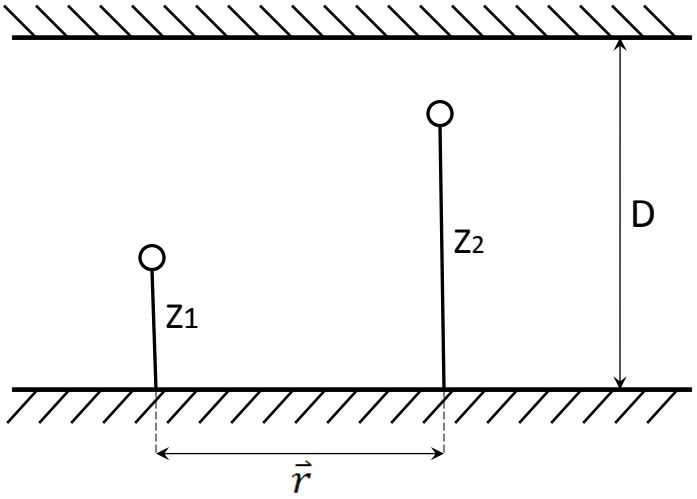

Figure 3.5: Illustration of the spin-spin correlation. The two open circles denote the positions of two spins whose correlation is calculated. z_1 and z_2 give the number of layers where the spins are located. $\vec{r}$ is the projection of the vector connecting the two spins onto the horizontal plane.

where z_1 and z_2 represent the number layers where the spins are located, $\vec{r_1}$ and $\vec{r_2}$ are the location of the two spins in the projected plane parallel to the surface of the film, $\vec{r}$ is the projection of the vector connecting the two spins onto the horizontal plane, $S(\vec{r_1})$ and $S(\vec{r_2})$. The relationship of these quantities is illustrated in Fig. 3.4. More information can be obtained by taking the 2-dimensional Fourier transformation with respect to $\vec{r}$ as follows

$$\tilde{C}(z_1, z_2; \vec{q}) = \int e^{i\vec{q}\cdot\vec{r}} Corr(z_1, z_2; \vec{r}) d\vec{r} \tag{3.36}$$

In this dissertation, we calculated the following correlation functions, which are shown schematically in Fig. 3.5

(1) Correlation within the surface layer: $Corr(1, 1; \vec{r})$ or equivalently $Corr(D, D; \vec{r})$

(2) Correlation within the interface layer: $Corr(\frac{D}{2}, \frac{D}{2}; \vec{r})$ or equivalently $Corr(\frac{D+1}{2}, \frac{D+1}{2}; \vec{r})$

(3) Correlation between the surface layer and interface layer: $Corr(1, \frac{D}{2}; \vec{r})$ or equivalently $Corr(\frac{D+1}{2}, D; \vec{r})$

and did the Fourier Transformation along the $\vec{x}$ direction as follows

$$\tilde{C}(z_1, z_2; q_x) = \int e^{iq_x x} C(z_1, z_2; \vec{r}) d\vec{r} \tag{3.37}$$

According to the non-local theory of Parry *et al.*, the correlation functions $\tilde{C}(1, \frac{D}{2}; q)$ and $\tilde{C}(\frac{D}{2}, \frac{D}{2}; q)$ in momentum space have the following format

$$\tilde{C}(1, \frac{D}{2}; q) \propto \frac{1}{\xi_\perp} \frac{e^{-q^2 \xi_{NL}^2/2}}{(1 + q^2 \xi_\parallel^2)} \tag{3.38}$$

$$\tilde{C}(\frac{D}{2}, \frac{D}{2}; q) \propto \frac{1}{(1 + q^2 \xi_\parallel^2)} \tag{3.39}$$

where $\xi_\perp$ is the interfacial roughness, $\xi_\parallel$ is the parallel correlation length. $\tilde{C}(1, 1; q)$ does not contain the information about the non-local correlation, so in most cases, we didn't calculate it. When performing the fourier transformation, although we only had data for finite r, we avoided this limit since our model was subject to periodic boundary conditions in both x and y directions.

According to the non-local theory of Parry *et al.* (see section 3.7), the correlation functions $\tilde{C}(1, \frac{D}{2}; q)$ and $\tilde{C}(\frac{D}{2}, \frac{D}{2}; q)$ in momentum space have the form shown in Eqn. 3.38 and 3.39; so, when the ratio between $\tilde{C}(1, \frac{D}{2}; q)$ and $\tilde{C}(\frac{D}{2}, \frac{D}{2}; q)$ is taken, we should have a simple decay as follows

$$\frac{\tilde{C}(1, \frac{D}{2}; q)}{\tilde{C}(\frac{D}{2}, \frac{D}{2}; q)} \propto e^{-q^2 \xi_{NL}^2/2} \tag{3.40}$$

According to the non-local theory, this simple decay is valid, at least for small q values. So by calculating and plotting the ratio as a function of q, we can test this theoretical prediction and also obtain information about ξ_{NL}. According to the predictions, ξ_{NL} has the D dependence $\xi_{NL} \propto \sqrt{D}$.

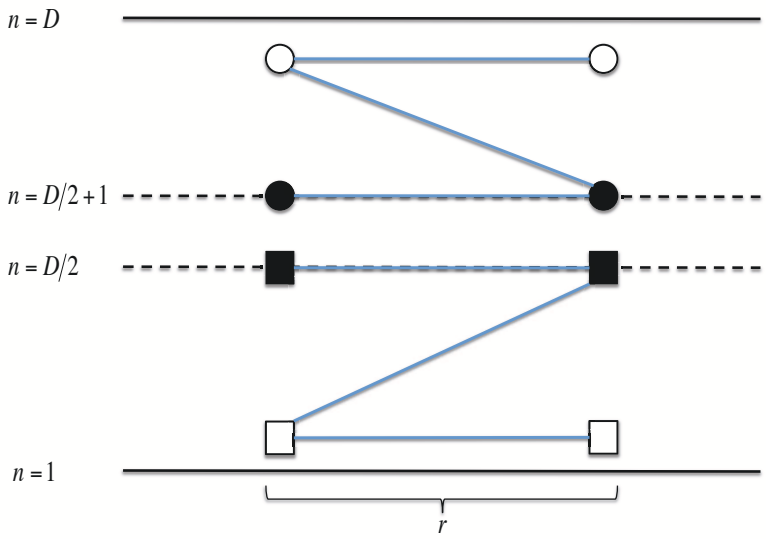

Figure 3.6: Schematic demonstration of the three different correlation functions evaluated. Open circles and squares represent the spins on the surface or bottom layers, while solid circles and squares represent the spins located in the interface layers. Note: for odd D, there is only one interface layer.

Chapter 4

Results - Ising thin films with both competing walls and a field gradient

4.1 Simulation Data and phase transitions

We concentrated on Ising films with lattice size $L = 128$, $D = 12$, applied with opposite surface fields $H_1 = -H_D = -0.55$, and a varying linear field gradient g. Typical correlation times of averaged magnetization are within 10 Monte Carlo steps (MCS). For most cases, MCS is at least 10^5 to obtain good statistics, and sometimes up to 4×10^7 for the study of probability distribution of the energy E and the order parameter M. To study the probability distribution of the order parameter, we also simulated different lattice sizes $L = 16, 32, 64$. A single Monte Carlo run of length 4×10^7 MCS takes about a week, and takes much longer for $L = 256$, so we took $L = 128$ as our primary lattice size.

We first examined the layer magnetization M_n as a function of layer number n when an extra non-zero linearly changing field was applied to the Ising films with both competing walls. Let's recall the behavior of the layer magnetization M_n in Fig. 2.9, obtained in previous Monte Carlo simulation on Ising films with only competing walls by Ferrenberg *et al.* [36]. When the temperature is higher than a critical temperature $T_c(D)$ dependent on the thickness of the film, the layer magnetization profile showed an symmetric pattern about the center of the film (midpoint between layer number $\frac{D}{2}$ and $\frac{D+1}{2}$, when D is even). One can take this midpoint as the location of the interface between positive magnetization and negative magnetization although one needs to keep in mind that the interface is actually fluctuating and this is just an average of the interface position. The fluctuation of M, i.e. the susceptibility was also measured. While when the temperature is below $T_c(D)$, the interface will get bound to either of the walls, and one can say that the system has two equivalent

phases (bound interface), instead of one phase with interface in the center at high temperature. The transition between these two states is called interface-unbinding phase transition. In our work, we studied a model which is almost exactly the same with the above work, except that we added a non-zero field gradient. According to the phase diagram predicted by Rogiers and Indekeu [54], when g is non-zero, the system will undergo a similar interface-unbinding phase transition at different temperatures depending upon the value of g. And we did observe the behavior predicted. Fig. 4.1 shows the profiles of the layer magnetization M_n plotted vs layer number n, for $g/J = 0.01$. We can see, at high temperatures above $J/k_BT = 0.22$, the interface is fluctuating in the center of the film. When the temperature decreases down to $J/k_BT = 0.25$, the interface is moving toward the surface, and finally is bound the wall. Depending on the initial configuration, the interface could be bound to either of the walls, and the positions of interfaces should be symmetric to each other. The kinks at both ends of the magnetization profiles are caused by opposite surface fields and the reduced number of interacting neighbors. According to the phase diagram predicted by Rogiers and Indekeu [54], when the temperature is fixed and the magnitude of the field gradient is swept from zero to certain value, two different situations of phase transition are expected to be observed. When the temperature is above $T_c(D)$ ($J/k_BT_c(D) \approx 0.2497$ [36]), two phase transitions are encountered; while when the temperature is below $T_c(D)$, only one phase transition occurs. Fig. 4.2 and Fig. 4.3 show what we observed in Monte Carlo simulations.

At $J/k_BT = 0.244$ (see Fig. 4.2), which is above $T_c(D)$, the system shows an interface fluctuating in the center of the film at zero g; by increasing the value of g to $g/J = 0.005$, the interface is already bound to the surface; at $g/J = 0.025$, the interface appears in the center of the film again, however, the magnetization in the layers above the interface becomes positive, while the magnitude of the layers below the interface turns to negative, although the top surface field is negative and bottom field is positive. We can see the effects of the field gradient competing with the effects of opposite walls. And at this temperature, the system goes through two phase transitions when the value of g is increased from zero. At a lower

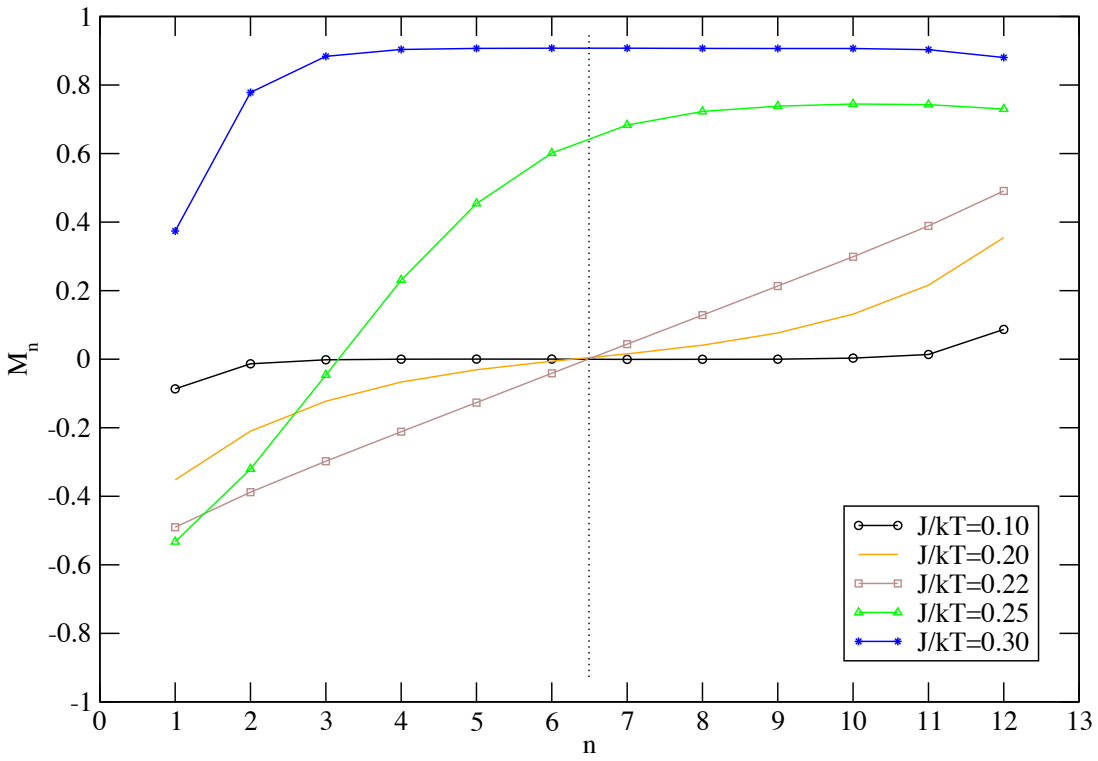

Figure 4.1: Profiles of the layer magnetization M_n vs layer number n, for $L = 128, D = 12, H_1/J = -H_D/J = -0.55, g/J = 0.01$ and various choices of inverse temperature. The dashed line indicate the position of the center of the film. The error bars are less than the size of the symbols.

temperature $J/k_BT = 0.303$ (see Fig. 4.3), which is below $T_c(D)$, only one phase transition, instead of two, occurs when the value of g is increased, since the system is already in the two-phase coexistence state at zero g.

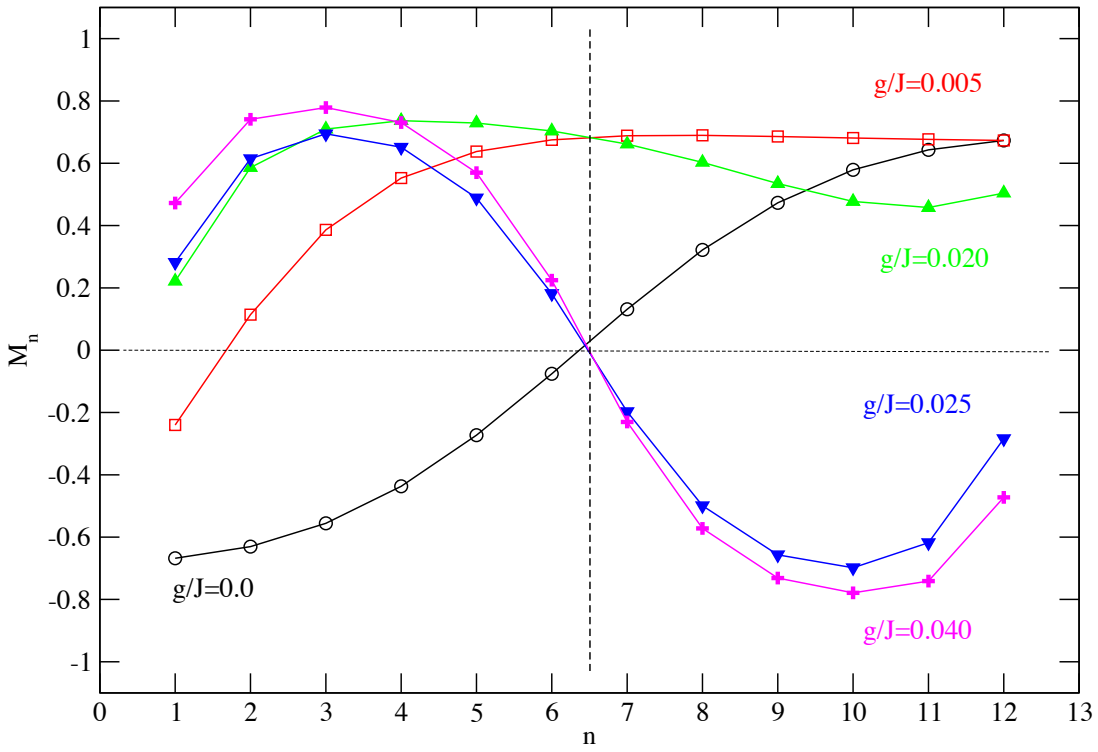

Figure 4.2: Profiles of the layer magnetization M_n vs layer number n, for $L = 128, D = 12, H_1/J = -H_D/J = -0.55, J/k_BT = 0.244$ and various choices of field gradient g. The dashed lines indicate the position of the center of the film and zero magnetization. The error bars are less than the size of the symbols.

4.2 The Interface Unbinding Phase Transitions

According to the theoretical prediction by Rogiers and Indekeu [54], for relatively small value of g, the phase transition when T varies is second order, while for large value of g, the phase transition turns to first order. There is a tricritical point separating them. In the following two sections, we will discuss the results we obtained for both kinds of phase transition.

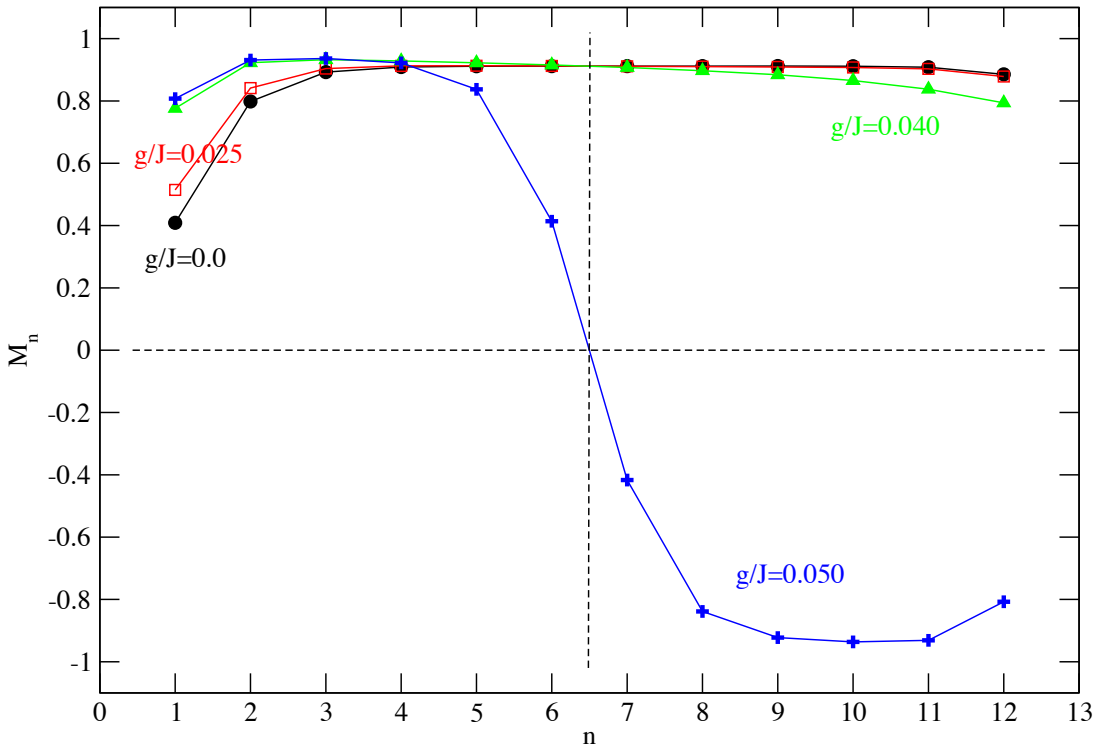

Figure 4.3: Profiles of the layer magnetization M_n vs layer number n, for $L = 128, D = 12, H_1/J = -H_D/J = -0.55, g/J = 0.10$ and various choices of inverse temperature. The dashed lines indicate the position of the center of the film and zero magnetization. The error bars are less than the size of the symbols.

4.2.1 Second-order Phase Transition

As mentioned in section 3.3.2, for second-order transitions, making plots of Binder cumulant as a function of temperature for different size lattices provides an efficient way for us to make a preliminary identification of the universality class from the value of U_4^* and obtain an estimate for T_c from the location of the crossing point. Based on a rough approximation of the phase diagram by measuring specific heat as a function of temperature and locating the peak

temperatures when g is fixed at different values. As an example, Fig. 4.4 shows our simulation results at $g/J = 0.015$, which we expect introduces second-order phase transition at certain critical temperature. We did Monte Carlo simulation for different lattice sizes, L=16, 32, 48, 64, 96, 128 and up to 192, and measured the Binder cumulant U_L for each lattice size at different temperatures. We can see from Fig. 4.4 that the curves for different sizes cross systematically with increasing lattice size due to the fact that the lattice sizes are not infinite. The value of U_L at crossing moves toward to the value of U_4^* of two-dimensional Ising model (0.615 [79]) asymptotically when extrapolated. Fig. 4.5 shows the finite size scaling analysis

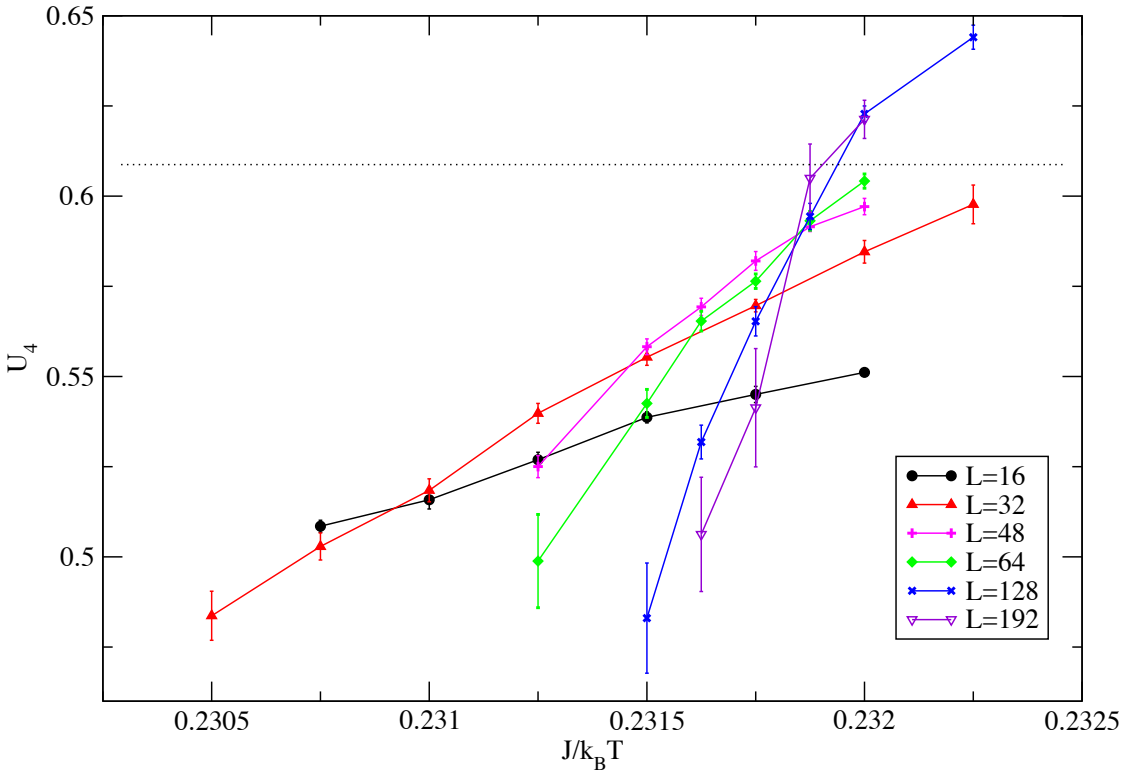

Figure 4.4: Binder cumulant U_4 plotted vs inverse temperature for $D = 12, H_1/J = -H_D/J = -0.55, g/J = 0.015$, and several choices of L. The dashed line indicates the position of U_4^* for two dimensional Ising model (0.615) [79].

on the above systematic crossing behavior in order to determine the transition temperature.

For $L' = 16, 32$ and 48, the inverse temperature at crossing with values for larger lattice sizes is plotted as a function of inverse of those lattice sizes. After doing linear fitting to data for each individual L', the fitting lines intersect at a same point at infinite L ($1/L = 0$). Thus the transition temperature is determined at $J/k_BT = 0.232 \pm 0.0012$ for $g/J = 0.015$. We also used histogram reweighting method to examine the probability distribution of order

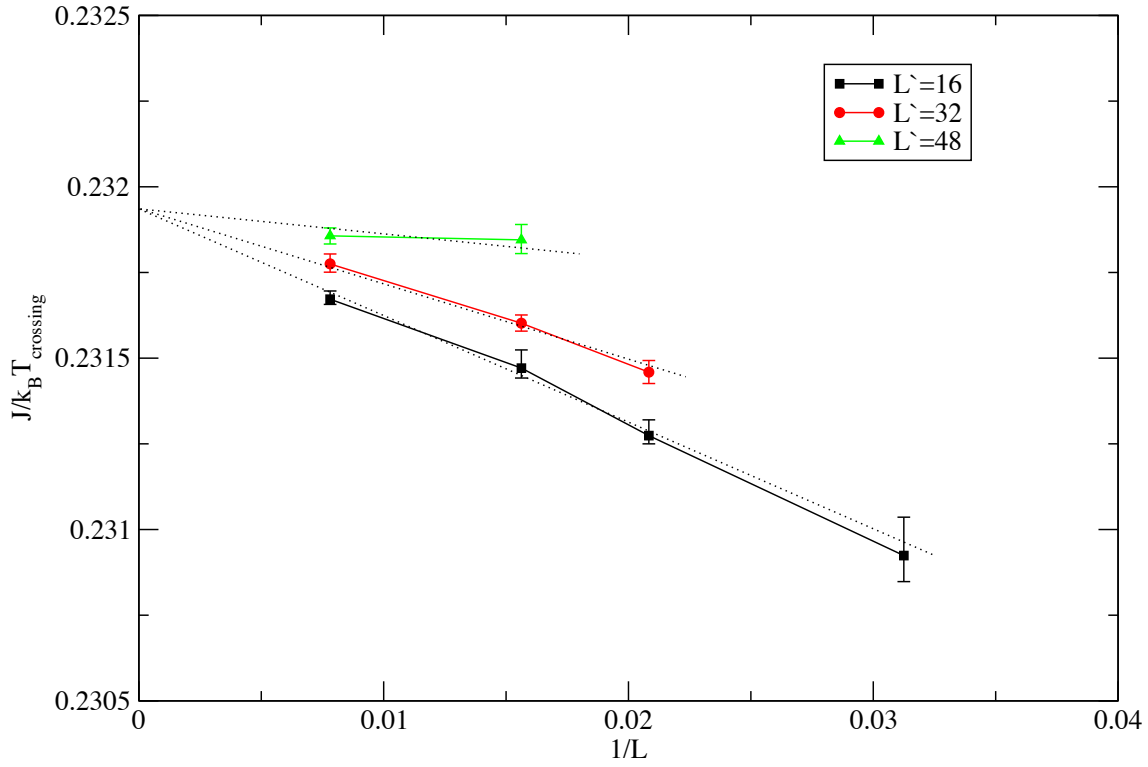

Figure 4.5: Extrapolation of the values of the inverse temperatures J/k_BT of crossing points vs. $1/L$ for different choices of reference lattice size L'. The dashed lines are straight lines fitted from the data.

parameter M (magnetization). As mentioned in section 3.5, scaling functions, such as P^* (see Eqn. 3.29), are characteristic of the corresponding universality class. In Fig. 4.6, the scaling function P^* at different temperatures for $g/J = 0.015$ is plotted as a function of $\tilde{M}$ together with the scaling function of two-dimensional Ising model. There is a difference

between the distribution of our model and 2-D Ising model, which we believe is from the finite size effects. Although we believe Ising film belongs to the same universality class with the 2-D Ising model, there is another dimension, thickness of the film. If the lattice size L is infinitely large, the thickness can be ignored and the Ising film gets closer to the 2-D Ising model. In Fig. 4.7, scaling function P^* (see Eqn. 3.29) is plotted for models with different lattice sizes $L = 128, 64, 32$ and 16. We also include the curve for 3-D Ising model for comparison. We can see, as the lattice size L decreases, the distribution gets closer to the 3-D Ising model form, since the effects of thickness cannot be ignored.

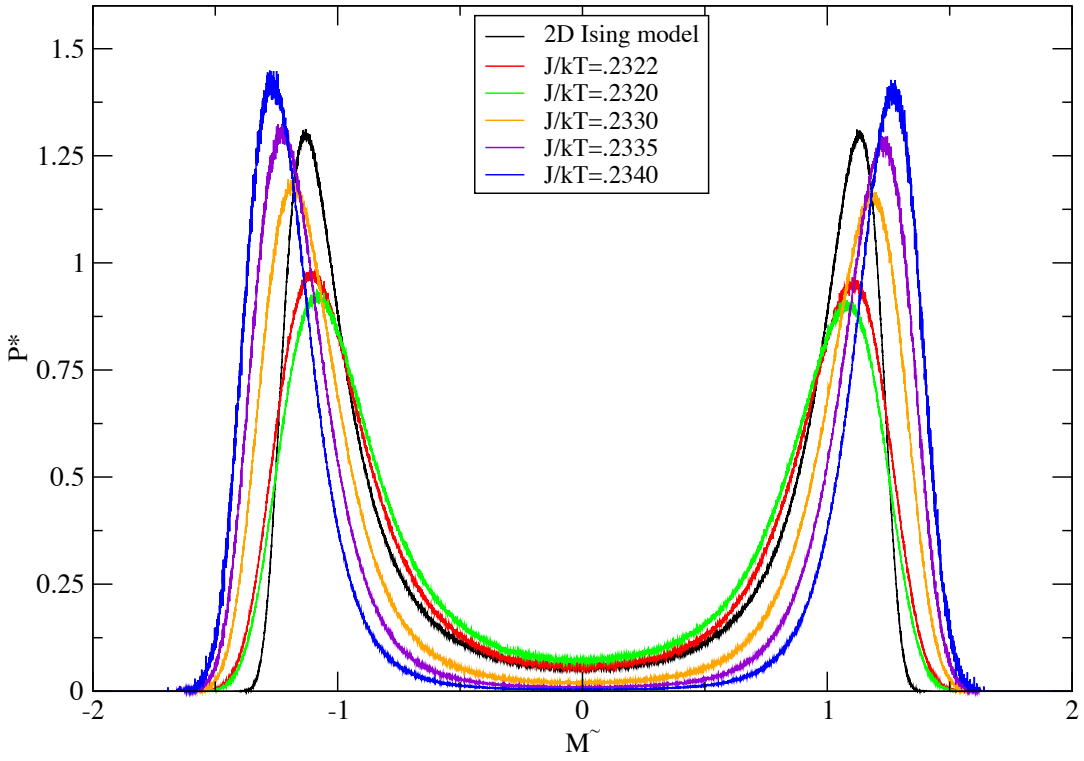

Figure 4.6: Scaled probability distribution P^* plotted vs $\tilde{M}$ for $L = 128, D = 12, H_1/J = -H_D/J = -0.55$ and $g/J = 0.015$. Monte Carlo runs are performed at inverse temperature $J/k_BT = 0.2322$, and the probability distribution are reweighted at other temperature close to it. The black curve represents the scaling function of 2-D Ising model with lattice size $L = 100$ at $T = 2.26918$ provided by Joao Plascak (private communication).

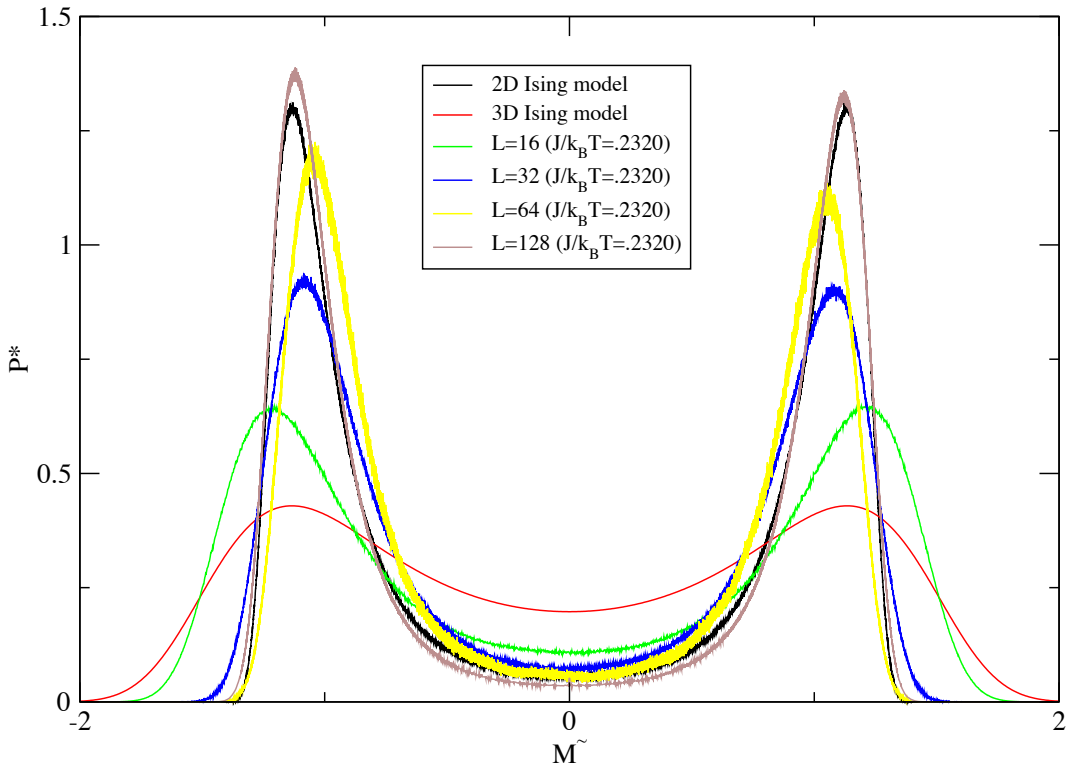

Figure 4.7: Scaled probability distribution P^* plotted vs scaled magnetization $\tilde{M}$ for $D = 12, H_1/J = -H_D/J = -0.55, g/J = 0.015$ and different choices of L at inverse temperature $J/k_BT = 0.2320$. Data for 2-D ($L = 100$) and 3-D ($L = 100$) Ising models (provided by Joao Plascak, private communication) are included for comparison.

4.2.2 First-order Phase Transition

For larger values of g,a first-order transition is expected. We first located the phase boundary approximately by examining hysteresis between sweeps of g or T in opposite directions. Then we used the free energy integration method described in section 3.4 to locate the transition. Fig. 4.8 shows the routes along which the free energy was integrated. Integrations were done along two opposite directions, one from high temperature (at $T \to \infty$, $U = 0$) to low

temperature, the other one from zero temperature (at zero T, $C = 0$) to high temperature. The intersection of these two integrations would be where the transition occurs. When g becomes larger and the phase boundary is steeper, we can choose to integrate the free energy along the direction of field gradient g instead of temperature. Similarly, we need to fix the temperature and do the integration in two opposite directions, one from zero g to larger value, the other one from large g to small values. Since it is hard to know beforehand what the free energy of the system is for certain value of g, we can perform an integration from infinite temperature to a position outside of the phase boundary, and then integrate towards the direction of smaller value of g. The intersection of two curves of free energy vs. g will tell us the value of g at transition. We first examined free energy integration for

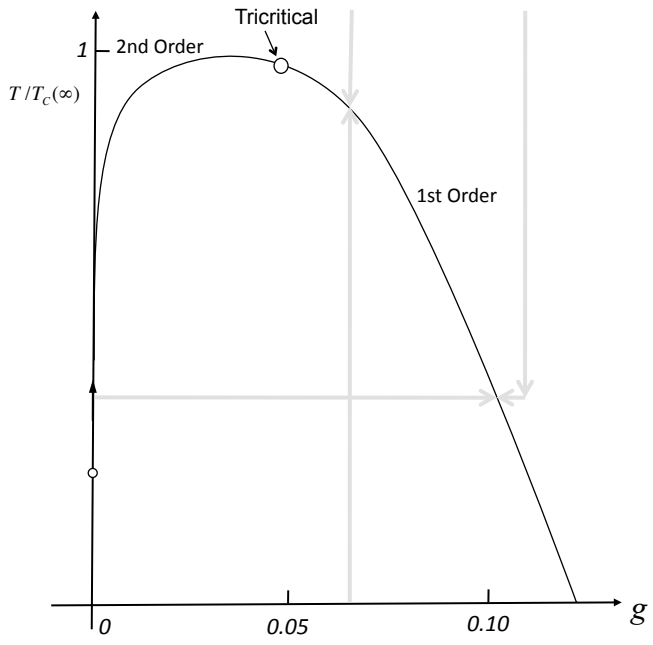

Figure 4.8: Illustration of routes along which the free energy integration is done. The phase diagram is from ref. [54].

a small field gradient $g/J = 0.01$, for which we know for certain is a second-order phase transition and the two integration curves should merge into each other smoothly. Fig. 4.9

shows the results we obtained for this low field gradient. The two curves don't intersect but overlap each other when they meet from opposite directions. Fig. 4.10 shows the free

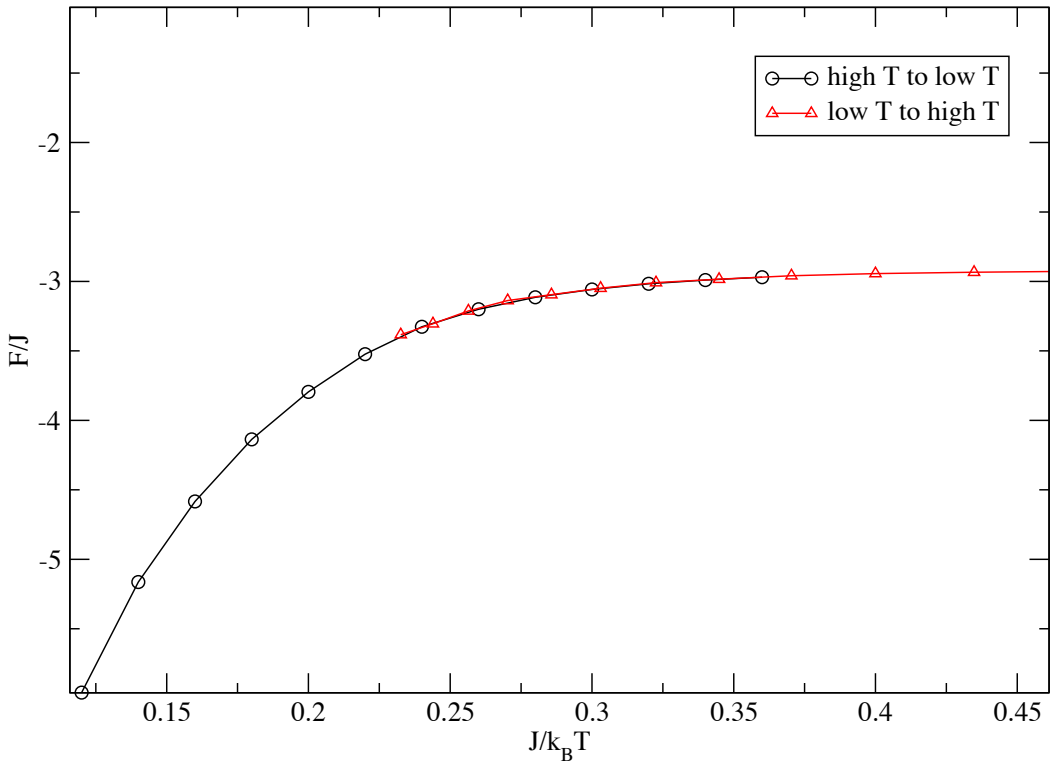

Figure 4.9: Free energy integration for $L = 128, D = 12, H_1/J = -H_D/J = -0.55$ and $g/J = 0.01$ along two opposite directions of temperature.

energy integration results for a higher field gradient $g/J = 0.025$. When the two curves meet each other from opposite directions, an obvious intersection occurs. So we can tell that the transition happening here is first-order, and the location of the transition temperature can be obtained from the intersection point ($J/k_BT = 0.255$). Fig. 4.11 shows the free energy integration results for a lower temperature at $J/k_BT = 0.467 \pm 0.006$. The two integration curves intersect at a field gradient $g/J = 0.0424 \pm 0.0008$, where a first-order phase transition occurs.

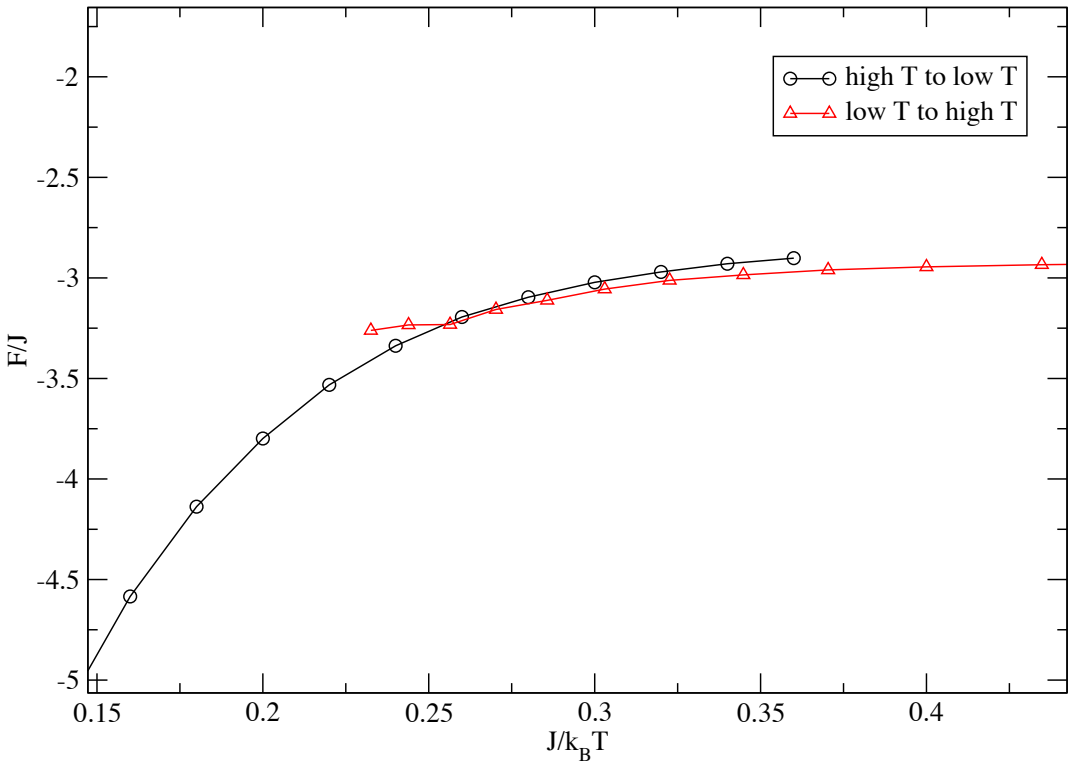

Figure 4.10: Free energy integration for $L = 128, D = 12, H_1/J = -H_D/J = -0.55$ and $g/J = 0.025$ along two opposite directions of temperature.

4.3 Phase Boundary

Fig. 4.12 shows the phase boundary we obtained from our Monte Carlo simulation. Two different y coordinates are labeled, T/T_{cb} ($T_{cb} = 0.227$, bulk critical temperature) and inverse temperature J/k_BT. As predicted by Rogiers and Indekeu [54], the phase boundary separates a bulk two-phase coexsistence region from a single disordered phase region. The addition of the field gradient g produces a re-entrant phase diagram in which, as g increases, the temperature bounding the bulk two-phase coexistence first goes up from $T_c(D)$, and then

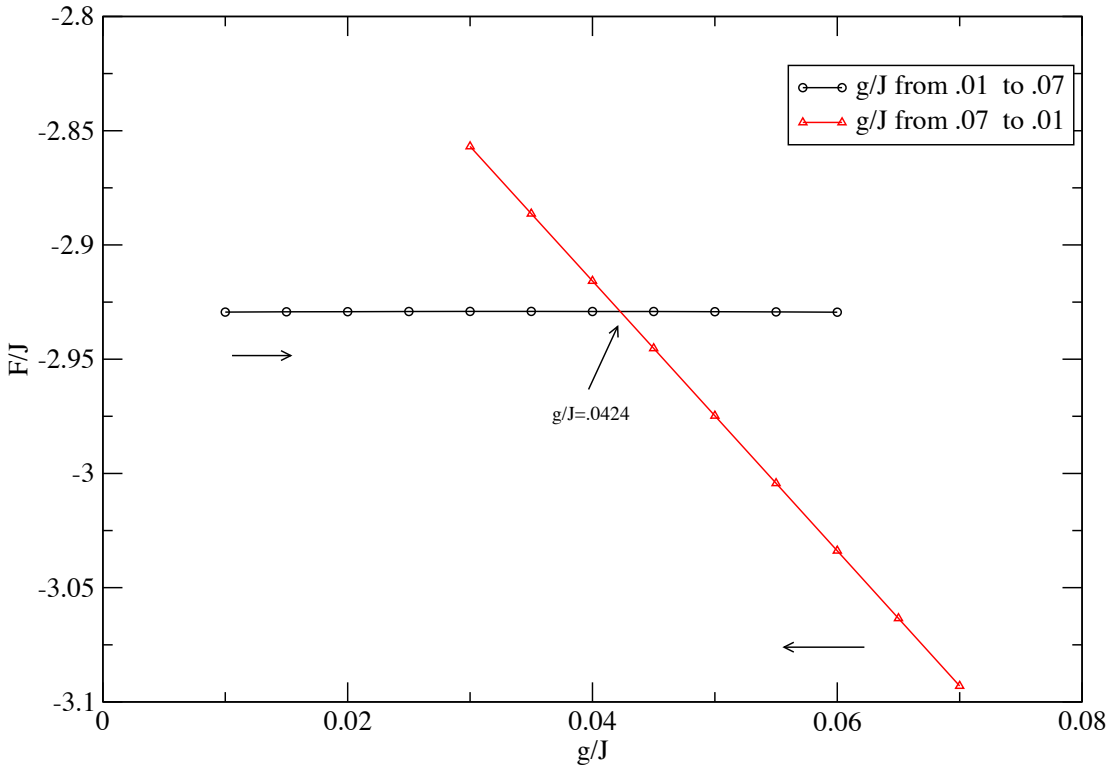

Figure 4.11: Free energy integration for $L = 128, D = 12, H_1/J = -H_D/J = -0.55$ and $J/k_BT = 0.467$ along two opposite directions of g.

decreases. For small g, the transition is second order, whereas for large g, the transition appears to be first order. A tricritical point is expected to be connecting first-order and second-order phase transition boundary. To locate the tricritical point which connects the second-order and first-order phase transition lines, first generate the probability distribution of the order parameter at a point estimated from the second-order and first-order phase transition lines, then use histogram reweighting method to reweight the distribution to close neighboring regime in two dimensions, both the temperature and the field, until a point is

reached, where the distribution function of the order parameter shows three peaks with the same height.

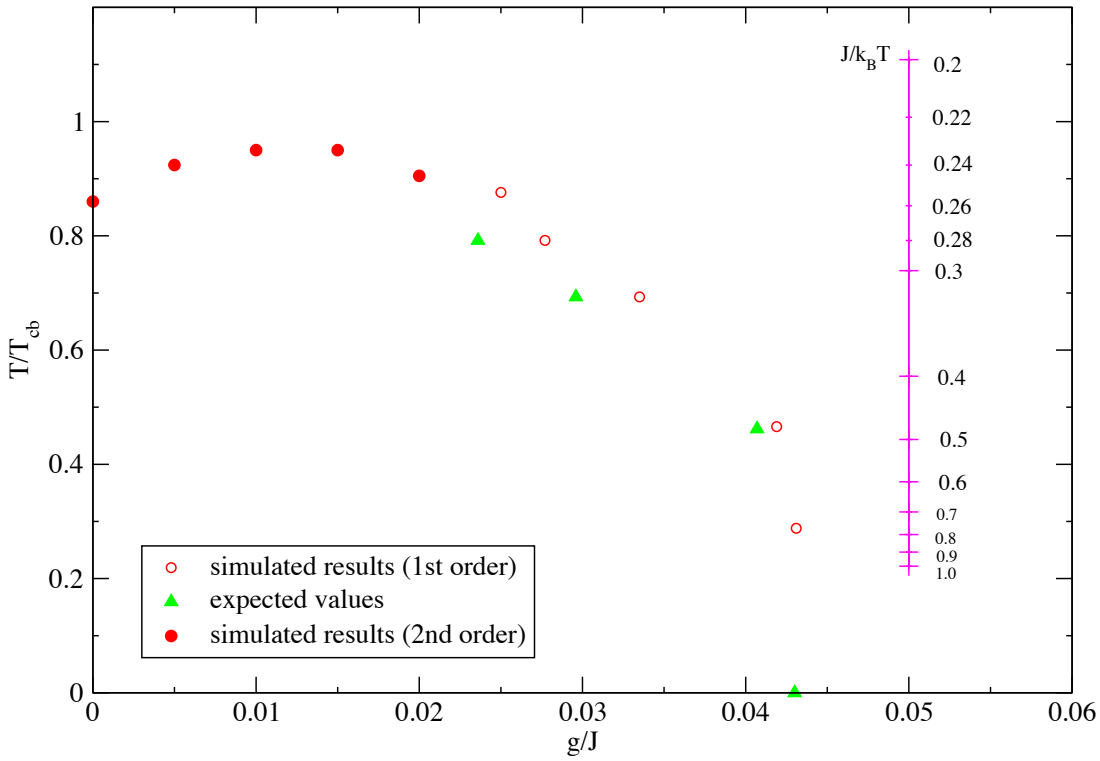

Figure 4.12: The phase diagram for the Ising film ($L = 128, D = 12$) subject to the opposite surface fields $H_1/J = -H_D/J = -0.55$ and a field gradient g. Solid circles denote second-order phase transition, while open circles denote first-order phase transitions. Solid triangles are calculated approximately by Binder (private communication).

4.4 Summary

In summary, extensive Monte Carlo simulations are used to study the interesting effects resulting from a linearly varying magnetic field on a thin Ising film. This linearly changing magnetic field is equivalent to applying gravity to the corresponding lattice-gas model. So, besides competing surface fields acting on two $L \times L$ free surfaces a distance D apart from

each other, we also applied a magnetic field g that varies linearly between the surfaces and which competes with the opposing surface fields. To determine the phase diagram, we looked for bulk two-phase coexistence at different values of g and temperature T. In situations with only competing surface fields applied, the interface unbinding transition [36] happens at temperature $T_c(D)$. The addition of the field gradient g competes with the surface field and produces a phase diagram as predicted by theoretical work by Rogiers and Indekeu [54]. As g increases, the temperature bounding bulk two-phase coexistence is re-entrant. For small g, the transition is second order, whereas for large g, the transition is first order. At temperatures above $T_c(D)$, one encounters two phase transitions when sweeping the magnitude of g starting from zero.

Chapter 5

Results - Non-local Correlation Length and the Wetting Transition

In this part of the work, we did extensive Monte Carlo simulation on Ising films with $L \times L \times D$ geometry with only competing surface fields ($H_1/J = -H_D/J = -0.55$) applied. A typical Monte Carlo run has 10^6 MCS or more, and the spin configurations in the surface and interface layers are obtained for spin-spin correlation calculation, which is rather time-consuming for large lattices. For $L = 512$, to measure a single one spatial correlation one needs about a month of CPU time. So for most of our work, we stopped at $L = 256$ since the results from it already provided a good estimate of the non-local correlation length that we are interested in.

5.1 Spin-Spin Correlation in Real Space

Spin-spin correlation functions were measured between different lateral positions as described in Section 3.7, in the surface and interface, within the interface layer and within the surface layer as a function of a two-dimensional vector $\vec{r}$, which is the projection of the vector connecting two spins whose correlation is measured. The temperature at which the simulations were performed was chosen to be below T_{cb} ($J/k_BT_{cb} = 0.227$ [36]) and above T_w ($J/k_BT_w \approx 0.250$ [36]), at $J/k_BT = 0.244$. After getting the real-space correlation function $Corr(z_1, z_2; \vec{r})$ (see Eqn. 3.35), an average is taken for all vectors $\vec{r}$ with the same magnitude, r. Thus, $C(z_1, z_2; r)$ is obtained, where r is a scalar.

Fig. 5.1 shows the averaged correlation function $C(1, \frac{D}{2}; r)$, $C(\frac{D}{2}, \frac{D}{2}; r)$, and $C(1, 1; r)$ (see Eqn. 3.35) for $L = 128, D = 12$ (for even D, the interface is in between middle layers), $H_1/J = -H_D/J = -0.55$ at $J/k_BT = 0.244$ on a logarithmic scale. All the three correlation

functions show a fast decay when q is close to zero, followed by an exponential decay regime of r. For larger r, a cut-off (around 40 here) happens, and correlation functions all fall into dramatic fluctuations although the absolute statistical errors are quite small (Note the plot is on a logarithmic scale). The correlation within the surface decays faster than the other two for small r and then decays with the same rate as the others for large r.

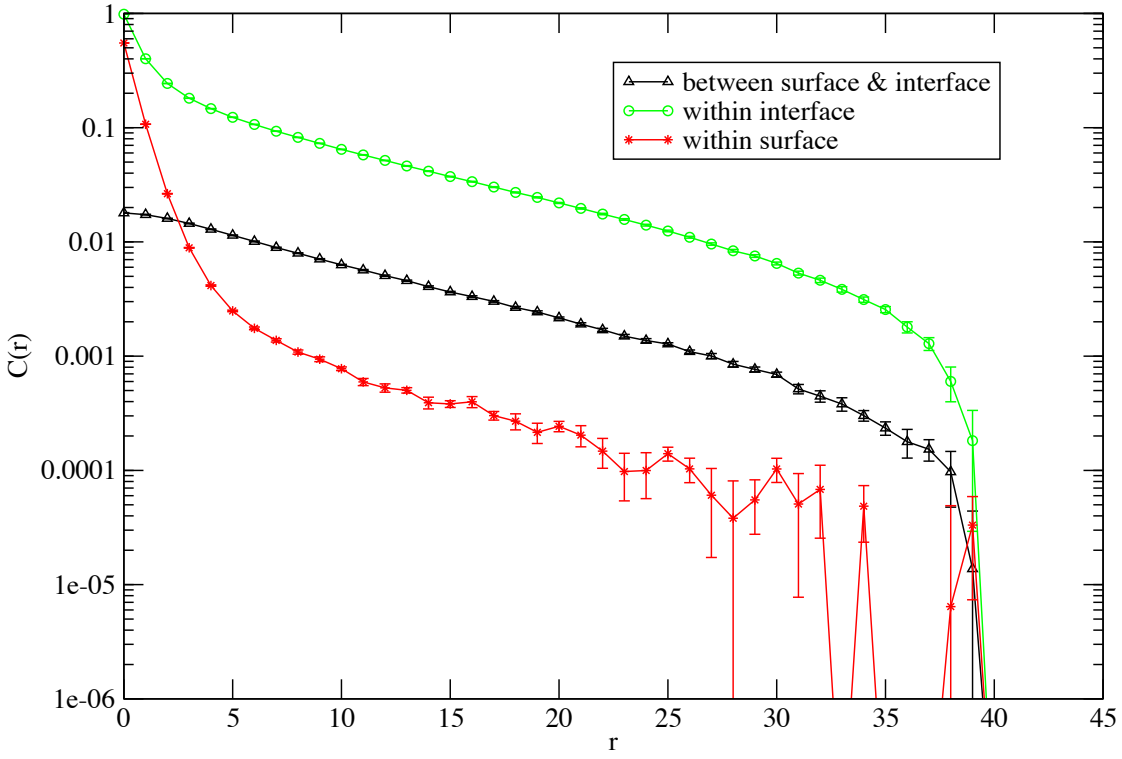

Figure 5.1: Correlation function plotted vs r for $L = 128, D = 12, H_1/J = -H_D/J = -0.55, J/k_BT = 0.244$, between surface and interface, within the interface and within the surface, respectively.

To determine the effect of finite lattice size L, Fig. 5.2 shows correlation functions $C(1, \frac{D}{2}; r)$ and $C(\frac{D}{2}, \frac{D}{2}; r)$ for $L = 128, 256$ and 512. ($C(1, 1; r)$ is not included here since according to non-local theory, it doesn't contain useful information about the non-local correlation length in which we are interested). We can see that they show some size dependence

and decay rate decreases systematically with the increase of L. The region of r where the correlation functions have exponential decay, i.e. linear decay on a semi-log plot, also extends systematically with the increase of L. For the work studying the D dependence of correlaition, we stopped at $L = 256$ since the bigger lattice sizes needs much more CPU time and don't bring very significant improvement. In Fig. 5.3 and 5.4, L is fixed at 256, and

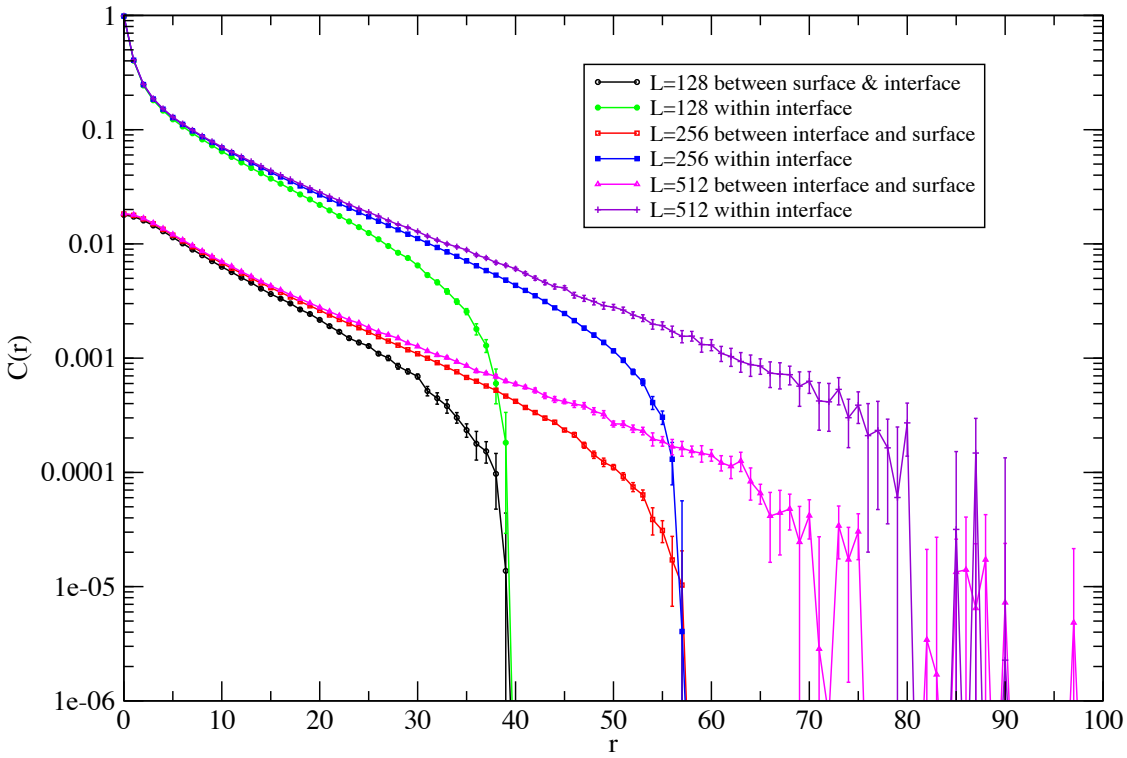

Figure 5.2: Real space spin-spin correlation function plotted vs r for $D = 12, H_1/J = -H_D/J = -0.55, J/k_BT = 0.244$, and multiple choices of L, $L = 128, 256, 512$, between surface and interface, within the interface, and within the surface, respectively.

D is given different values, $D = 6, 8, 10, 12, 13$ in order to study the D dependence of the non-local correlation length ξ_{NL}. The correlation functions $C(1, \frac{D}{2}; r)$ and $C(\frac{D}{2}, \frac{D}{2}; r)$ show a very obvious systematic behavior with the increase of value of D, decaying more slowly when D is increased and having larger value of r where cut-off happens.

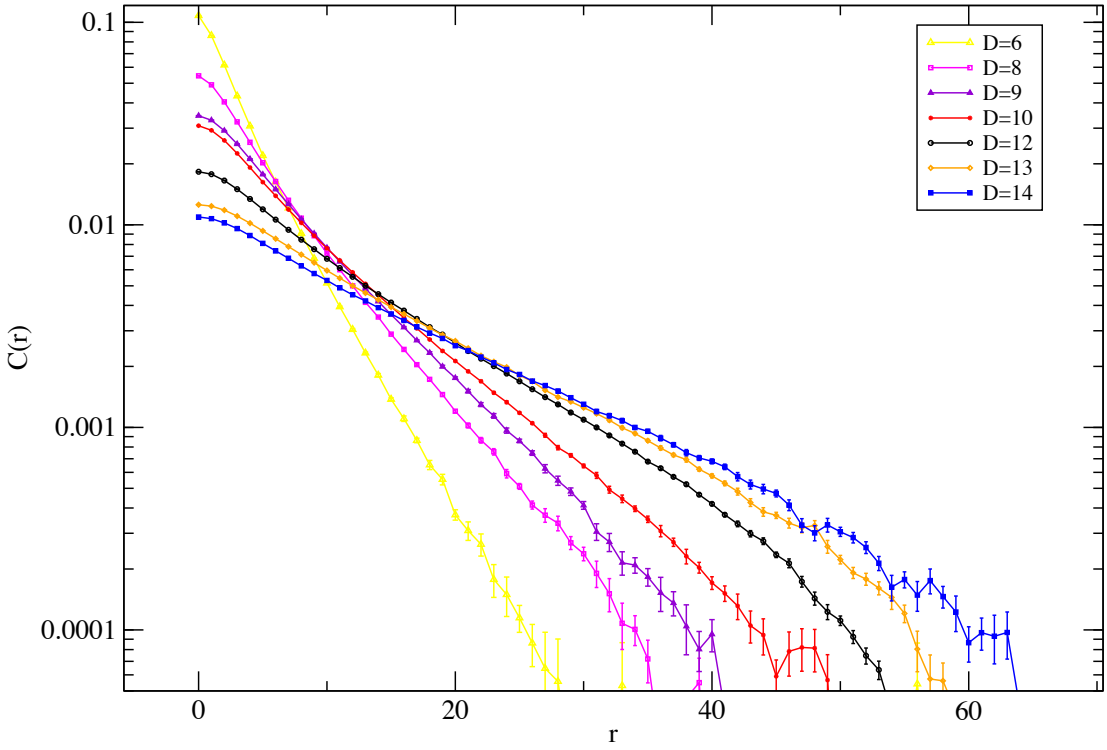

Figure 5.3: Real space correlation function plotted vs r for $L = 256, H_1/J = -H_D/J = -0.55, J/k_BT = 0.244$, and multiple choices of D, $D = 6, 8, 10, 12, 13$, between surface and interface.

5.2 Correlation in Momentum Space

While performing fourier transformation of the correlation functions to get the momentum space values $\tilde{C}(q)$, we did a linear fitting to the straight line parts of the curves, and extrapolated in r. For $\vec{r}$ whose magnitude r falls outside of the linear fitting regime, we used the extrapolated values instead of simulation results when doing the integration over x and y. Thus, we obtained good estimates of correlation functions $\tilde{C}(q)$ in momentum space.

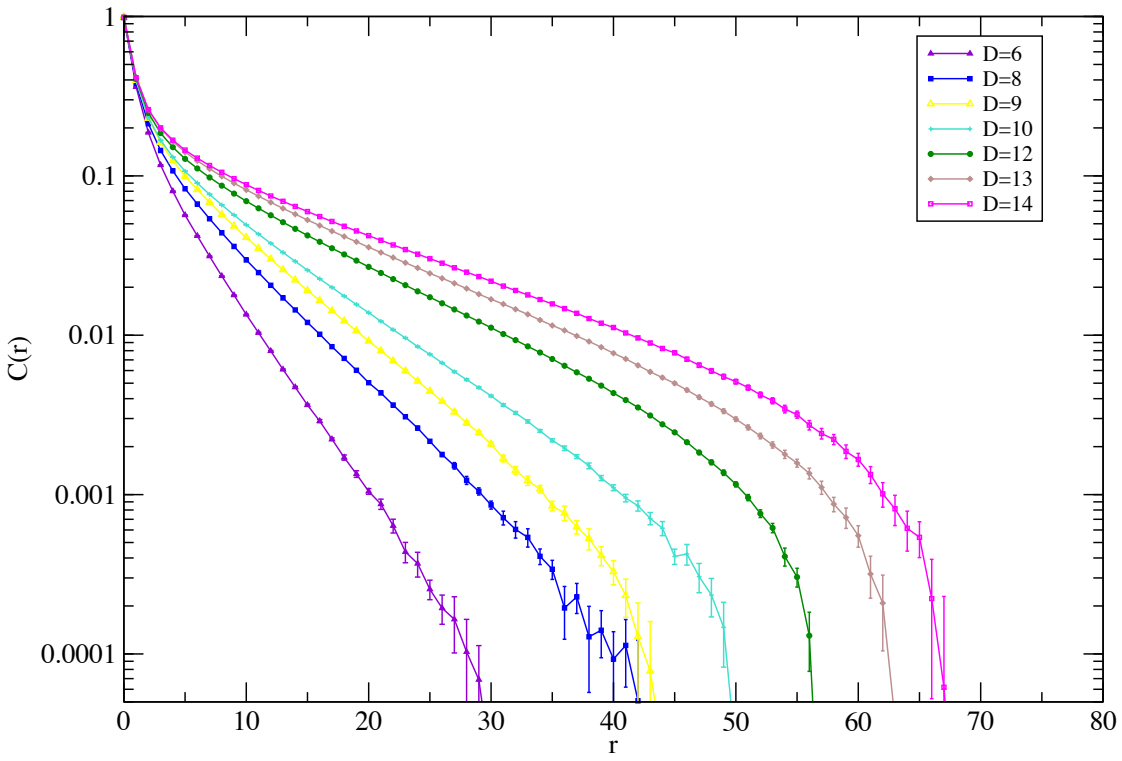

Figure 5.4: Real space correlation function plotted vs r for $L = 256, H_1/J = -H_D/J = -0.55, J/k_BT = 0.244$, and multiple choices of D, $D = 6, 8, 10, 12, 13$, within the interface.

Fig. 5.5 shows the correlation functions in momentum space for $L = 128, D = 12$ (in accordance with Fig. 5.1). The correlation between surface and interface decays much faster than the other two as seen in Fig. 5.2, and shows dramatic fluctuations when q gets bigger. The size dependence of our results is seen in Fig. 5.6 which shows the Fourier transformation of correlation functions shown in Fig. 5.2 for different L. The correlations show obvious size dependence only when q is very close to zero since the values of $C(q)$ when q is small mainly come from $C(r)$ at large r, where dramatic fluctuations happen and the real space

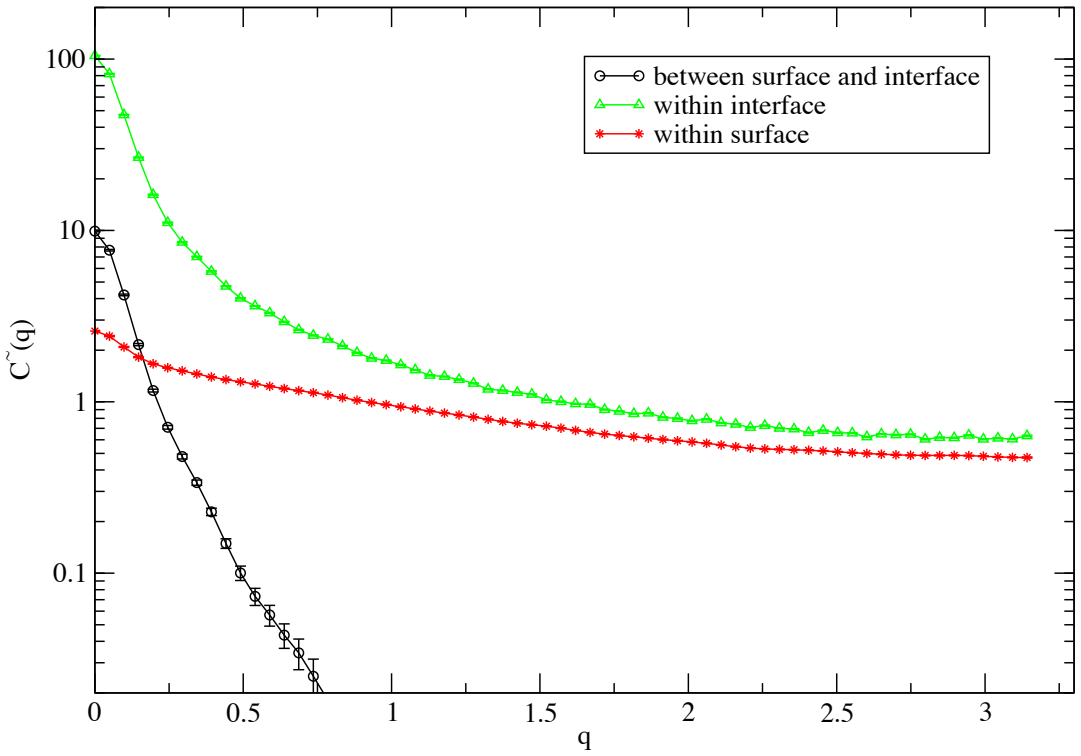

Figure 5.5: Fourier transformed (momentum space) correlation function plotted vs r for $L = 128, D = 12, H_1/J = -H_D/J = -0.55, J/k_BT = 0.244$ between surface and interface, within interface and within surface, separately. Where not shown, the error bars are less than the size of symbols.

correlations depend upon L. The correlation within the interface has very small fluctuations even when q is big, while between surface and interface, the fluctuation becomes dramatic when q is larger than ~ 0.75. Fig. 5.7 gives the Fourier transformation of correlations shown in Fig. 5.3 and Fig. 5.4 for different choices of D with fixed $L = 256$. The correlation within the interface shows systematic dependence upon D when q is small, while the correlation

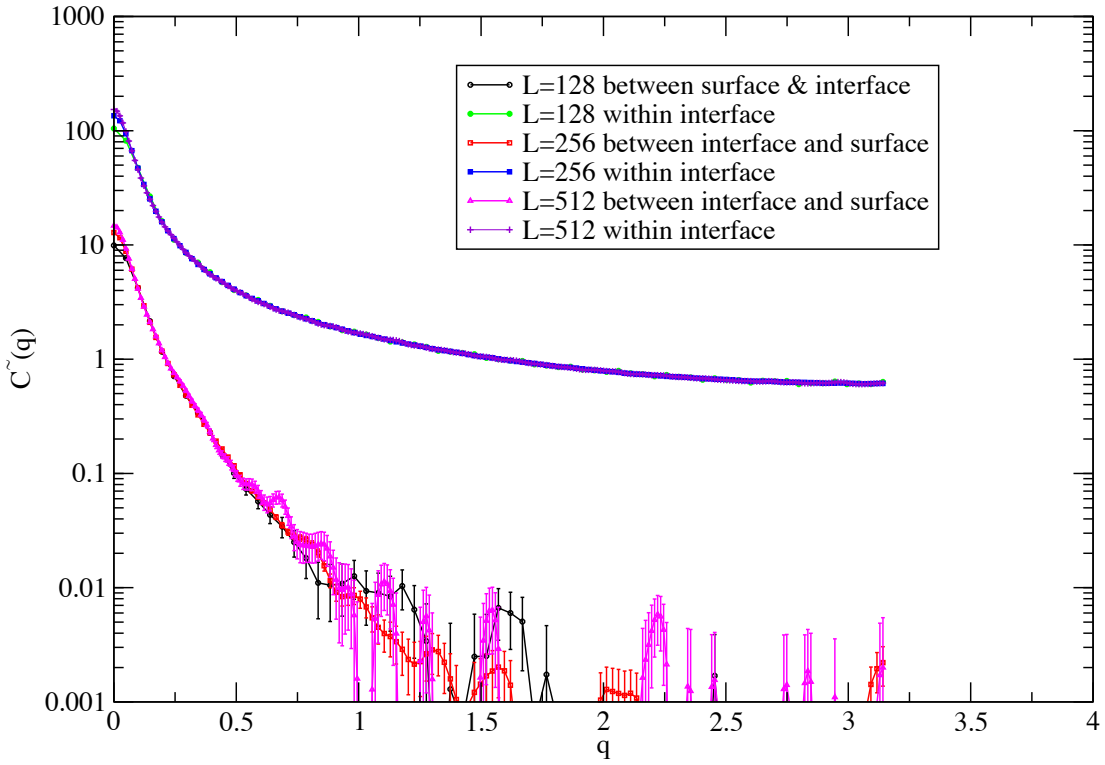

Figure 5.6: Fourier transformed correlation function plotted vs q for $D = 12, H_1/J = -H_D/J = -0.55, J/k_BT = 0.244$ and multiple choices of L, $L = 128, 256, 512$, between surface and interface, and within the interface.

between the interface and surface shows strong systematic D dependence over the entire range of q.

5.3 Ratio of Correlation $\frac{\tilde{C}(1,\frac{D}{2};q)}{\tilde{C}(\frac{D}{2},\frac{D}{2};q)}$ and non-local correlation length

Fig. 5.8 shows the ratio $\frac{\tilde{C}(1,\frac{D}{2};q)}{\tilde{C}(\frac{D}{2},\frac{D}{2};q)}$ as a function of q for $L = 128$ on a linear scale. The curve demonstrates a fast decay to around zero. Then, we plotted it on a semi-logarithmic scale in

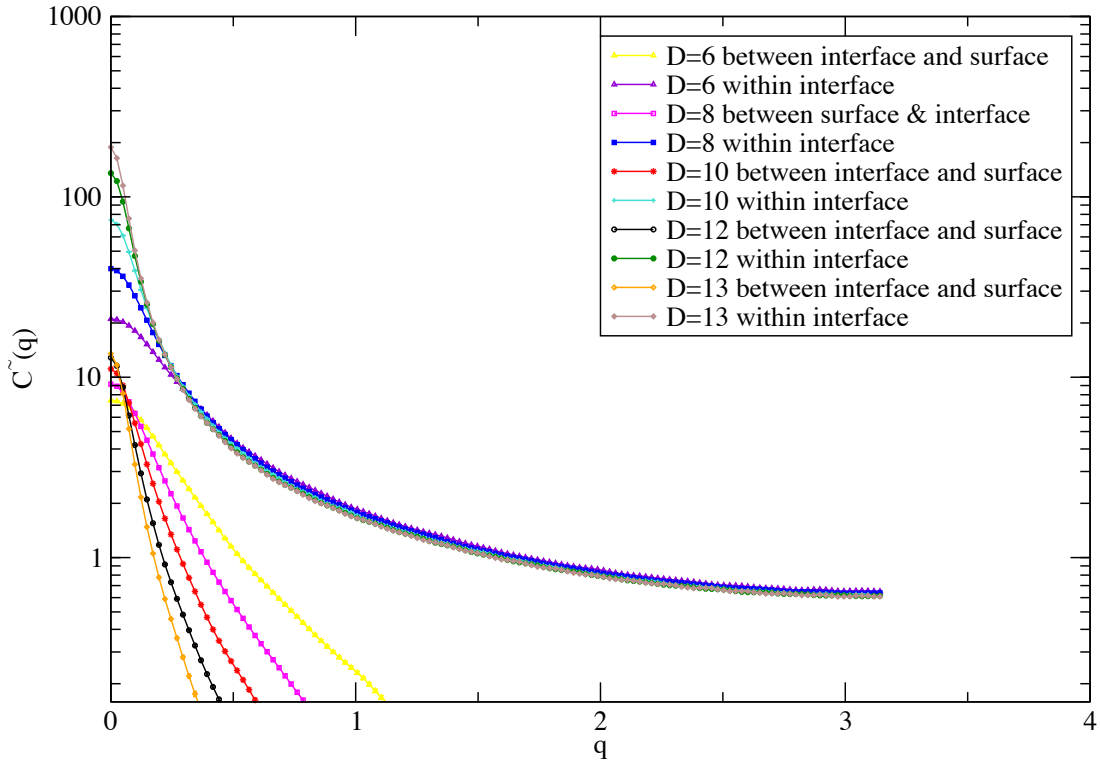

Figure 5.7: Fourier transformed correlation function plotted vs q for $L = 256, H_1/J = -H_D/J = -0.55, J/k_BT = 0.244$ and multiple choices of D, $D = 6, 8, 10, 12, 13$ between surface and interface, and within the interface. The error bars are less than the size of symbols.

Fig. 5.9, and found that it indeed has exponential decay behavior for small q. When q gets bigger, the error bars get very big and the curve fluctuates dramatically. Fig. 5.10 compares the ratio curves for $L = 128$ and a larger lattice size $L = 256$. We can see, the ratio's L dependence is not obvious.

Fig. 5.11 shows the ratio curves for a bigger lattice size $L = 256$ and multiple choices of D ($D = 6, 8, 10, 12, 13$). We can see the obvious exponential decay pattern for small q ($q^2 < 0.2, q < 0.45$ for most of these curves). Fig. 5.12 zooms the exponential decaying part

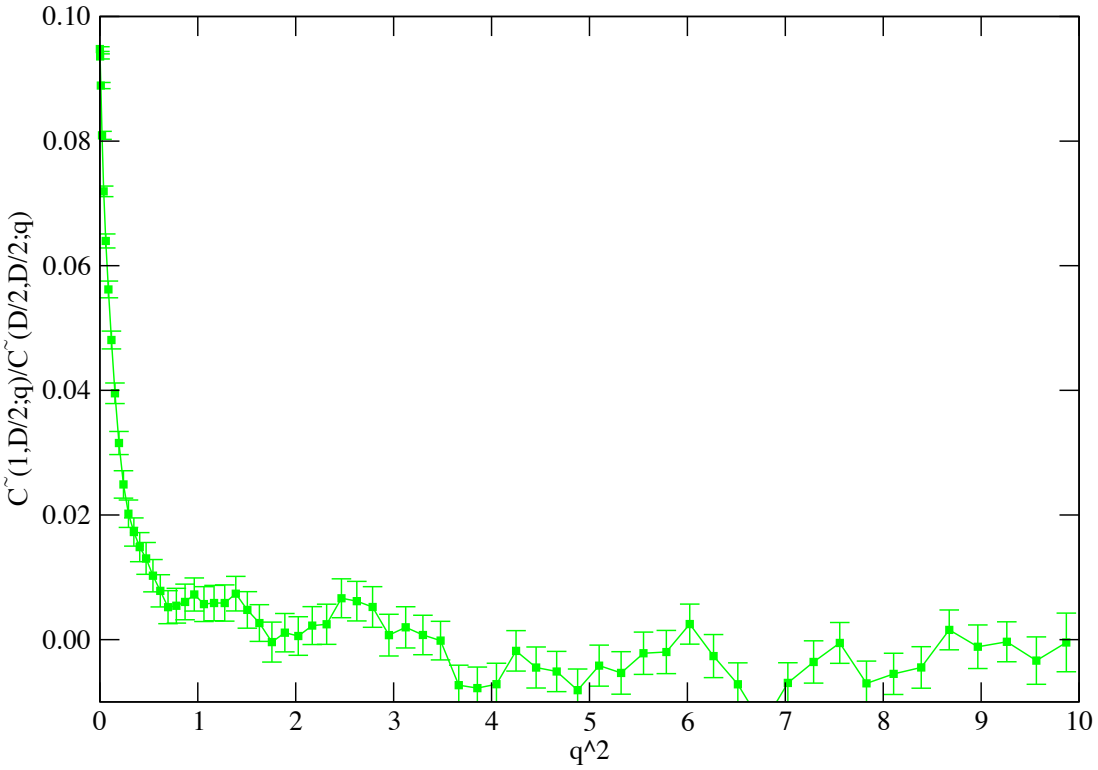

Figure 5.8: Ratio between Fourier transformed correlation functions plotted vs q^2 for $L = 128, D = 12, H_1/J = -H_D/J = -0.55, J/k_BT = 0.244$. Plotted on linear scale.

of the curves. Linear fitting was done for the ratios at small q, and the slopes of the fitted straight lines were plotted as a function of the film thickness D in Fig. 5.13. According to the non-local theory predictions, $\xi_{NL} \propto \sqrt{D}$, hence, the slopes of the fitted straight lines should be $\xi_{NL}^2/2$ and be proportional to D. We can see from Fig. 5.13, for all even numbers of D, the data for slopes do not fall onto a straight line within error bars, while in log-log plot Fig. 5.14, they fall onto a perfect straight line within error bars, which tells us that the relationship is a simple power law. By fitting the straight line, we can estimate the value of

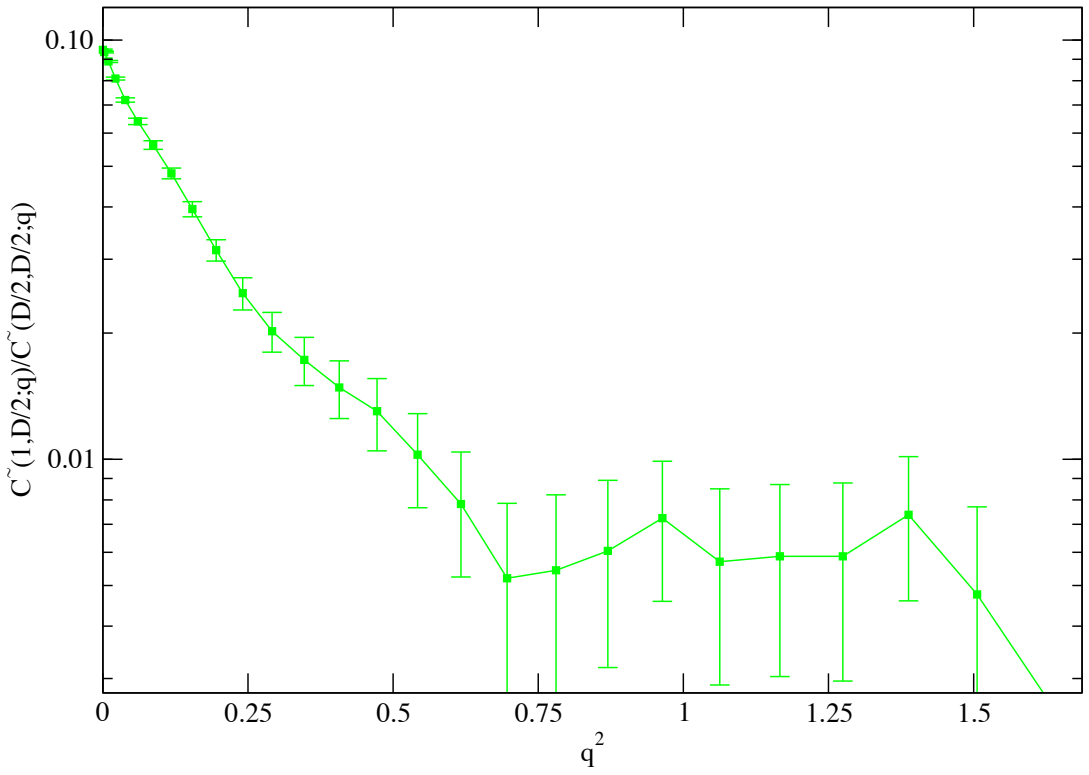

Figure 5.9: Ratio between Fourier transformed correlation function plotted vs q^2 for $L = 128, D = 12, H_1/J = -H_D/J = -0.55, J/k_BT = 0.244$. Plotted on logarithmic scale.

the slope, which turns out to be 1.20 ± 0.0131. For odd D, the slope is slightly different from even D. We can also see that the curves for even D and odd D are apart due to the face that for odd D, the interface is in the middle layer while for even D, the interface is in between two middle layers. The square root of the slopes gives the estimated values of non-local correlation length, ξ_{NL}, which are plotted in Fig. 5.15.

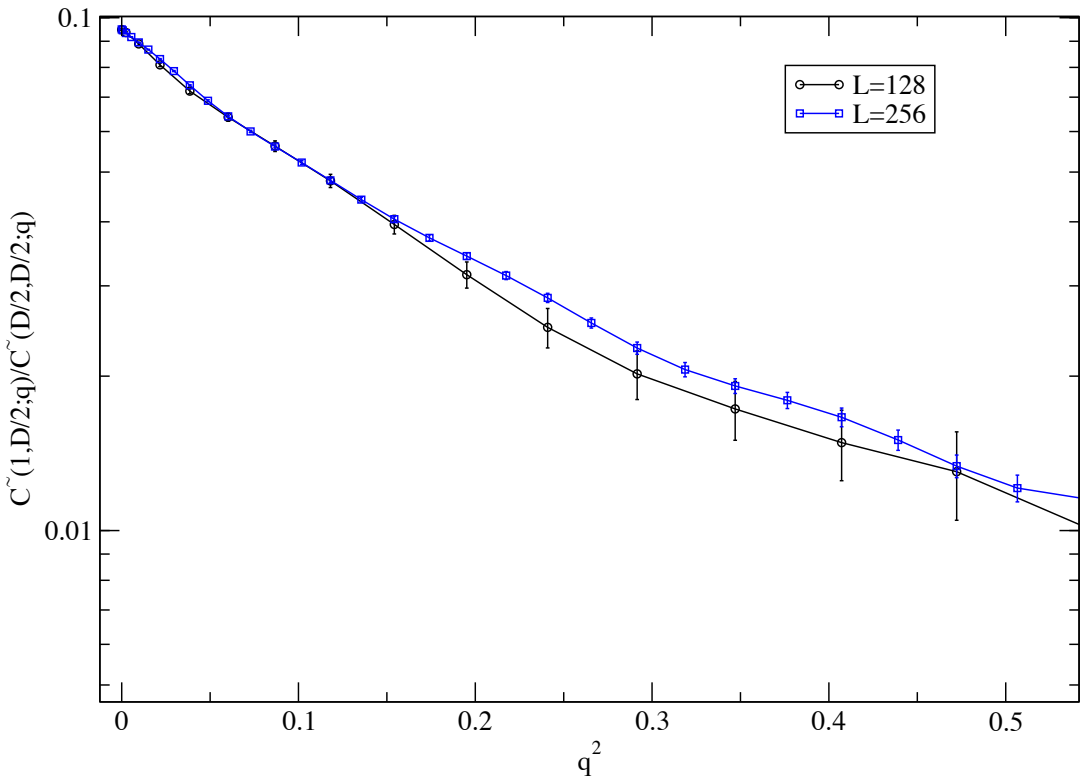

Figure 5.10: Ratio between Fourier transformed correlation function plotted vs q^2 for $L = 256, 512, D = 12, H_1/J = -H_D/J = -0.55, J/k_BT = 0.244$.

5.4 Summary

In summary, extensive Monte Carlo simulations are done for Ising films with $L \times L \times D$ geometry and applied with an opposite surface fields at the temperature $T_w < T < T_{cb}(J/k_BT = 0.244)$. Spin-spin correlations $C(z_1, z_2; \vec{r})$ are calculated for multiple choices of L and D. Three choices of z_1, z_2 combination are chosen, between surface and interface, within interface and within surface, separately. Multiple independent runs are done to estimate the statistical errors. Fourier transformation of these correlations are calculated, and also the ratio

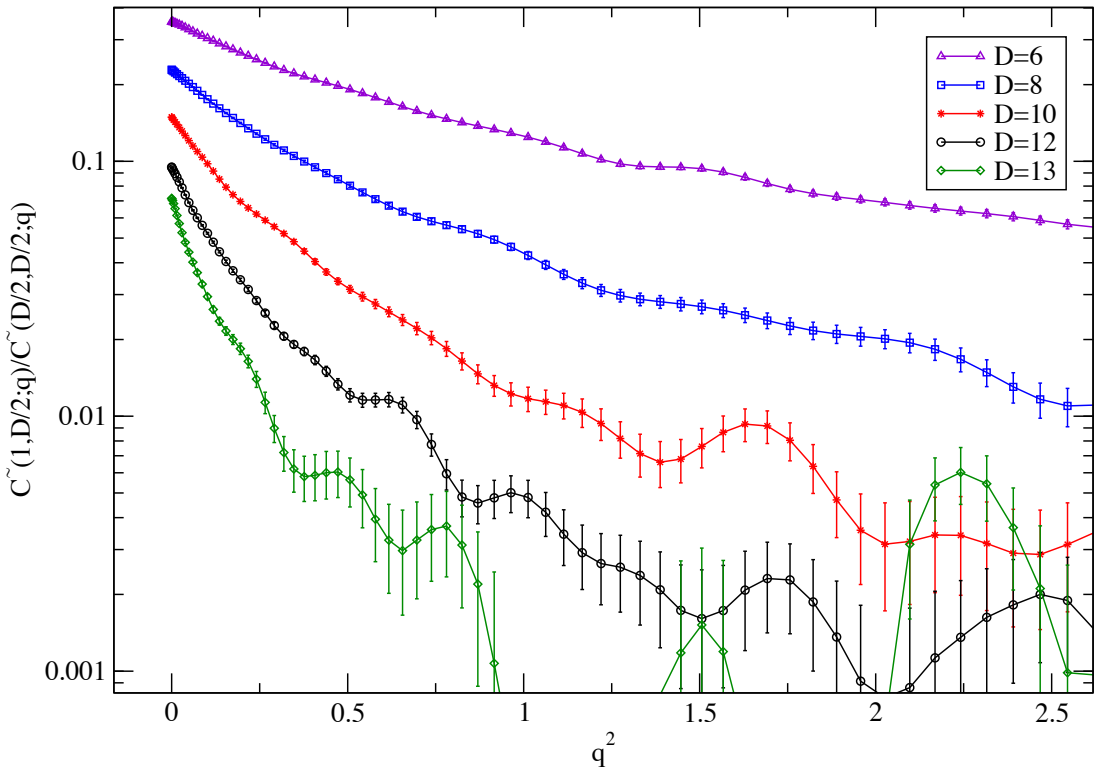

Figure 5.11: Ratio between Fourier transformed correlation function plotted vs q^2 for $L = 256, H_1/J = -H_D/J = -0.55, J/k_BT = 0.244$ and multiple choices of D, $D = 6, 8, 10, 12, 13$.

between the Fourier transformed correlations. We found that the ratio does decay exponentially as the non-local theory predicted, in the region of small q. The linear D dependence of the non-local correlation length ξ_{NL} is not confirmed, instead, we observed a power law relationship with the power of 1.20. The values of ξ_{NL} is also estimated. So, we believe Parry *et al.*'s non-local theory partly solved the long lasting controversy in renormalization group theory, and our simulation results provide the first and most direct confirmation.

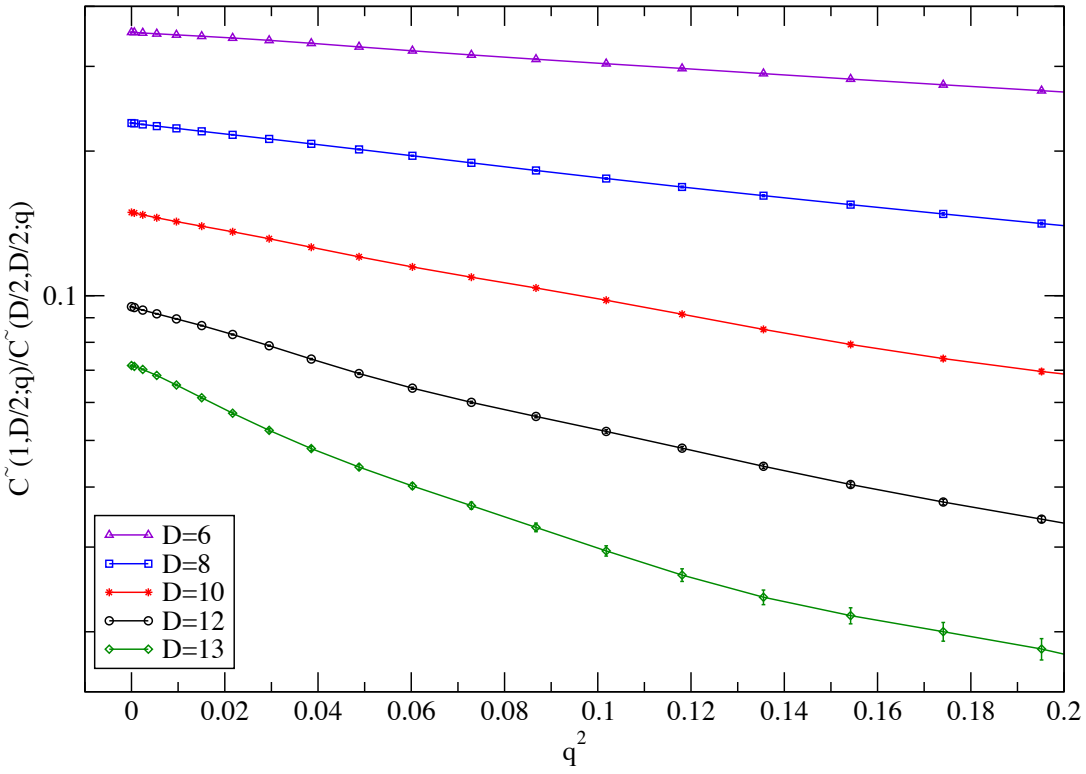

Figure 5.12: Exponential part of the curves shown in Fig. 5.9. Ratio between Fourier transformed correlation function plotted vs q^2 for $L = 256, H_1/J = -H_D/J = -0.55, J/k_BT = 0.244$ and multiple choices of D, $D = 6, 8, 10, 12, 13$.

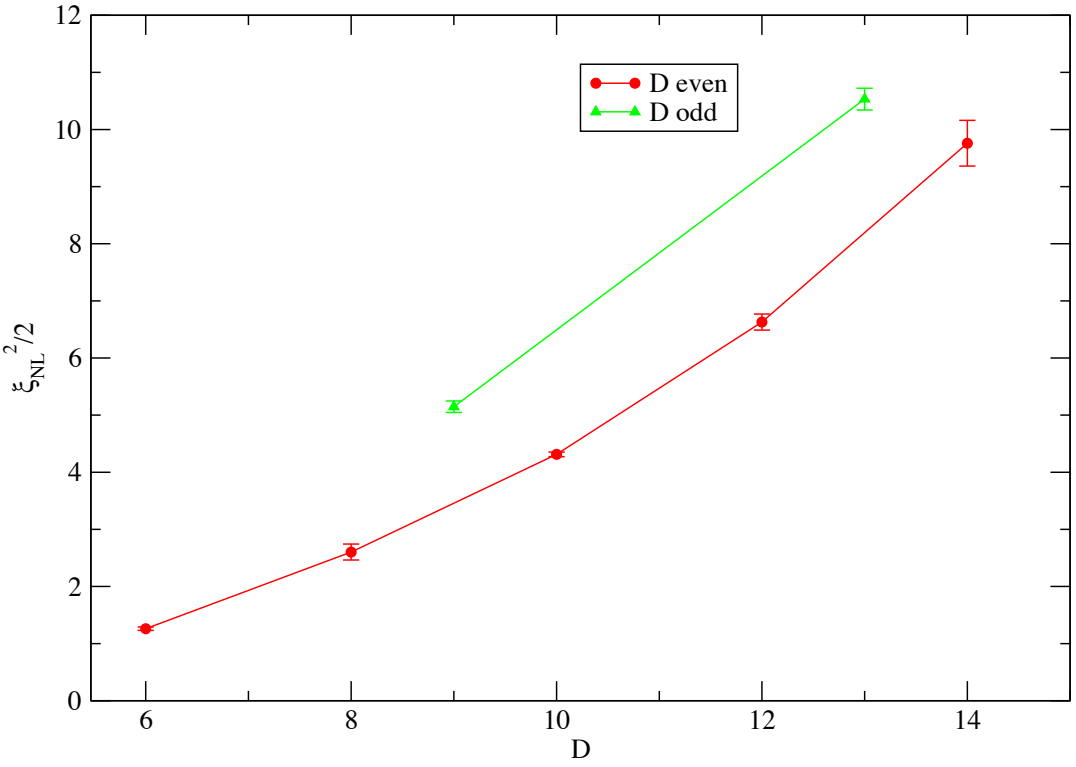

Figure 5.13: Estimation of $\xi_{NL}^2/2$ for different choice of film thickness D. The data are calculated from correlations for $L = 256, H_1/J = -H_D/J = -0.55, J/k_BT = 0.244$.

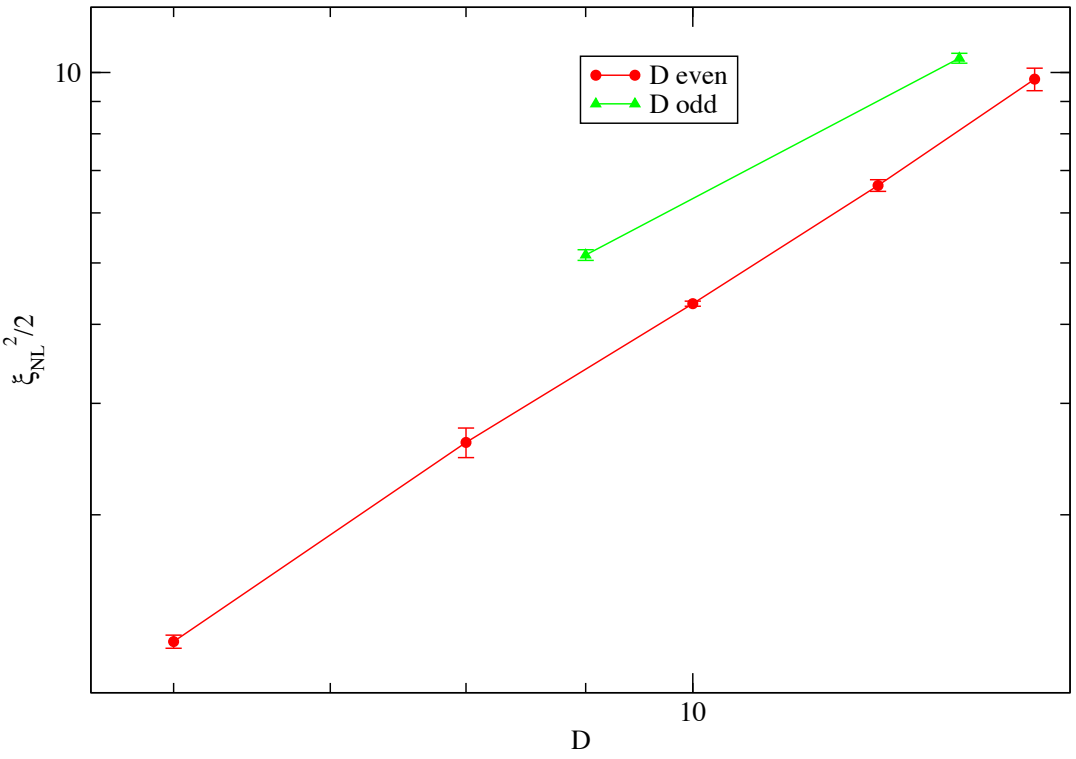

Figure 5.14: Estimation of $\xi_{NL}^2/2$ for different choice of film thickness D in log-log plot. The data are calculated from correlations for $L = 256, H_1/J = -H_D/J = -0.55, J/k_BT = 0.244$.

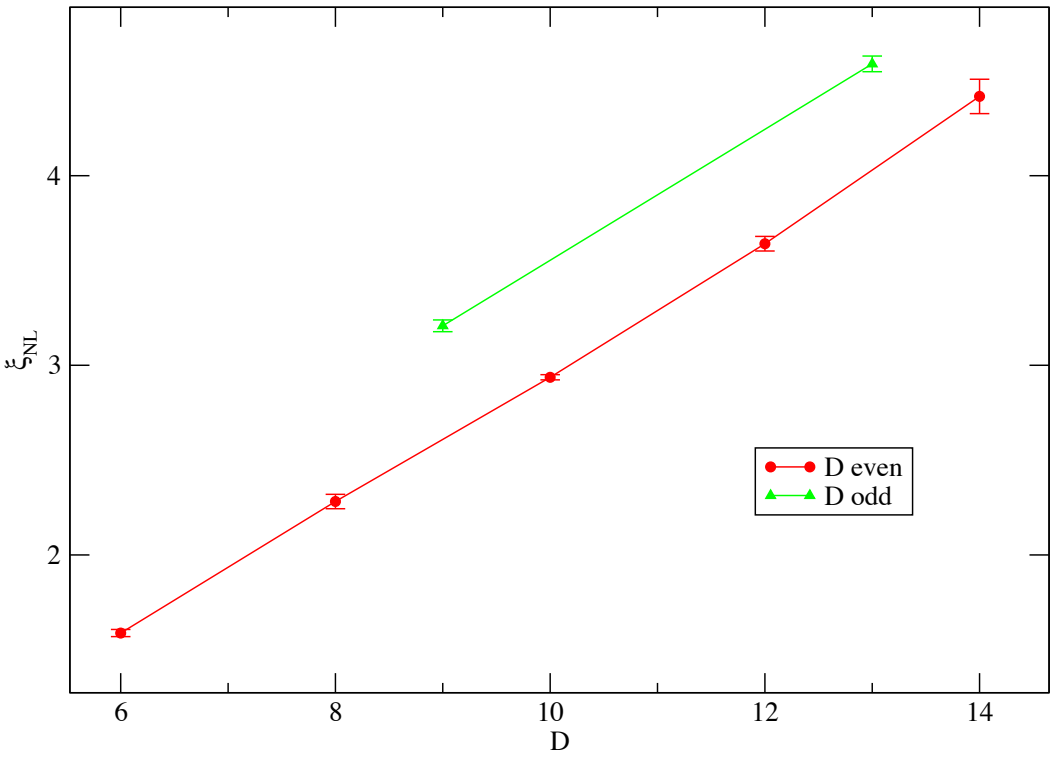

Figure 5.15: Estimation of ξ_{NL} for different choice of film thickness D. The data are calculated from correlations for $L = 256, H_1/J = -H_D/J = -0.55, J/k_BT = 0.244$.

Chapter 6

Conclusion

By making use of the Ising film-liquid-surface analogy we examine two wetting problems.

We studied effects resulting from a linearly varying magnetic field on a thin Ising film, which is equivalent to applying gravity to the corresponding lattice-gas model. We determined the phase diagram by looking for bulk two-phase coexistence at different values of g and temperature T. The addition of the field gradient g competes with the surface field. We confirmed the qualitative phase diagram predicted by theoretical work by Rogiers and Indekeu [54]. As g increases, the temperature bounding bulk two-phase coexistence is re-entrant: For small g, the transition is second order, whereas for large g, the transition is first order. At temperatures above $T_c(D)$, one will encounter phase transitions twice when sweeping the magnitude of g starting from zero.

Using extensive Monte Carlo simulations, we also studied non-local correlation functions in Ising films with the opposite surface fields. Spin-spin correlations are calculated for multiple choices of L and D. Three different choices of correlation are chosen, between surface and interface, within surface, and within the interface. Fourier transformation of these correlations are calculated, and also the ratio between the Fourier transformed correlations. We found that the ratio does decay exponentially as the non-local theory predicted, in the region of small q. The linear D dependence of the non-local correlation length ξ_{NL} is not confirmed, instead, we observed a power law relationship with the power of 1.20. The values of ξ_{NL} is also estimated. Thus, we believe Parry *et al.*' s non-local theory partly solved the long lasting controversy in renormalization group theory, and our simulation provides a direct confirmation.

Bibliography

[1] T. Young. Philos. Trans. Roy. Soc. (London) **95**, 65 (1805).

[2] K. Binder and P. C. Hohenberg, Phys. Rev. B **6**, 3461(1972).

[3] J. W. Cahn, J. Chem. Phys. **66**, 3667 (1977).

[4] C. Ebner and W. F. Saam, Phys. Rev. Lett. **38** 1486 (1977).

[5] D. E. Sullivan, J. Chem. Phys. **74**, 2604 (1981).

[6] H. Nakanishi and M. E. Fisher, Phys. Rev. Letter. **49**, 1565 (1982).

[7] R. Pandit and M. Wortis, Phys. Rev. B **25**, 3226 (1982)

[8] R. Pandit, M. Schick and M. Wortis, Phys. Rev. B **25**, 5112(1982)

[9] K. Binder, Phase Transitions and Critical Phenomena, Domb C and Lebowitz J L, eds. (Academic, New York, 1983), Vol. 8, p.1.

[10] E. Brézin, B. I. Halperin and S. Leibler S, Phys.Rev. Lett. **50**, 1387 (1983).

[11] R. Lipowsky, D. M. Kroll and R. K. P. Zia, Phys. Rev. B **27**, 4499 (1983).

[12] R. Lipowsky and G. Gompper, Z. Phys. B **29**, 5213 (1984)

[13] D. S. Fisher and D. A. Huse, Phys. Rev. B **32**, 247 (1985).

[14] R. Lipowsky, Phys. Rev. B **32**, 1731 (1985)

[15] D. E. Sullivan and M. M. Telo da Gama, Fluid Interfacial Phenomena, ed C A Croxton (London: Wiley) (1986).

[16] M. R. Moldover and J. W. Cahn, Science **207**, 1073 (1980)

[17] Kwon *O*'D, D. Beaglehole, W. W. Webb, B. Widom, J. W. Schmidt, J. W. Cahn, M. R. Moldover, and R. Stephenson, Phys. Rev. Lett. **48**, 185 (1982)

[18] D. W. Pohl and I. Goldburg, Phys. Rev. Lett. **48**, 1111 (1982)

[19] X. L. Wu, M. Schlossman and C. Franck, Phys. Rev. B **33**, 402 (1986)

[20] A. D. Milgone, J. Krim, J. G. Dash, and J. Suzanne, Phys. Rev. B **31**, 7643 (1985)

[21] K. Binder, D. P. Landau and D. M. Kroll, Phys. Rev.Lett. **56**, 2272 (1986).

[22] K. Binder and D. P. Landau, Phys. Rev. B **37**, 1745 (1988).

[23] K. Binder, D. P. Landau and S. Wansleben, Phys. Rev. B **40**, 6979 (1989).

[24] K. Binder, D. P. Landau and M. Muller, J. Stat. Phys. **110**, 1411(2003).

[25] *Fluid Interfacial Phenomena*, edited by Croxton C A (Wiley, New York, 1986); *Liquids at Interface*, edited by Charvolin J, Joanny J F, and Zinn-Justin J (North-Holland, Amsterdam, 1990)

[26] *Physics of Polumer Surfaces and Interfaces*, edited by Sachez I C (Butterworth-Heinemann, Boston, 1992)

[27] H. Nakanishi and M. E. Fisher, J. Chem. Phys. **78**, 3279 (1983).

[28] E. V. Albano, K. Binder, D. W. Heermann, and W. Paul, Surf. Sci. **223**, 15 (1989).

[29] A. O. Parry and R. Evans, Phys. Rev. Lett. **64**, 439 (1990).

[30] M. R. Swift, A. L. Owczarek and J. O. Indekeu, Europhys. Lett. **14**, 475 (1991).

[31] A. O. Parry and R. Evans, Physica A **181**, 250 (1992).

[32] K. Binder, A. M. Ferrenberg and D. P. Landau, Ber. Bunsenges, Phys. Chemie **98**, 340 (1994)

[33] Y. Rouault, J. Baschnagel and K. Binder, J. Stat. Phys. **80**, 1009 (1995)

[34] T. Kerle, J. Klein and K. Binder K, Phys. Rev. Lett. **77**, 1318 (1996)

[35] A. Werner, F. Schmid, K. Binder and J. Mueller, Chem. Phys. **107**, 8175 (1997)

[36] K. Binder, D. P. Landau, and A. M. Ferrenberg, Phys. Rev. E **51**, 2823 (1995);Phys.Rev.Lett. **74**, 298 (1995).

[37] K. Binder, R. Evans, D. P. Landau and A. M. Ferrenberg, Phys Rev. E **53**, 5023 (1996)

[38] M. E. Fisher and A. J. Jin, Phys. Rev. B **44**, 1430 (1991).

[39] A. J. Jin and M. E. Fisher, Phys. Rev. B **47**, 7365 (1993).

[40] M. E. Fisher and A. J. Jin, Phys. Rev. Lett. **69**, 792 (1992).

[41] A. J. Jin and M. E. Fisher, Phys. Rev. B **48**, 1897 (1993).

[42] M. E. Fisher, A. J. Jin and A. O. Parry, Bunsenges. Phys. Chem. **98**, 357 (1994).

[43] C. J. Boulter and A. O. Parry, Phys. Rev. Lett. **74**, 3403 (1995).

[44] A. O. Parry and C. J. Boulter, Physica A **218**, 77 (1995).

[45] C. J. Boulter and A. O. Parry, Physica A **218**, 109 (1995).

[46] P. S. Swain and A. O. Parry, Europhys. Lett. **37**, 207 (1997).

[47] A. O. Parry and P. S. Swain, Physica A **250**, 167, (1998).

[48] A. O. Parry, M. G. Greenall and J. M. Romero-Enrique, J. Phys.: Condens. Matter **24**, 1169 (2004).

[49] A. O. Parry, A. J. Wood and C. Rascón, J. Phys.: Condens. Matter **13**, 4591(2001).

[50] M. E. Fisher and H. Nakanishi, J. Chem. Phys. **75**, 5857 (1981).

[51] A. O. Parry and R. Evans, Phys. Rev. Lett. **64**, 439 (1990)

[52] A. O. Parry and R. Evans, Physica A ***A***, 250 (1992)

[53] F. Brochard-Wyart and P. G. De Gennes, C. R. Acad. Sci. Paris II **297**, 223 (1983).

[54] J. Rogiers and J. O. Indekeu, Europhys. Lett. **24**, 21 (1993).

[55] E. Carlon and A. Drzewiński, Phys. Rev. Lett. **79**, 1591 (1997).

[56] E. Carlon and A. Drzewiński, Phys. Rev. E **57**, 2626 (1998)

[57] D. P. Landau and K. Binder, *A Guide to Monte Carlo Simulations in Statistical Physics.* (Cambridge University Press, Cambridge, 2000).

[58] For reviews of wetting, see Dietrich S, *Phase Transitions and Critical Phenomena.* vol 12, ed C Domb and J L Lebowitz (New York: Academic, 1988).

[59] For a review, see Evans R, *J. Phys. Condens. Matter* 2: 8989, 1990.

[60] C. Rascón and A. O. Parry, Phys. Rev. Lett. **94**, 096103 (2005).

[61] A. O. Parry, M. G. Greenall and J. M. Romero-Enrique, Phys. Rev. Lett. **90**, 046101 (2003).

[62] M. G. Greenall, A. O. Parry and J. M. Romero-Enrique, J. Phys.: Condens.Matter **16**, 2515 (2004).

[63] A. O. Parry, J. M. Romero-Enrique, N. R. Bernardino and C. Rascón, J. Phys.: Condens.Matter **20**, 505102 (2008).

[64] A. O. Parry, J. M. Romero-Enrique and A. Lazarides, Phys. Rev. Lett. **93**, 086104 (2004).

[65] A. O. Parry, C. Rascón, N. R. Bernardino and J. M. Romero-Enrique, Phys.Rev.Lett. **100**, 136105 (2008).

[66] A. O. Parry, C. Rascón, N. R. Bernardino and J. M. Romero-Enrique, J. Phys.: Condens. Matter **18**, 6433 (2006).

[67] A. O. Parry, C. Rascón, N. R. Bernardino and J. M. Romero-Enrique, J. Phys.: Condens. Matter **19**, 416105 (2007).

[68] G. S. Pawley, R. H. Swendsen, D. J. Wallace and K. G. Wilson K G, Phys. Rev. B **29**, 4030 (1984).

[69] K. Binder, D. P. Landau and S. Wansleben, Phys. Rev. B **40**, 6971 (1989).

[70] A. M. Ferrenberg and D. P. Landau, Phys. Rev. B **44**, 5081 (1991).

[71] J. M. J. Van Leeuwen and J. V. Sengers, Physica A **128**, 99 (1984); **138**, 1 (1986).

[72] A. O. Parry and R. Evans, Phys. Rev. Lett. **66**, 2175 (1991).

[73] J. O. Indekeu, A. L. Owczarek and M. R. Swift, Phys. Rev. Lett. **66**, 2174 (1991).

[74] N. Metropolis and S. Ulam, Journal of the American Statistical Association **44**, 335 (1949).

[75] N. Metropolis, A. W. Rosebluth, M. N. Rosenbluth, A. M. Teller, and E. Teller, J. Chem. Phys. **21**, 1087 (1953).

[76] M. Hasenbusch, K. Pinn and S. Vinti, Phys. Rev. B **59**, 11471 (1999).

[77] M. Creutz, Phys. Rev. D **21**, 2308 (1980).

[78] K. Binder, Z. Phys. B **43**, 119 (1981).

[79] T. W. Burkhardt and B. Derrida, Phys. Rev. B **32**, 7273 (1985); A. D. Bruce, J. Phys. A **18**, L873 (1985); D. P. Landau and D. Stauffer, J. Phys. (Paris) **50**, 509 (1989).

[80] see website http://www.physik.uni-leipzig.de/ janke/CompPhys07/Folien/selke-poster2.pdf

[81] H. B. Callen, Thermodynamics And An Introduction to Thermostatistics (2nd Ed.) John Wiley and Sons, New York (1985).

[82] A. D. Bruce, J. Phys. C **14**, 3667 (1981).

[83] D. P. Landau and D. Stauffer, J. Phys. (Paris) **50**, 509 (1989).

[84] D. Nicolaides and A. D. Bruce, J. Phys. A **21**, 233 (1988).

[85] J. A. Plascak and D. P. Landau, Phys. Rev. E **67**, 015103 (R) (2003).

[86] M. M. Tsypin and H. W. J. Blöte, Phys. Rev. E **62**, 73 (2000).

[87] A. D. Bruce and N. B. Wilding, Phys. Rev. Lett. **68**, 193 (1992); N. B. Wilding and A. D. Bruce, J. Phys.: Condens. Matter **4**, 3087 (1992); N. B. Wilding, Phys. Rev. E **52**, 602 (1995).

[88] K. Rummukainen, M. Tsypin, K. Kajantie, M. Laine, and M. Shaposhnikov, Nucl. Phys. B **532**, 283 (1998).

[89] C. Alexandrou, A. Borici, A. Feo, P. de Forcrand, A. Galli, F. Jegerlehner, and T. Takaishi, Phys. Rev. D **60**, 034504 (1999).

[90] M. E. Fisher in *Critical Phenomena*, edited by M. S. Green (Academic, New York, 1971).

[91] A. M. Ferrenberg and R. H. Swendsen, Phys. Rev. Lett. **61**, 2635 (1988).

[92] D. Ross, D. Bonn and J. Meunier, Nature **400**, 737 (1999).

[93] F. Matsubata, A. Sato, O. Koseki and T. Shirakura, Phys. Rev. Lett. **78**, 3237 (1997)

Appendix

Fortran code

```
C*************************************************************
C This is the main function of Monte Carlo simulation.
      Program SurfAsy
      INCLUDE 'sparam.h'
      INTEGER ISeed,I,K,i1,j1,k1,Itry
      INTEGER SMPLRTIO(L3),J
      REAL*8 DLayer,AC,Seed,DL3
      REAL*8 Erg(L3),RLM(L3),E(L3),E2(L3)
      REAL*8 MA(L3),M1(L3),M2(L3),M3(L3),M4(L3)
      REAL*8 MAT,MT1,MT2,MT3,MT4
      REAL*8 ET,ET2,BMT,BET,SUS1,SUSN(L3),SPH(L3)
      REAL*8 SP

      DL3 = 1.0D0/DBLE(L3)
      DLayer = 1.0D0/DBLE(L*L)

      NumLeft = 0


      ISeed = IOSeed
C** Initialize the random number generator
      CALL InitRan(ISeed)
C**  Assign the spins and sublattices
      CALL Init(SMPLRTIO,AC)
C**  Simulation for equilibrium
      DO I = 1,NToss
        CALL Prefer(SMPLRTIO,AC)
      END DO

      SUS1 = 0.0D0
      MAT = 0.0D0
      MT1 = 0.0D0
      MT2 = 0.0D0
      MT3 = 0.0D0
      MT4 = 0.0D0
```

```
      ET = 0.0D0
      ET2 = 0.0D0

      DO J = 1,L3
        MA(J) = 0.0D0
        M1(J) = 0.0D0
        M2(J) = 0.0D0
        M3(J) = 0.0D0
        M4(J) = 0.0D0
        SUSN(J)= 0.0D0
        SPH(J)= 0.0D0
        E(J) = 0.0D0
        E2(J) = 0.0D0
      END DO

C**   Simulation for data
      write(20,*) 'NMCS=',NMCS

      DO I = 1,NMCS

        CALL Prefer(SMPLRTIO,AC)
C**   Now make measurements and accumulate things:
        CALL CalcEM(Erg,RLM,DLayer)
C**   First do Mag:  RLM(J) is the magnetization/spin in plane J

          write(9, 19) (RLM(Itry), Itry=1,12)
19        Format(12F8.4)
        BMT = 0.0D0
        DO J = 1,L3
          BMT = BMT + RLM(J)
          MA(J) = MA(J)+DABS(RLM(J))
          M1(J) = M1(J)+RLM(J)
          M2(J) = M2(J)+RLM(J)*RLM(J)
          M3(J) = M3(J)+RLM(J)*RLM(J)*RLM(J)
          M4(J) = M4(J)+RLM(J)*RLM(J)*RLM(J)*RLM(J)
        END DO
        BMT = BMT*DL3
        MAT = MAT + DABS(BMT)
        MT1 = MT1 + BMT
        MT2 = MT2 + BMT*BMT
        MT3 = MT3 + BMT*BMT*BMT
        MT4 = MT4 + BMT*BMT*BMT*BMT
C**   Now do things dealing with the energy.
C**   Erg(J) is the nearest-neighbor part of the energy (in energy/spin)
C**   for plane J initially, then the magnetic part is added.
        BET = 0.0D0
C        Erg(1) = Erg(1) - H(1)*RLM(1)
```

```
C        Erg(L3) = Erg(L3) - H(L3)*RLM(L3)
         DO J=1,L3
            Erg(J)=Erg(J)- H(J)*RLM(J)
         END DO
         DO J = 1,L3
           BET = BET + Erg(J)
           E(J) = E(J) + Erg(J)
           E2(J) = E2(J) + Erg(J)*Erg(J)
         END DO
         BET = BET*DL3
         write(10,18) BET
18       Format(D16.8)
         ET = ET + BET
         SUS1=SUS1+BMT*(RLM(1)+RLM(L3))
         DO J = 1,L3
           Susn(J) = Susn(J) + BMT*RLM(J)
           SPH(J) = SPH(J) + BET*Erg(J)
         END DO
         ET2 = ET2 + BET*BET
       END DO
        DO K = 1,L3
          DO J = 1,L
             DO I = 1,L
                Write(32, 50) S(I,J,K)
             END DO
          END DO
        END DO
50     Format(I3)



C**  Write out information to the raw data file
       SP=128*128*12*1.111*1.111*(ET2/500-(ET/500)*(ET/500))
       WRITE(44,11) ET2,ET, SP
11     FORMAT(1X, D18.12, D18.12, D18.12)
       WRITE(60,*) L,L3,NMCS,TInvs,Asym,LBulk
C       WRITE(60,*) NMCS,MAT,MT1,MT2,MT3,MT4,ET,ET2,SUS1
       WRITE(60,*) NMCS,MAT,MT1,MT2,MT3,MT4
       WRITE(60,12) ET
       WRITE(60,12) ET2
       WRITE(60,*) SUS1
12     FORMAT(1X,D18.12)
       DO J = 1,L3
         WRITE(60,*) MA(J),M1(J),M2(J),M3(J),M4(J),E(J),E2(J),
      *             SUSN(J),SPH(J)
       END DO
```

```
      CLOSE(UNIT=20)
      CLOSE(UNIT=60)

      END


C*********************************************************************
C This subroutine is used to initialize the model.
      SUBROUTINE Init(SMPLRTIO,AC)
      INCLUDE 'sparam.h'
      INTEGER SMPLRTIO(L3),II2,L33,IIRan
      REAL*8 DSMPLRTIO(L3),DD0,DD1,DD2,g
      REAL*8 AC,A,DIA,DL3A,ARGUMENT
      INTEGER I,J,II,JJ,K
      INTEGER Im,Jm,ID,INum,JMin,JMax,I1
      CHARACTER*60 DLine
      g=0.010
C**
C**  Read in the parameters for the run
C**
      READ(*,*) TInvs,HSurf,JSurf,HBulk,ASym,LStart,HStart
C**
C**  Calculate the magnetic fields
C**
      IF (HStart .EQ. 0) THEN
C**
C**  Symmetric or antisymmetric case with no field gradient
C**
        DO I = 1,L3
          H(I) = HBulk
        END DO
        H(1) =  H(1) + HSurf
        H(L3) =  H(L3) + Asym*HSurf
      ELSE IF (HStart .EQ. 1) THEN
C**
C**  Antisymmetric case with linear field gradient
C**
        IF (Asym .NE. -1) THEN
          WRITE(*,*) 'Asym must be -1 for field gradient.'
          STOP
        END IF
        H(1)=HBulk+HSurf+g*L3M1
        H(L3)=HBulk+Asym*HSurf-g*L3M1
        DO I = 2,L3-1
          H(I) = HBulk+g*(L3 + 1 - 2*I)
        END DO
```

```
      ELSE IF (HStart .EQ. 2) THEN
C**
C**  Antisymmetric case with 1/r^3 field gradient
C**
        IF (Asym .NE. -1) THEN
          WRITE(*,*) 'Asym must be -1 for field gradient.'
          STOP
        END IF
        L33 = L3*L3*L3
        DD0 = HSurf*DBLE(L33)/DBLE(L33 - 1)
        DO I = 1,L3
          DD1 = 1.0D0/DBLE(I*I*I)
          II2 = L3 + 1 - I
          DD2 = 1.0D0/DBLE(II2*II2*II2)
          H(I) = DD0*(DD1 - DD2)
        END DO
      END IF

C**
C**  Open the output (UNIT 20) and raw (UNIT 60) data files
C**
        OPEN(UNIT=20,STATUS='OLD')
        OPEN(UNIT=60,STATUS='OLD')
C**
C**  Write out the header information for the output data file
C**
      WRITE(20,*) '*****************************************'
      WRITE(20,*) ' Ising program, version 2.0:  6/26/96'
      WRITE(20,*) ' Scalar simulation'
      WRITE(20,*) ' Heatbath algorithm, slab geometry'
      WRITE(20,*) ' Free BC in Z direction'
      WRITE(20,*) ' Periodic BC in X and Y directions'
      WRITE(20,*) ' Symmetrization of quantities included'
      WRITE(20,*) ' Linear and cubic field gradients included'
      WRITE(20,*) ' New quantities added to output'
      WRITE(20,*) ' Cumulant added to output'
      WRITE(20,*) ' Antisymmetric surface fields'
      WRITE(20,*) ' R250 random number generator'
      WRITE(20,*) ' New output format'
      WRITE(20,*) '*****************************************'
      WRITE(20,*)
      WRITE(20,*) '*****************************************'
      WRITE(20,*) 'Run parameters:'
      WRITE(20,*)
      WRITE(20,*) 'L       = ',L
      WRITE(20,*) 'L3      = ',L3
      WRITE(20,*) 'NMax    = ',NMax
```

```
      WRITE(20,*) 'NGrid   = ',NGrid
      WRITE(20,*) 'NSkip   = ',NSkip
      WRITE(20,*) 'RTio    = ',RTio
      WRITE(20,*) 'LBulk   = ',LBulk
      WRITE(20,*) 'TInvs   = ',TInvs
      WRITE(20,*) 'SurfCpl = ',JSurf
      WRITE(20,*) 'HBlk    = ',HBulk
      WRITE(20,*) 'HSurf   = ',HSurf
      WRITE(20,*) 'IOSeed  = ',IOSeed
      WRITE(20,*) 'LStart  = ',LStart
      WRITE(20,*) 'ASym    = ',ASym
      WRITE(20,*) 'HStart  = ',HStart
      WRITE(20,*) '****************************************'


C**
C**  Boltzmann weights for the bulk:  with bulk field
C**  Bolt(I) is the probability that the spin is up.
      DO J = 1,L3
        DO I = -6,6
          ARGUMENT = 2.0D0*TInvs*(DBLE(I) + H(J))
          BOLT(I,J) = IMax/(1.0D0 + DEXP(-ARGUMENT))
        END DO
      END DO

C**
C**  Boltzmann weights for the surface layers
C**
      DO J = -1,1,2
        DO I = -4,4
          ARGUMENT = 2.0D0*TInvs*(JSurf*DBLE(I) + DBLE(J) + H(1))
          BOLTST(I,J) = IMax/(1.0D0 + DEXP(-ARGUMENT))
          ARGUMENT = 2.0D0*TInvs*(JSurf*DBLE(I) + DBLE(J) + H(L3))
          BOLTSB(I,J) = IMax/(1.0D0 + DEXP(-ARGUMENT))
        END DO
      END DO

C**  Initialize the preferential sampling array
      IF (RTio .EQ. 0.0D0) THEN
        DO I = 1,L3
          SMPLRTIO(I) = 1.0D0
        END DO
      ELSEIF (RTio .GT. 0.0D0) THEN
        A = DLOG(RTIO + DSQRT(RTIO*RTIO - 1.0D0))/(0.5D0*(L3 - 2))
        DO I = 1,L3/2
          DIA = DBLE(I)*A
          DL3A = DBLE(L3)*A
```

```
          SMPLRTIO(I) = 0.5D0*DEXP(-0.5D0*DL3A) *
     &                  (DEXP(DIA) + DEXP(DL3A - DIA)) + 1.0D-3
          SMPLRTIO(L3-I+1) = SMPLRTIO(I)
        END DO
       ELSE
        A = DLOG(DABS(RTIO) + DSQRT(RTIO*RTIO - 1.0D0))/(0.5D0*(L3 - 2))
        DO I = 1,L3/2
          DIA = DBLE(I)*A
          DL3A = DBLE(L3)*A
          DSMPLRTIO(I) = 2.0D0*DEXP(0.5D0*DL3A) /
     &                  (DEXP(DIA) + DEXP(DL3A - DIA)) + 1.0D-3
          DSMPLRTIO(L3-I+1) = DSMPLRTIO(I)
        END DO
        DO I = 1,L3
          SMPLRTIO(I) = IDNINT(DSMPLRTIO(I)/DSMPLRTIO(1))
        END DO
       END IF
C**  Write out the preferential sampling array
       WRITE(20,*)
       WRITE(20,*)
       WRITE(20,*) 'Sample-ratios for layers'
       WRITE(20,*)
       IF (L3 .LT. 16) THEN
         WRITE(20,1) (SMPLRTIO(I), I = 1,L3)
1          FORMAT(1X,16I4)
       ELSE
         II = L3/16
         DO J = 1,II
           JMin = (J - 1)*16 + 1
           JMax = J*16
           WRITE(20,1) (SMPLRTIO(I), I = JMin,JMax)
         END DO
         J = L3 - 16*II
         JMin = JMax + 1
         JMax = L3
         WRITE(20,1) (SMPLRTIO(I), I = JMin,JMax)
       END IF
C**  Normalize and integrate the sampling array
       AC = 0.0D0
       DO I = 1,L3
         AC = AC + DBLE(SMPLRTIO(I))
       END DO
       DO I = 2,L3
         ID = 0.0D0
         DO J = 1,L3+1-I
           ID = ID + SMPLRTIO(J)
         END DO
```

```
        SMPLRTIO(L3+2-I) = ID
      END DO
      SMPLRTIO(1) = 0

C**  Now initialize the spins.  This depends on the parameter LStart
C**    LStart = -N ---> Bulk ferro, top N layers ferro but opposite bulk
C**    LStart = 1  ---> Bulk ferro, surface ferro
C**    LStart = 2  ---> Bulk and surface random
C**    Lstart = 3  ---> Input initial configuration from file
      IF (LStart .GT. 3) THEN
        WRITE(*,*) 'Error: LStart must be less than or equal to two.'
        STOP
      ELSE IF (LStart .LT. -L3/2) THEN
        DLine='Error: LStart must be greater than or equal to -L3/2'
        WRITE(*,*) DLine
        STOP
      ELSE IF (LStart .EQ. 0) THEN
        DLine='Antiferromagnetic initialization (LStart = 0) is not'
        WRITE(*,*) DLine
        DLine='supported in this version of the program.  Sorry.'
        WRITE(*,*) DLine
        STOP
      END IF

C**  For rest, start all spins up
      DO K = 1,L3
        DO J = 1,L
          DO I = 1,L
            S(I,J,K) = 1
          END DO
        END DO
      END DO
C**  Now make the necessary changes
C**  For LStart=1, no changes are needed
      IF (LStart .LT. 0) THEN
        DO K = IABS(LStart)+1, L3
          DO J = 1,L
            DO I = 1,L
              S(I,J,K) = -1
            END DO
          END DO
        END DO
           DO K = 1,L3
             DO J = 1,L
               DO I = 1,L
                   write(35, 70) S(I,J,K)
               END DO
```

```
            END DO
          END DO
70        Format(I3)

      ELSE IF (LStart .EQ. 2) THEN
        DO K = 1,L3
          CALL GetRan(NLayer)
          IIRan = 250
          DO J = 1,L
            DO I = 1,L
              IF (RanVec(IIRan+I) .LT. IMax2) S(I,J,K) = -1
            END DO
            IIRan = IIRan + L
          END DO
        END DO
      Else if (LStart .EQ. 3) then
         OPEN(UNIT=30, FILE='initconfig.dat', STATUS='OLD')
          DO K = 1,L3
            DO J = 1,L
              DO I = 1,L
                  Read (30, 50) S(I,J,K)
                  write(33, 50) S(I,J,K)
              END DO
            END DO
          END DO
50        Format(I3)
         CLOSE(30)
      END IF

      RETURN
      END


C**********************************************************************
C This subroutine is used to do the sampling in the bulk layers.
      SUBROUTINE MCBulk(IZ,IZM1,IZP1)
      INCLUDE 'sparam.h'
      INTEGER I,J,Im,Jm,Ip,Jp,NSum,IRan,NumRan
      INTEGER IZ,IZM1,IZP1

      CALL GetRan(NLayer)

C**  Do the (4*L - 2) spins on the boundary
C**  First the four corners
C**    S(1,1)
      NSum = S(L,1,IZ)+S(2,1,IZ)+S(1,L,IZ)+S(1,2,IZ)+
     *       S(1,1,IZM1) + S(1,1,IZP1)
```

```
       S(1,1,IZ) = -1
       IF (RanVec(251) .LT. Bolt(NSum,IZ)) S(1,1,IZ) = 1

C**    S(1,L)
      NSum = S(L,L,IZ)+S(2,L,IZ)+S(1,LM1,IZ)+S(1,1,IZ)+
     *       S(1,L,IZM1) + S(1,L,IZP1)

       S(1,L,IZ) = -1
       IF (RanVec(252) .LT. Bolt(NSum,IZ)) S(1,L,IZ) = 1

C**    S(L,1)
      NSum = S(LM1,1,IZ)+S(1,1,IZ)+S(L,L,IZ)+S(L,2,IZ)+
     *       S(L,1,IZM1) + S(L,1,IZP1)

       S(L,1,IZ) = -1
       IF (RanVec(253) .LT. Bolt(NSum,IZ)) S(L,1,IZ) = 1

C**    S(L,L)
      NSum = S(LM1,L,IZ)+S(1,L,IZ)+S(L,LM1,IZ)+S(L,1,IZ)+
     *       S(L,L,IZM1) + S(L,L,IZP1)

       S(L,L,IZ) = -1
       IF (RanVec(254) .LT. Bolt(NSum,IZ)) S(L,L,IZ) = 1

C**  Now do rest of J = 1
       DO I = 2,LM1
         NSum = S(I-1,1,IZ)+S(I+1,1,IZ)+S(I,L,IZ)+S(I,2,IZ)+
     *          S(I,1,IZM1)+S(I,1,IZP1)

          S(I,1,IZ) = -1
          IF (RanVec(253+I) .LT. Bolt(NSum,IZ)) S(I,1,IZ) = 1
        END DO

C**  Now do rest of J = L
       NumRan = 253 + LM2
       DO I = 2,LM1
         NSum = S(I-1,L,IZ)+S(I+1,L,IZ)+S(I,LM1,IZ)+S(I,1,IZ)+
     *          S(I,L,IZM1)+S(I,L,IZP1)

          S(I,L,IZ) = -1
          IF (RanVec(NumRan + I) .LT. Bolt(NSum,IZ)) S(I,L,IZ) = 1
        END DO

C**  Now do rest of I = 1
       NumRan = NumRan + LM2
       DO J = 2,LM1
```

```
          NSum = S(L,J,IZ)+S(2,J,IZ)+S(1,J-1,IZ)+S(1,J+1,IZ)+
     *           S(1,J,IZM1)+S(1,J,IZP1)

          S(1,J,IZ) = -1
          IF (RanVec(NumRan+J) .LT. Bolt(NSum,IZ)) S(1,J,IZ) = 1
        END DO

C**  Now do rest of I = L
        NumRan = NumRan + LM2
        DO J = 2,LM1
          NSum = S(LM1,J,IZ)+S(1,J,IZ)+S(L,J-1,IZ)+S(L,J+1,IZ)+
     *           S(L,J,IZM1)+S(L,J,IZP1)

          S(L,J,IZ) = -1
          IF (RanVec(NumRan+J) .LT. Bolt(NSum,IZ)) S(L,J,IZ) = 1
        END DO

C**  Now do the rest of the layer
       NumRan = NumRan + LM2
       DO J = 2,LM1
         DO I = 2,LM1,2
           NSum = S(I-1,J,IZ)+S(I+1,J,IZ)+S(I,J-1,IZ)+S(I,J+1,IZ)+
     *            S(I,J,IZM1)+S(I,J,IZP1)

           S(I,J,IZ) = -1
           IF (RanVec(NumRan+I) .LT. Bolt(NSum,IZ)) S(I,J,IZ) = 1

           NSum = S(I,J,IZ)+S(I+2,J,IZ)+S(I+1,J-1,IZ)+S(I+1,J+1,IZ)+
     *            S(I+1,J,IZM1)+S(I+1,J,IZP1)

           S(I+1,J,IZ) = -1
           IF (RanVec(NumRan+I+1) .LT. Bolt(NSum,IZ)) S(I+1,J,IZ) = 1
         END DO
         NumRan = NumRan + LM2
       END DO

       RETURN
       END


C**********************************************************************
C The following two subroutines are used to do the sampling on the both surfaces.
       SUBROUTINE MCTop
       INCLUDE 'sparam.h'
       INTEGER I,J,Im,Jm,Ip,Jp,NSum,IRan,NumRan

       CALL GetRan(NLayer)
```

```
C**  Do the (4*L - 2) spins on the boundary
C**  First the four corners
C**    S(1,1)
      NSum = S(L,1,1) + S(2,1,1) + S(1,L,1) + S(1,2,1)
      S(1,1,1) = -1
      IF (RanVec(251) .LT. BoltST(NSum,S(1,1,2))) S(1,1,1) = 1

C**    S(1,L)
      NSum = S(L,L,1) + S(2,L,1) + S(1,LM1,1) + S(1,1,1)
      S(1,L,1) = -1
      IF (RanVec(252) .LT. BoltST(NSum,S(1,L,2))) S(1,L,1) = 1

C**    S(L,1)
      NSum = S(LM1,1,1) + S(1,1,1) + S(L,L,1) + S(L,2,1)
      S(L,1,1) = -1
      IF (RanVec(253) .LT. BoltST(NSum,S(L,1,2))) S(L,1,1) = 1

C**    S(L,L)
      NSum = S(LM1,L,1) + S(1,L,1) + S(L,LM1,1) + S(L,1,1)

      S(L,L,1) = -1
      IF (RanVec(254) .LT. BoltST(NSum,S(L,L,2))) S(L,L,1) = 1

C**  Now do rest of J = 1
      DO I = 2,LM1
        NSum = S(I-1,1,1) + S(I+1,1,1) + S(I,L,1) + S(I,2,1)

        S(I,1,1) = -1
        IF (RanVec(253+I) .LT. BoltST(NSum,S(I,1,2))) S(I,1,1)=1
      END DO

C**  Now do rest of J = L
       NumRan = 253 + LM2
       DO I = 2,LM1
         NSum = S(I-1,L,1) + S(I+1,L,1) + S(I,LM1,1) + S(I,1,1)

         S(I,L,1) = -1
         IF (RanVec(NumRan+I).LT.BoltST(NSum,S(I,L,2))) S(I,L,1)=1
       END DO

C**  Now do rest of I = 1
       NumRan = NumRan + LM2
       DO J = 2,LM1
         NSum = S(L,J,1) + S(2,J,1) + S(1,J-1,1) + S(1,J+1,1)

         S(1,J,1) = -1
```

```
          IF (RanVec(NumRan+J).LT.BoltST(NSum,S(1,J,2))) S(1,J,1)=1
        END DO

C**  Now do rest of I = L
        NumRan = NumRan + LM2
        DO J = 2,LM1
          NSum = S(LM1,J,1) + S(1,J,1) + S(L,J-1,1) + S(L,J+1,1)

          S(L,J,1) = -1
          IF (RanVec(NumRan+J).LT.BoltST(NSum,S(L,J,2))) S(L,J,1) = 1
        END DO

C**  Now do the rest of the layer
       NumRan = NumRan + LM2
       DO J = 2,LM1
         DO I = 2,LM1,2
C**  Sum of the in-plane neighbors
           NSum = S(I-1,J,1)+S(I+1,J,1)+S(I,J-1,1)+S(I,J+1,1)

           S(I,J,1) = -1
           IF (RanVec(NumRan+I).LT.BoltST(NSum,S(I,J,2))) S(I,J,1)=1

           NSum = S(I,J,1)+S(I+2,J,1)+S(I+1,J-1,1)+S(I+1,J+1,1)

           S(I+1,J,1) = -1
           IF (RanVec(NumRan+I+1).LT.BoltST(NSum,S(I+1,J,2)))
     *         S(I+1,J,1)=1
         END DO
         NumRan = NumRan + LM2
       END DO

       RETURN
       END

C**********************************************************************
       SUBROUTINE MCBot
       INCLUDE 'sparam.h'
       INTEGER I,J,Im,Jm,Ip,Jp,NSum,IRan,NumRan

       CALL GetRan(NLayer)

C**  Do the (4*L - 2) spins on the boundary
C**  First the four corners
C**    S(1,1)
       NSum = S(L,1,L3) + S(2,1,L3) + S(1,L,L3) + S(1,2,L3)

       S(1,1,L3) = 1
```

```
      IF (RanVec(251).GT.BoltSB(NSum,S(1,1,L3M1))) S(1,1,L3)=-1

C**    S(1,L)
      NSum = S(L,L,L3) + S(2,L,L3) + S(1,LM1,L3) + S(1,1,L3)

      S(1,L,L3) = 1
      IF (RanVec(252).GT.BoltSB(NSum,S(1,L,L3M1))) S(1,L,L3)=-1

C**    S(L,1)
      NSum = S(LM1,1,L3) + S(1,1,L3) + S(L,L,L3) + S(L,2,L3)

      S(L,1,L3) = 1
      IF (RanVec(253).GT.BoltSB(NSum,S(L,1,L3M1))) S(L,1,L3)=-1

C**    S(L,L)
      NSum = S(LM1,L,L3) + S(1,L,L3) + S(L,LM1,L3) + S(L,1,L3)

      S(L,L,L3) = 1
      IF (RanVec(254).GT.BoltSB(NSum,S(L,L,L3M1))) S(L,L,L3)=-1

C**  Now do rest of J = 1
      DO I = 2,LM1
        NSum = S(I-1,1,L3) + S(I+1,1,L3) + S(I,L,L3) + S(I,2,L3)

        S(I,1,L3) = 1
        IF (RanVec(253+I).GT.BoltSB(NSum,S(I,1,L3M1)))
     *       S(I,1,L3) = -1
      END DO

C**  Now do rest of J = L
       NumRan = 253 + LM2
       DO I = 2,LM1
         NSum = S(I-1,L,L3) + S(I+1,L,L3) + S(I,LM1,L3) + S(I,1,L3)

         S(I,L,L3) = 1
         IF (RanVec(NumRan+I).GT.BoltSB(NSum,S(I,L,L3M1)))
     *     S(I,L,L3) = -1
       END DO

C**  Now do rest of I = 1
       NumRan = NumRan + LM2
       DO J = 2,LM1
         NSum = S(L,J,L3) + S(2,J,L3) + S(1,J-1,L3) + S(1,J+1,L3)

         S(1,J,L3) = 1
         IF (RanVec(NumRan+J).GT.BoltSB(NSum,S(1,J,L3M1)))
     *     S(1,J,L3) = -1
```

```
       END DO

C**  Now do rest of I = L
       NumRan = NumRan + LM2
       DO J = 2,LM1
         NSum = S(LM1,J,L3) + S(1,J,L3) + S(L,J-1,L3) + S(L,J+1,L3)

         S(L,J,L3) = 1
         IF (RanVec(NumRan+J).GT.BoltSB(NSum,S(L,J,L3M1)))
     *     S(L,J,L3) = -1
       END DO

C**  Now do the rest of the layer
      NumRan = NumRan + LM2
      DO J = 2,LM1
        DO I = 2,LM1,2
C**  Sum of the in-plane neighbors
          NSum = S(I-1,J,L3) + S(I+1,J,L3) + S(I,J-1,L3) + S(I,J+1,L3)

          S(I,J,L3) = 1
          IF (RanVec(NumRan+I).GT.BoltSB(NSum,S(I,J,L3M1)))
     *      S(I,J,L3)= -1

          NSum = S(I,J,L3) + S(I+2,J,L3)+S(I+1,J-1,L3)+S(I+1,J+1,L3)

          S(I+1,J,L3) = 1
          IF (RanVec(NumRan+I+1).GT.BoltSB(NSum,S(I+1,J,L3M1)))
     *      S(I+1,J,L3)= -1
        END DO
        NumRan = NumRan + LM2
      END DO

      RETURN
      END


C**********************************************************************
C This subroutine is used to calculate the energy and magnetization.
      SUBROUTINE CalcEM(E,AM,DLayer)
      INCLUDE 'sparam.h'
      INTEGER EIn(L3),EBet(L3),Mag(L3),I,J,Im,Jm,IZ,IZM1
      REAL*8 E(L3),DLayer,AM(L3)

      IZM1 = L3
      DO IZ = 1,L3
C**  S(1,1)
        EIn(IZ) = S(1,1,IZ)*(S(L,1,IZ) + S(1,L,IZ))
```

```
        EBet(IZ) = S(1,1,IZ)*S(1,1,IZM1)
        Mag(IZ) = S(1,1,IZ)

C**  Now do the rest of I = 1
       DO J = 2,L
          EIn(IZ) = EIn(IZ) + S(1,J,IZ)*(S(L,J,IZ) + S(1,J-1,IZ))
          EBet(IZ) = EBet(IZ) + S(1,J,IZ)*S(1,J,IZM1)
          Mag(IZ) = Mag(IZ) + S(1,J,IZ)
        END DO
C**  Now do the rest of J = 1
       DO I = 2,L
          EIn(IZ) = EIn(IZ) + S(I,1,IZ)*(S(I-1,1,IZ) + S(I,L,IZ))
          EBet(IZ) = EBet(IZ) + S(I,1,IZ)*S(I,1,IZM1)
          Mag(IZ) = Mag(IZ) + S(I,1,IZ)
        END DO
C**  Now do the rest of the layer
        DO J = 2,L
          DO I = 2,L
            EIn(IZ) = EIn(IZ) + S(I,J,IZ)*(S(I-1,J,IZ) + S(I,J-1,IZ))
            EBet(IZ) = EBet(IZ) + S(I,J,IZ)*S(I,J,IZM1)
            Mag(IZ) = Mag(IZ) + S(I,J,IZ)
          END DO
        END DO
        IZM1 = IZ
      END DO

C**  The nearest-neighbor contribution to the energy consists of the
C**  in-plane energy plus half the inter-plane energy above and below,
C**  except for the top and bottom layers.

      E(1) = JSurf*EIn(1) + 0.5D0*EBet(2)
      E(L3)= JSurf*EIn(L3)+ 0.5D0*EBet(L3)

      DO I = 2,L3M1
        E(I) = EIn(I) + 0.5D0*(EBet(I) + EBet(I+1))
      END DO
      DO I = 1,L3
        E(I) = -E(I)*DLayer
        AM(I) = Mag(I)*DLayer
      END DO

      RETURN
      END


C*********************************************************************
C This subroutine is used to realize the preferential layer selection.
```

```
      SUBROUTINE Prefer(SMPLRTIO,AC)
      INCLUDE 'sparam.h'
      INTEGER II,I,SMPLRTIO(L3),J
      REAL*8 AC,RND,IRan

      DO J = 1,NGrid
        IF (NumLeft .LT. L3) THEN
          CALL GetRan(LayNum)
          DO I = 1,LayNum
            LayVec(I) = RanVec(I + 250)
          END DO
          NumLeft = LayNum
        END IF

        DO II = 1,L3
          RND = AC*LayVec(II+LayNum-NumLeft)*DMax

          I = L3 + 1
C**  Find the plane to update
7777      I = I - 1
          IF (RND .LT. SMPLRTIO(I)) GOTO 7777

C          WRITE(*,*) 'I = ',I,'  RND = ',RND
          IF (I.EQ.1) THEN
            CALL MCTop
          ELSEIF (I.EQ.L3) THEN
            CALL MCBot
          ELSE
            CALL MCBulk(I,I-1,I+1)
          END IF
        END DO
        NumLeft = NumLeft - L3
      END DO

      RETURN
      END


C**********************************************************************
C This subroutine is used to generate random numbers.
       SUBROUTINE InitRan(ISeed)
       INCLUDE 'sparam.h'
       INTEGER ISeed,IMod,I,J,K
       REAL*8 RMod,PMod

       RMod = DBLE(ISeed)
       PMod = 2147483647.0D0
```

```
       DO I = 1,1000
         RMod = RMod*16807.0D0
         IMod = RMod*DMax
         RMod = RMod - PMod*IMod
       END DO

       DO I = 1,250
         RanVec(I) = 0
         DO J = 0,30
           DO K = 1,36
             RMod = RMod*16807.0D0
             IMod = RMod*DMax
             RMod = RMod - PMod*IMod
           END DO
           RMod = RMod*16807.0D0
           IMod = RMod*DMax
           RMod = RMod - PMod*IMod
           IF (RMod .GT. 0.5D0*PMod) RanVec(I) = IBSET(RanVec(I),J)
         END DO
       END DO

       CALL GetRan(1000)

       RETURN
       END

C**********************************************************************
      SUBROUTINE GetRan(Number)
      INCLUDE 'sparam.h'
      INTEGER Number,I,Temp1,Temp2

c      integer _KII1, _KII2
c      double precision _KDD1 (257)

      Temp2 = MAX0(Number/4,0)
      Temp1 = Temp2*4 + 1
      DO I = 1,Number-3,4
        RanVec(I+250) = IEOR(RanVec(I),   RanVec(I+147))
        RanVec(I+251) = IEOR(RanVec(I+1), RanVec(I+148))
        RanVec(I+252) = IEOR(RanVec(I+2), RanVec(I+149))
        RanVec(I+253) = IEOR(RanVec(I+3), RanVec(I+150))
      END DO
      DO I = Temp1,Number
        RanVec(I+250) = IEOR(RanVec(I),RanVec(I+147))
      END DO
```

```
      DO I = 1,247,4
        RanVec(I) = RanVec(I+Number)
        RanVec(I+1) = RanVec(I+Number+1)
        RanVec(I+2) = RanVec(I+Number+2)
        RanVec(I+3) = RanVec(I+Number+3)
      END DO
      do I=249,250,1
        RanVec(I) = RanVec(I+Number)
      end do

      RETURN
      END

C**********************************************************************
C This program is used to do the post calculations after Monte Carlo.
      PROGRAM PostCalc
      IMPLICIT NONE
      INTEGER L3MAX
      PARAMETER(L3MAX = 4096)
      REAL*8 SUS1,ET,ET2
      REAL*8 MAT,MT1,MT2,MT3,MT4
      REAL*8 MA(L3MAX),M1(L3MAX),M2(L3MAX),M3(L3MAX),M4(L3MAX)
      REAL*8 E(L3MAX),E2(L3MAX)
      REAL*8 Sym(L3MAX),SymE(L3MAX),ErgErr
      REAL*8 SUSN(L3MAX),SPH(L3MAX),Denom,SD,DD
      REAL*8 D0,D1,D2,D3,D4,D5,D6
      REAL*8 D0Av,D1Av,D2Av,D3Av,D4Av,D5Av,D6Av
      REAL*8 D0Av2,D1Av2,D2Av2,D3Av2,D4Av2,D5Av2,D6Av2
      REAL*8 CumAv,CumAv2,DD1
      INTEGER J,I,Asym
      REAL*8 CHIN,SUSC,CHI1,CHI11,SPH1,SPH11,SPECHEB,CHIB,CHIT
      REAL*8 CUM,CUM1,SSPECHEB,SCHIB,EB,SPECHET
      REAL*8 SMB1,SMB2,SSpecB1,SSpecB2,SChiB1,SChiB2,SMB,SEB
      REAL*8 SSpecB,SpecB,EB1,EB2,ChiB1,ChiB2,SpecT1,SpecT2
      REAL*8 ChiT1,ChiT2,ChiT3,SEB1,SEB2,SpecB1,SpecB2,MB1,MB2,MB
      CHARACTER*72 B
      CHARACTER*6 DWord
      INTEGER L,L3,NMCS,LBulk,NLayer,Vol,LHelp1,LHelp2
      REAL*8 TInvs

      READ(*,*) L,L3,NMCS,TInvs,Asym,LBulk
C**      READ(*,*) NMCS,MAT,MT1,MT2,MT3,MT4,ET,ET2,SUS1
      READ(*,*) NMCS,MAT,MT1,MT2,MT3,MT4
      READ(*,12) ET
      READ(*,12) ET2
      READ(*,*) SUS1
12    FORMAT(D18.12)
```

```
      Write(55,77) ET2, ET
77    Format(1X, D18.12, D18.12)

      LHelp1 = L3/2 - LBulk/2 + 1
      LHelp2 = L3/2 + LBulk/2
      NLayer = L*L
      Vol = NLayer*L3
C**  Normalize the measured quantities
      Denom = 1.0D0/DBLE(NMCS)

C** First, moments of the total magnetization
      MAT = MAT*Denom
      MT1 = MT1*Denom
      MT2 = MT2*Denom
      MT3 = MT3*Denom
      MT4 = MT4*Denom
C** Now moments of the total energy
      ET = ET*Denom
      ET2 = ET2*Denom
      SUS1 = SUS1*Denom

      DO J = 1,L3
C** Now moments of the layer magnetizations
        READ(*,*) MA(J),M1(J),M2(J),M3(J),M4(J),E(J),E2(J),
     *             SUSN(J),SPH(J)
        MA(J) = MA(J)*Denom
        M1(J) = M1(J)*Denom
        M2(J) = M2(J)*Denom
        M3(J) = M3(J)*Denom
        M4(J) = M4(J)*Denom
C** Finally moments of the layer energies and susceptibilities
        E(J) = E(J)*Denom
        E2(J) = E2(J)*Denom
        SUSN(J) = SUSN(J)*Denom
        SPH(J) = SPH(J)*Denom
      END DO

C---- DATA ANALYSIS
C**  First the layer magnetizations
      WRITE(*,*)
      WRITE(*,*)
C---- CALCULATE STANDARD DEVIATION FOR EACH LAYER AND PRINT RESULTS
      DO J = 1,L3
        Sym(J) = M1(J)
      END DO
C**  Antisymmetrize the magnetization and write out results
```

```
      WRITE(*,*)
      WRITE(*,*)
      B= '  #  Magnetization  Sym. Magnet.'
      WRITE(*,5) B
      B= ' --- ------------ --------------'
      WRITE(*,5) B
5       FORMAT(1X,A72)
      DO J = 1,L3/2
        D1Av = 0.5D0*(Sym(L3-J+1) + Asym*Sym(J))
        WRITE(*,2) J,Sym(J),D1Av
2         FORMAT(1X,I3,2(1X,F13.7))
      END DO
      DO J = L3/2+1,L3
        D1Av = 0.5D0*(Asym*Sym(L3-J+1)+Sym(J))
        WRITE(*,2) J,Sym(J),D1Av
      END DO

C**  Next the layer energies
C**  Calculate energy and standard deviation for each layer
      DO J = 1,L3
        Sym(J) = E(J)
      END DO
C**  Symmetrize the energy and write out results
      WRITE(*,*)
      WRITE(*,*)
      B= '  #     Energy      Sym. Energy'
      WRITE(*,5) B
      B= ' --- ------------ -------------'
      WRITE(*,5) B
      DO J = 1,L3
        D1Av = 0.5D0*(Sym(J) + Sym(L3-J+1))
        WRITE(*,2) J,Sym(J),D1Av
      END DO

C**  Specific heat by layer
C**  Calculate Cnn
      WRITE(*,*)
      DO J = 1,L3
        Sym(J) = NLayer*TINVS*TINVS*(E2(J) - E(J)*E(J))
      END DO
C**  Symmetrize Cnn and write out results
      WRITE(*,*)
      WRITE(*,*) 'Cnn = L*L*Beta*Beta*(E2(J) - E(J)*E(J))'
      WRITE(*,*)
      B= '  #       Cnn       Symm.  Cnn'
      WRITE(*,5) B
      B= ' --- ------------ ------------'
```

```
      WRITE(*,5) B
      DO J = 1,L3
        D1Av = 0.5D0*(Sym(J) + Sym(L3-J+1))
        WRITE(*,3) J,Sym(J),D1Av
3         FORMAT(1X,I3,2(1X,F13.6))
      END DO
C**   Calculate Cn
      DO J = 1,L3
        Sym(J) = Vol*TINVS*TINVS*(SPH(J)-ET*E(J))
      END DO
C**   Symmetrize Cn and write out results
      WRITE(*,*)
      WRITE(*,*) 'Cn = L*L*L3*Beta*Beta*(SPH(J) - ET*E(J))'
      WRITE(*,*)
      B= '  #       Cn         Sym.   Cn'
      WRITE(*,5) B
      B= ' --- ------------- -------------'
      WRITE(*,5) B
      DO J = 1,L3
        D1Av = 0.5D0*(Sym(J) + Sym(L3-J+1))
        WRITE(*,3) J,Sym(J),D1Av
      END DO

C**   Susceptibilities
C**   Calculate CHIn
      DO J = 1,L3
        Sym(J) = Vol*TINVS*(SUSN(J) - MT1*M1(J))
      END DO
C**   Symmetrize CHIn and write out results
      WRITE(*,*)
      WRITE(*,*)
      B= '  #      CHIn       Sym.   CHIn'
      WRITE(*,5) B
      B= ' --- ------------- -------------'
      WRITE(*,5) B
      DO J = 1,L3
        D1Av = 0.5D0*(Sym(J) + Sym(L3-J+1))
        WRITE(*,3) J,Sym(J),D1Av
      END DO

C**   Calculate CHInn
      DO J = 1,L3
        Sym(J) = NLAYER*TINVS*(M2(J) - M1(J)*M1(J))
      END DO
C**   Symmetrize CHInn and write out results
      WRITE(*,*)
      WRITE(*,*)
```

```
      B= '  #      CHInn      Sym.  CHInn'
      WRITE(*,5) B
      B= ' --- ------------- -------------'
      WRITE(*,5) B
      DO J = 1,L3
        D1Av = 0.5D0*(Sym(J) + Sym(L3-J+1))
        WRITE(*,3) J,Sym(J),D1Av
      END DO

C**   Calculate the 4th order cumulant
      DO J = 1,L3
        Sym(J) = 1.0D0 - M4(J)/(3.0D0*M2(J)*M2(J))
      END DO
C**   Symmetrize U and write out results
      WRITE(*,*)
      WRITE(*,*)
      B= '  #        U        Sym.    U'
      WRITE(*,5) B
      B= ' --- ------------- -------------'
      WRITE(*,5) B
      DO J = 1,L3
        D1Av = 0.5D0*(Sym(J) + Sym(L3-J+1))
        WRITE(*,2) J,Sym(J),D1Av
      END DO

C**   Calculate moments of layer susceptibility
      D0 = 0.0D0
      D1 = 0.0D0
      D2 = 0.0D0
      D3 = 0.0D0
      D4 = 0.0D0
      DO J = 1,L3
        SUSC = NLAYER*TINVS*(M2(J) - M1(J)*M1(J))
        DD = DBLE(J)
        D0 = D0 + SUSC
        D1 = D1 + SUSC*DD
        D2 = D2 + SUSC*DD*DD
        D3 = D3 + SUSC*DD*DD*DD
        D4 = D4 + SUSC*DD*DD*DD*DD
      END DO
      D1 = D1/D0
      DD1 = D1
      D2 = D2/D0
      D3 = D3/D0
      D4 = D4/D0
      CUM = 1.0D0 - D4/(3.0D0*D2*D2)
C**   Write out the moments of the distribution:
```

```
      WRITE(*,*)
      WRITE(*,*)
      WRITE(*,*) 'CHInn Distribution Results:  Non-Central moments'
      WRITE(*,*)
      WRITE(*,*) '   Quantity         Value'
      WRITE(*,*) '   --------     -------------'
      DWord = 'Mean'
      WRITE(*,7) DWord,D1
7       FORMAT(4X,A6,6X,F13.6)
      DWord = 'Cumu.'
      WRITE(*,7) DWord,CUM
C**  Calculate central moments
      D0 = 0.0D0
      D2 = 0.0D0
      D4 = 0.0D0
      DO J = 1,L3
        SUSC = NLAYER*TINVS*(M2(J) - M1(J)*M1(J))
        DD = DBLE(J) - DD1
        D0 = D0 + SUSC
        D2 = D2 + SUSC*DD*DD
        D4 = D4 + SUSC*DD*DD*DD*DD
      END DO
      D2 = D2/D0
      D4 = D4/D0
      CUM = 1.0D0 - D4/(3.0D0*D2*D2)

C**  Write out Binder parameter for central moments
      WRITE(*,*)
      WRITE(*,*)
      WRITE(*,*) 'CHInn Distribution Results:  Central moments'
      WRITE(*,*)
      WRITE(*,*) '   Quantity         Value'
      WRITE(*,*) '   --------     -------------'
      DWord = 'Var.'
      WRITE(*,7) DWord,D2
      DWord = 'Cumu.'
      WRITE(*,7) DWord,CUM

C**  Calculate Z quantities
      D0 = 0.0D0
      D1 = 0.0D0
      D2 = 0.0D0
      D3 = 0.0D0
      DO J = 1,L3
        SUSC = NLAYER*TINVS*(M2(J) - M1(J)*M1(J))
        DD = DBLE(J) - 0.5D0*DBLE(L3+1)
        D0 = D0 + SUSC
```

```
        D1 = D1 + SUSC*DD
        D2 = D2 + SUSC*DD*DD
        D3 = D3 + SUSC*DABS(DD)
      END DO
      D1 = D1/D0
      D2 = D2/D0
      D3 = D3/D0
      DD1 = D1

C**  Write out the moments of the distribution:
      WRITE(*,*)
      WRITE(*,*)
      WRITE(*,*) 'CHInn Distribution Results:  Z quantities'
      WRITE(*,*)
      WRITE(*,*) '   Quantity         Value'
      WRITE(*,*) '   --------     -------------'
      DWord = 'ZX'
      WRITE(*,7) DWord,D1
      DWord = 'ZX2'
      WRITE(*,7) DWord,D2
      DWord = 'ZXSYM'
      WRITE(*,7) DWord,D3


C**  Calculate properties of the total magnetization
      D0Av = MAT
      D1Av = MT1
      D2Av = MT2
      D3Av = MT3
      D4Av = MT4
      DD = MT2 - MT1*MT1
      D5Av = DD
      DD = MT4 - MT2*MT2
      D6Av = DD

C**  Write out the moments of the magnetization'
      WRITE(*,*)
      WRITE(*,*)
      WRITE(*,*) 'Total magnetization results'
      WRITE(*,*)
      WRITE(*,*) '   Quantity         Value'
      WRITE(*,*) '   --------     -------------'
      DWord = 'MABS'
      WRITE(*,7) DWord,D0Av
      DWord = 'M'
      WRITE(*,7) DWord,D1Av
      DWord = 'M2'
```

```
      WRITE(*,7) DWord,D2Av
      DWord = 'M3'
      WRITE(*,7) DWord,D3Av
      DWord = 'M4'
      WRITE(*,7) DWord,D4Av
      DWord = 'M2Conn'
      WRITE(*,7) DWord,D5Av
      DWord = 'M4Conn'
      WRITE(*,7) DWord,D6Av
      DWord = 'CUMU'
      WRITE(*,7) DWord,(1.0D0 - D4Av/(3.0D0*D2Av*D2Av))
      ChiT1 = Vol*TInvs*(MT2 - MT1*MT1)
      ChiT2 = Vol*TInvs*(MT2 - D0Av*D0Av)
      ChiT3 = Vol*TInvs*MT2
      DWord = 'Chi1'
      WRITE(*,7) DWord,ChiT1
      DWord = 'Chi2'
      WRITE(*,7) DWord,ChiT2
      DWord = 'Chi3'
      WRITE(*,7) DWord,ChiT3


C** Initialize the total susceptibility and specific heat
      ChiT1 = 0.0D0
      ChiT2 = 0.0D0
      ChiT3 = 0.0D0
      SpecT1 = 0.0D0
C**  Initialize the bulk quantities
      EB1 = 0.0D0
      ChiB1 = 0.0D0
      MB1 = 0.0D0
      SpecB1 = 0.0D0
C**  Initialize the surface excess quantities
      SEB1 = 0.0D0
      SChiB1 = 0.0D0
      SMB1 = 0.0D0
      SSpecB1 = 0.0D0

C**  First calculate total quantities (Chi and Spec)
      ChiT1 = Vol*TInvs*(MT2 - MT1*MT1)
      SpecT1 = Vol*TInvs*Tinvs*(ET2 - ET*ET)

C**  Now calculate bulk properties:  Loop over LBulk layers from
C**  LHelp1 (= L3/2 - LBulk/2 + 1) to LHelp2 (=L3/2 + LBulk/2)
      EB=0.0D0
      MB=0.0D0
      SpecB=0.0D0
```

```
      ChiB=0.0D0
      DO J=LHELP1,LHELP2
        EB = EB + E(J)
        ChiB =  ChiB + Vol*TINVS*(SUSN(J) - MT1*M1(J))
        MB = MB + M1(J)
        SpecB = SpecB + Vol*TINVS*TINVS*(SPH(J)-ET*E(J))
      END DO
      EB1 = EB/DBLE(LBulk)
      ChiB1 =  ChiB/DBLE(LBulk)
      MB1 = MB/DBLE(LBulk)
      SpecB1 = SpecB/DBLE(LBulk)

C**  Calculate surface excess quantities
      SEB=0.0D0
      SMB=0.0D0
      SSpecB=0.0D0
      SChiB=0.0D0
      DO J=1,L3
        SEB = SEB + E(J) - EB1
        SMB = SMB + M1(J) - MB1
        SPH1 = Vol*TINVS*TINVS*(SPH(J)-ET*E(J))
        SSpecB = SSpecB + SPH1 - SpecB1
        CHIN = Vol*TINVS*(SUSN(J) - MT1*M1(J))
        SChiB = SChiB + CHIN - ChiB1
      END DO

      SEB1 = SEB
      SChiB1 = SChiB
      SMB1 = SMB
      SSpecB1 = SSpecB

      WRITE(*,*)
      WRITE(*,*) 'Summary of results for the Energy'
      WRITE(*,*) '   Quantity         Value'
      WRITE(*,*) '   --------     -------------'
      DWord = 'Total'
      WRITE(*,7) DWord,ET
      DWord = 'Bulk'
      WRITE(*,7) DWord,EB1
      DWord = 'Excess'
      WRITE(*,7) DWord,SEB1
      WRITE(*,*)
      WRITE(*,*) 'Summary of results for the Magnetization'
      WRITE(*,*) '   Quantity         Value'
      WRITE(*,*) '   --------     -------------'
      DWord = 'Total'
      WRITE(*,7) DWord,MT1
```

```
DWord = 'Bulk'
WRITE(*,7) DWord,MB1
DWord = 'Excess'
WRITE(*,7) DWord,SMB1
WRITE(*,*)
WRITE(*,*) 'Summary of results for the Susceptibility'
WRITE(*,*) '   Quantity         Value'
WRITE(*,*) '   --------     -------------'
DWord = 'Total'
WRITE(*,7) DWord,ChiT1
DWord = 'Bulk'
WRITE(*,7) DWord,ChiB1
DWord = 'Excess'
WRITE(*,7) DWord,SChiB1
WRITE(*,*)
WRITE(*,*)
WRITE(*,*) 'Summary of results for the Specific Heat'
WRITE(*,*) '   Quantity         Value'
WRITE(*,*) '   --------     -------------'
DWord = 'Total'
WRITE(*,7) DWord,SpecT1
DWord = 'Bulk'
WRITE(*,7) DWord,SpecB1
DWord = 'Excess'
WRITE(*,7) DWord,SSpecB1
END
```